CHEMICAL REVIEWS

Review

pubs.acs.org/CR

Synthesis and Development of Graphene–Inorganic Semiconductor Nanocomposites

Nan Gao and Xiaosheng Fang*

Department of Materials Science, Fudan University, Shanghai 200433, People's Republic of China

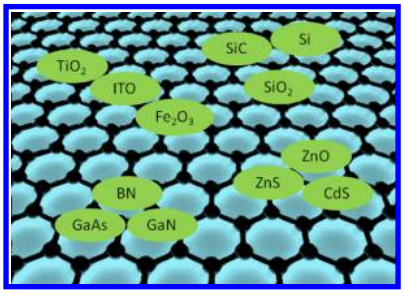

CONTENTS

1. INTRODUCTION

Over the past decade, graphene research has attracted increasing interest from researchers in physics, materials science, chemistry, etc. Graphene consists of an unusual single-layer honeycomb lattice of C atoms, which differs from all other materials of this element. More specifically, the C atoms of graphene are sp^2-bonded and densely packed in a crystal lattice. This closely resembles the basic building block found in graphitic materials of different dimensionalities.[1] It has been demonstrated that graphene exhibits some special characteristics, such as a high electron mobility of up to 230 000 $cm^2\ V^{-1}\ s^{-1}$ at low temperatures,[2] an exceptional thermal conductivity approaching 5000 W mK^{-1},[3] and superior mechanical properties with a large Young's modulus, exceeding 1.0 TPa,[4,5] the latter being comparable to those of single-walled nanotubes and even diamonds.

With these intriguing physical and chemical properties, it is not surprising that graphene has been intensively investigated to exploit its functions as a promising material for future applications. Typical examples of graphene research focus are (1) the synthesis of pristine graphene in inorganic chemistry, (2) the chemical modification of graphene, (3) graphene characterization (its properties and functions), (4) the investigation of graphene–polymer composites, and (5) graphene and inorganic materials either exclusively combined or in integrated electronic systems with other components.

The fourth and fifth examples above demonstrate the potential applications of graphene when conjugated with a range of other materials. For example, in the case of optoelectronic and electrochemical devices, inorganic semiconductors are potentially competitive candidates for exploring micro- and nanoscale phenomena and studying the dependence of functional properties on size and dimensionality. Indeed, due to their low work functions, high aspect ratios, and high mechanical stability, the inherent nanostructure design of many inorganic semiconductors provides unique features for a diverse range of systems used in electronic applications.[6] In fact, it is possible to build up an effective link between conventional solid-state nanostructures and 2-dimensional molecular structures using hybrid materials of graphene and inorganic semiconductors.[7] In this review, the focus is on the heterogeneous structures of graphene and inorganic semiconductors. Of interest is the fact that, although the research on nanostructures of C-based materials, for example, of carbon nanotubes (CNTs),[8,9] to prepare enhanced composites with inorganic semiconductors was developed many years ago, little was known about the atomically thin graphene sheets

Received: October 25, 2013
Published: August 3, 2015

DOI: 10.1021/cr400607y
Chem. Rev. 2015, 115, 8294–8343

themselves. This is despite another fact that unrolled CNTs are dimensionally equivalent to such sheets. About a decade ago, systematic research on the single-layer structure of C atoms was initiated in the Manchester laboratory of Geim and Novoselov.[10] One of the reasons for using graphene with inorganic semiconductors was to achieve large-scale integration of nanoelectronic devices, based on conventional means, with the continued scaling of the individual components.[11] When restrained within nanoscale dimensions, graphene can demonstrate the unique electronic properties of CNTs.[12] This leads to effective transport phenomena from the viewpoint of electronics, allowing the composite systems of inorganic semiconductors based on graphene to obtain prompted charge transport. In addition, the creation of composite inorganic semiconductor−graphene systems overcomes the inherent disadvantages of bulk nanotubes, namely, their relatively low tensile strength. In fact, even before the production of single-layer graphene sheets was officially reported, research involving graphene material on a semiconductor substrate (Si) had already been achieved, not without any experimental support.[13]

Sometime after the discovery of graphene, it became clear that when a graphene nanosheet was combined with some inorganic semiconductors, the zero-gap shortcomings that had limited the electrical and optical characteristics of graphene itself in potential applications, especially for high-speed electronic devices, could be considerably reduced or even avoided. Charge carriers in graphene demonstrate charge-conjugation symmetry between electrons and holes and possess an internal degree of freedom similar to "chirality" for ultrarelativistic elementary particles, and this results in a gapless graphene semiconductor.[14] An electronic band gap in graphene can be created by patterning graphene with size constrictions, or introducing strain-induced curvature (disorder) directly onto the graphene nanosheet. This can be achieved through attaching nanoscaled materials, including inorganic semiconductors.[15,16] One valid question is how to effectively connect the inorganic semiconductors with the graphene. In fact, recent studies have shown that a great number of inorganic semiconductors are compatible, to varying extents, with graphene in forming hybrid materials. Since different methods are used to produce the graphene, the compatibility between graphene and the inorganic semiconductors changes drastically. More relevantly, so do the optical and electronic properties of the ensuing hybrid materials. In the case of revealing graphene under a microscopic instrument, distinct yet interesting features in visibility can be observed. Another interesting aspect is the isolation of graphene onto the supporting substrates. The characteristics of isolated graphene sheets, from different sources, on semiconductor substrates can vary. The production techniques, on the other hand, are related to the classified groups and structures of the semiconductors. In addition, as well as induced physical/chemical absorption, interactions between some inorganic semiconductors and graphene with respect to charge transport are also present. Charge carriers can be activated in nanoscaled semiconductor structures typically under light irradiation. The resulting electronic interactions between the coupled semiconductor and graphene will trigger efficient charge separation and transportation. With graphene working as the electron conductor, the fate of these charge carriers and the accompanying physical and chemical changes in the semiconductor nanostructures can then be studied without the issue of fast recombination.[17,18] In the search for a better understanding of such integrated graphene−semiconductor systems, Raman scattering, a range of imaging techniques such as atomic force microscopy (AFM), scanning electron microscopy (SEM), and transmission electron microscopy (TEM), and X-ray diffraction (XRD) measurements have all yielded important information.

A perusal of the nanomaterial literature reveals that research into hybrid graphene−inorganic semiconductor materials is a relatively new interdisciplinary field where optoelectronic, electrochemical, and photochemical methods as well as the underlying theories are encountered. Recent progress confirms that graphene is a rising star in the quest for new-generation materials that are predicted to make an essential difference in both the electronics and composite industries. In this review, we put a particular emphasis on the chemical and physical properties of the hybrid materials, focusing on the synthetic conditions used. In addition, we categorize the hybrid materials into relevant groups while discussing the interplay between the inorganic semiconductors and graphene. This approach is reflected through the main body of this review, in particular where the diverse heterogeneous structures of graphene and inorganic semiconductors in various functional devices are concerned. Since the scope of this review is not limited to a specific group of inorganic semiconductors, a wide range of relevant research appealing to a broad range of readers is covered. For example, on one hand, it should be of general interest to researchers working on composite materials and functional nanostructures because the review covers work involving the combination of two (or more) constituent materials with different chemical or physical properties, the treatment of the resulting composite materials for a particular function such as field emission or photocatalysis, as well as their characterization. On the other hand, the composite materials made of graphene and inorganic semiconductors are categorized into groups with relevant examples, and this should attract intense attention from those researchers whose activities are focused on optoelectronic and electrochemical applications.

2. GROUP IV SEMICONDUCTORS (ELEMENTAL AND COMPOUND) AND GRAPHENE

2.1. Silicon and Graphene

Although the replacement of Si by new materials has been regularly predicted, and is to some extent even desired, progress at the moment toward this goal shows that this is unlikely to occur anytime soon.[19] Even as the nanotechnology for future electronics is advancing rapidly, it is still reasonable to expect that the use of Si will be enhanced for at least another decade or so, with new add-on features on conventional Si platforms dominating.[20] For example, to date, graphene, with its excellent electronic properties, has been intensively investigated with a view to making combined nanoelectronic devices with Si.[21] Back in 2002, Hirono et al. deposited C films with remarkable mechanical and electrical properties onto Si substrates.[13] The resulting C films were then considered as graphene sheets due to the fact that they had electron patterns similar to that of graphite, although the evidence to show the existence of such single-layer graphene sheets was yet to be enhanced by the work of Geim and Novoselov in forthcoming years. The fact that early achievements have driven further developments in the field of graphene research makes it worthwhile to look at the characteristics of such Si−graphene hybrid materials.

Eda et al. collected field emission data from randomly but nonlaterally oriented graphene in polymer hosts. They noticed

DOI: 10.1021/cr400607y
Chem. Rev. 2015, 115, 8294−8343

that only when the graphene sheets stood on their edges (not lying laterally flat) on Si substrates could the advantage of high-field enhancement be efficiently taken.[22] It should be noted, therefore, that the geometrical features of graphene play an important role in the resulting electronic device performance. Similarly, to investigate the field electron emission properties, Pandey et al. fabricated both planar graphene and morphologically disordered graphene on p-doped Si substrates.[23] They achieved this by transferring pregrown graphene synthesized through thermal chemical vapor deposition (CVD) onto Cu foil. The morphologically disordered graphene was shown to have improved field emission properties compared with the planar graphene. Of particular interest is the fact that the maximum emission current density was increased by "a factor of 500". The planar graphene exhibited a maximum current density of 0.007 mA cm^{-2}, under an electric field intensity of 4.26 V μm^{-1}, while the morphologically disordered graphene sample reached 3.52 mA cm^{-2}. It was argued that the incorporation of morphological disorder, induced during the transfer process, in the graphene created more emission sites due to the additional defects, edges, and atomic-scale ripples.

It is worth noting that the additional transfer process of graphene onto a substrate is frequently adopted, although it is not always favorable. Likewise, Fan et al. assembled Schottky junction solar cells by coating graphene films onto n-type Si nanowire arrays. The resulting structures showed enhanced light trapping and faster carrier transport compared with the graphene/planar Si structure.[24] The improved efficiency was mainly attributed to the relatively large surface areas of the Si nanowires and the suppression of reflectance caused by periodic spacing among the nanowire structures. On one hand, the Si nanowires not only provided direct pathways to increase the charge carrier collection and transport for light harvesting, but also suppressed the reflection of the Si–graphene junction surface, compared with the bulk Si. On the other hand, the graphene acted as a transparent electrode favorable for collection of the photoexcited holes generated out of the Si nanowires. This leads to the junction exhibiting high optical absorption. The graphene they used was synthesized employing a methane CVD method using Ni foils as the substrate. Afterward, these were transferred to the top of the array to make a junction. Xie et al. constructed Schottky junction solar cells by transferring a single-layer graphene film, which was also produced on a Cu foil (as the catalyst) via the CVD method at 1000 °C by using a gas mixture of CH_4 and H_2, onto a Si nanowire array in turn prepared using a Ag-assisted chemical etching method.[25] Jeong et al. made top electrodes by transferring the graphene layer, grown on a Cu substrate at 1000 °C using CH_4 gas, with the assistance of poly(methyl methacrylate) (PMMA), onto vertical Si nanowire bundles made from boron-doped p-type Si wafers.[26] The transferred graphene acted as a supporting layer for the further deposition of an Al metal electrode. On the other hand, Yan et al. recently managed to directly grow a bilayer of CVD graphene on heavily doped Si wafers coated with a 500 nm thick insulating layer of SiO_2.[27] This creates a possible pathway for the scalable growth of bilayer graphene with direct compatibility twith device construction. Another direct growth technique for graphene on substrates was reported by Kumar et al.[28] They fabricated vertical graphene nanosheets in a N_2 plasma (with 20% CH_4) on Si nanograss made from the Si substrate in a CF_4 + O_2 plasma-based process.

However, while the growth of graphene on metal (mainly Ni and Cu) substrates was found to either follow the diffusion–segregation–precipitation of C atoms (on Ni) or develop as a consequence of a surface-adsorption process (on Cu),[30] the growth mechanism of graphene on Si remains unclear. In a relatively early paper, Shang et al. studied the direct growth of a uniform multilayer graphene nanoflake film on a Si substrate.[31] They used a microwave-assisted plasma CVD method without using any metallic catalyst or surface pretreatments. The grown film exhibited sharp edges and a preferentially vertical orientation relative to the Si substrates. The mechanism, however, was not systematically shown. In a very similar way, Hong et al. synthesized graphene on a silicon-on-insulator (SOI) substrate without metallic catalyst.[29] They suggested that graphene growth on the Si surface followed a process involving surface reaction, adsorption, decomposition, and accumulation. It was also proposed, as shown schematically in Figure 1, that

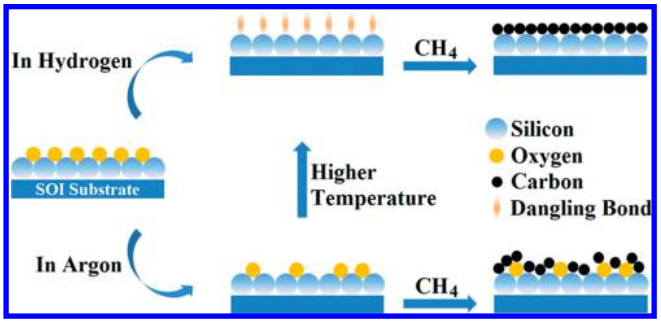

Figure 1. Schematic of the graphene growth mechanism on the SOI substrate. Reprinted with permission from ref 29. Copyright 2012 AIP Publishing LLC.

when Si was heated at high temperatures (up to 1000 °C), the surface oxide decomposed and the Si atoms became reactive with free dangling bonds. Hydrogen could then react with and remove SiO_2 at the surface. When CH_4 was adsorbed onto a clean active Si surface, it was found to crack into C atoms at high temperatures. The Si dangling bonds would then stick strongly to the C atoms, so that the surface-adsorbed C atoms no longer moved freely on the Si surface but instead accumulated to form graphene. It was also observed that although hydrogen could be replaced by argon for graphene growth, the SOI surface seemed to be much less reactive.

In view of the importance of inherent geometrical features, it is not surprising that these are relevant, not only in field enhancement, but also in some other Si–graphene-related areas such as in high-performance lithium ion batteries. From an efficiency point of view, Si-based materials are believed to be suitable for making Li ion battery anodes because each Si atom can accommodate 4.4 Li atoms. In theory, this leads to a specific insertion capacity of 4200 mA h g^{-1}, which is considerably higher than that of the graphitic counterpart (~372 mA h g^{-1}).[33,34] However, Si suffers from a large volume change of more than 300% during Li alloying and dealloying, and this frequently results in structural pulverization and electrical disconnection from the current collector, leading to a rapid decline in cell capacity.[32] Recent studies have shown that Si nanowires can accommodate large strains without pulverization, provide good electronic contact and conduction, and display short Li insertion distances.[35,36] Furthermore, it has been demonstrated that modification of Si nanostructures with C materials can provide enhanced mechanical support and

DOI: 10.1021/cr400607y
Chem. Rev. 2015, 115, 8294–8343

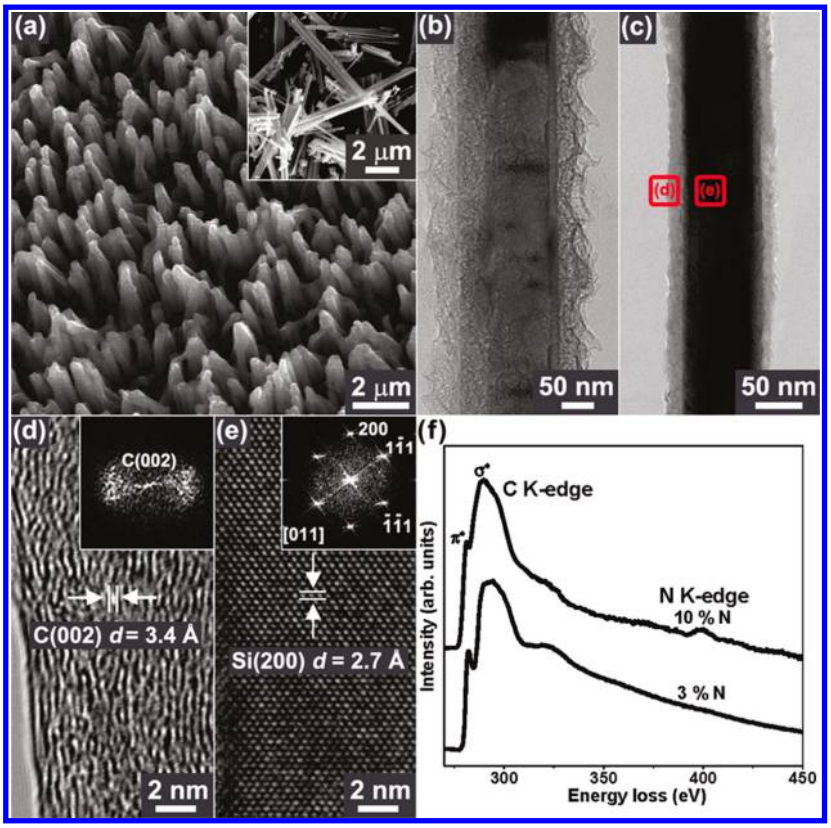

Figure 2. (a) SEM micrograph of the vertically aligned Si−C nanocable array synthesized on a Si substrate. The inset corresponds to the Si−C nanocables separated from the substrate. HRTEM images show Si−C nanocables with 50 nm (b) and 20 nm (c) thick shells. The lattice-resolved TEM images and Fourier-transformed electron diffraction patterns (insets) confirm the crystalline graphitic layer shells (d) and the single-crystalline Si nanowire core (e) with the [100] growth direction. (f) Electron energy-loss spectroscopy (EELS) spectra show the N contents of 3% doping and 10% doping in the graphitic layers. Reprinted from ref 32. Copyright 2011 American Chemical Society.

efficient electron-conducting pathways.[37,38] To understand the detailed mechanism for modifying Li ion batteries and with a view to extending the range of applications of C-containing nanostructures, Cho et al. sheathed pregrown (through metal-assisted chemical etching) Si nanowires with shell-like graphitic layers using CVD.[32] They suggested that increasing the thickness of the undoped graphitic layers from 20 to 50 nm should lead to an increase in the charge capacity of the Li ion battery from 800 to 1040 mA h g^{-1} after 45 cycles. The thicknesses of the graphitic layers were controlled by adjusting the deposition time. As shown in Figure 2a (the inset shows the SEM image of the Si−C nanocables separated from the substrate), Si−C core−shell nanocable (or nanowire) arrays were vertically aligned on Si substrates. The high-resolution TEM (HRTEM) image shows the homogeneously coated graphitic layers on the Si nanocable core (diameter about 80 nm) with thicknesses of about 50 nm (Figure 2b) and 20 nm (Figure 2c). Parts d and e of Figure 2 show the lattice-resolved images of the C shell and the Si core, respectively, for a selected 20 nm thick Si−C nanocable. For the nitrogen-doped graphitic layers that were deposited on the Si nanowire arrays with a N content of either 3% or 10%, the structures were reported to be quite similar to those of the Si−C nanocable reference samples. Nevertheless, the authors noted that doping of C materials further enhanced the charge capacity of the Li ion batteries. That is, a 3% N-doping in the 50 nm thick shell increased the charge capacity by 21% (i.e., to 1260 mA h g^{-1}), whereas a 10% N-doping in the 20 nm thick shell increased it by 36% (i.e., to 1090 mA h g^{-1}). The electron energy-loss spectroscopy (EELS) spectra of these samples show their N content in the relevant graphitic layers (Figure 2f).

Given that graphene, as the conducting and buffering matrix, can greatly improve the capacity of Li ion batteries, it is, however, important to be aware of an alternative way to ensure the interaction between the graphene sheets and the electroactive material. When Si is present in the form of nanoparticles, rather than relatively "large" wafers, anchoring the nanoparticles to the surface of the graphene sheet appears to be necessary to maintain good structural stability and electron conduction of the Si electrode during discharging and charging. Lee et al. prepared composites consisting of Si nanoparticles (H-terminated, <30 nm) and stacks of graphene sheets to form anodes for use in Li ion batteries.[39] In their work, suspensions of graphene oxide (GO) were prepared by oxidizing graphite and then added into Si dispersions (in water). Afterwards the mixture was suction filtered and settled, in a specified order, to form self-standing Si−GO composite papers. Figure 3a shows the SEM image of the Si−GO composite with a stack of GO sheets. As can be seen in Figure 3b, after reduction of GO (in a flow of 10% H_2 in Ar), the sheets appeared crumpled and pockets of void space were visible. The sheetlike morphology is also observed in the TEM image of the composite (Figure 3c). It was reported that electrodes with high storage capacities of 2200 mA h g^{-1}, after 50 cycles, were obtainable from these composites, provided that the Si nanoparticles were well dispersed between the GO sheets and the portions of the GO sheet stacks reconstituted to form a network of graphite, as shown in Figure 3d.

DOI: 10.1021/cr400607y
Chem. Rev. 2015, 115, 8294−8343

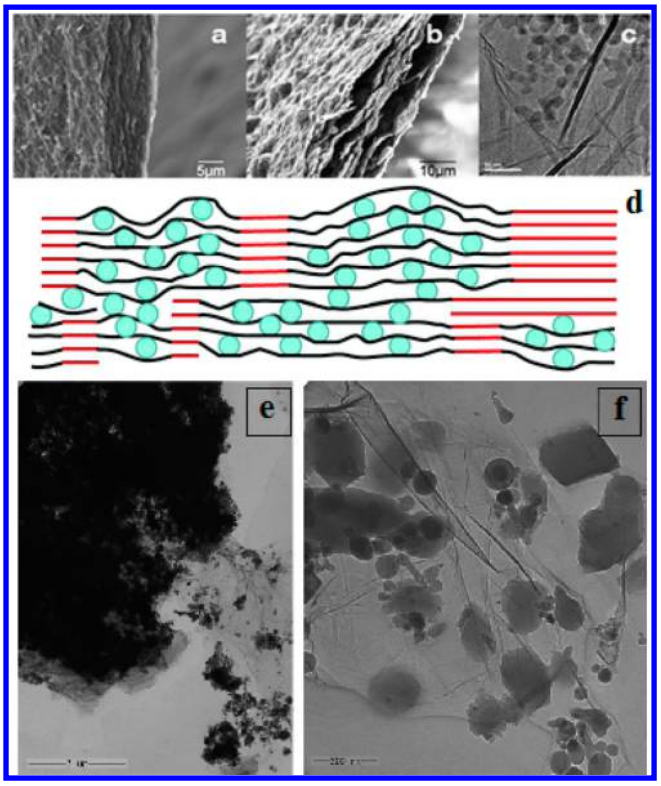

Figure 3. (a, b) Edge-view SEM images of Si−GO and Si−RGO composite papers: (a) Si−GO; (b) Si−RGO. (c) TEM image of the Si−RGO composite paper. (d) Cross-sectional schematic showing a network of graphite (red) anchoring regions of graphene-Si composite. Blue circles: Si nanoparticles; black lines: graphene sheets. (e, f) TEM images of the Si−Ph−G nanocomposite: (e) ×15000; (f) ×100000. Images a−d reprinted with permission from ref 39. Copyright 2010 Royal Society of Chemistry. Images e and f reprinted with permission from ref 40. Copyright 2012 Royal Society of Chemistry.

However, Evanoff et al. claimed that the high surface area of graphene used in these composites would lead to large irreversible capacity losses, and therefore, they employed a vapor deposition method (low-pressure decomposition of high-purity SiH_4) to synthesize porous Si- and graphene-containing nanocomposites.[41] The nanocomposites thus obtained were found to have a reduced surface area: the specific surface area, from 940 $m^2\ g^{-1}$ of produced graphene to 5 $m^2\ g^{-1}$ of produced composite, was reduced by over 100 times. The anode which was composed of the nanocomposite particles exhibited a specific capacity in excess of 2000 mA h g^{-1} at a current density of 140 mA g^{-1} and also exhibited a stable performance for 150 cycles. Yang et al. reported that when Si nanoparticles of 50−200 nm size were covalently bound to graphene (G) sheets via phenyl (Ph) linkers using diazonium chemistry, the Si−Ph−G nanocomposites obtained, as shown in parts e and f of Figure 3, delivered a capacity of 828 mA h g^{-1} for up to 50 cycles, at a current density of 300 mA g^{-1}.[40] The electrodes exhibited a reversible capacity of 350 mA h g^{-1} in the 40th cycle at a rate of 4000 mA g^{-1}. It was argued that the covalent linkages between the Si nanoparticles and the graphene sheets ensured a fast and stable kinetics for the Si electrodes by maintaining structural integrity and high electronic conduction during the cycling process. This type of research strategy is also frequently adopted in fabricating graphene composites with other semiconductor materials. These will be discussed in subsequent sections.

2.2. Silicon Dioxide (SiO_2) and Graphene

To observe and optimize the growth conditions, it is necessary to map and characterize large areas of graphene during the device fabrication. However, the correct identification of graphene on a sample using ordinary optical microscopy is dependent on the nature of the substrate, unless additional imaging modes are suitably employed.[42] In fact, the only way the graphene sheets reported in early research papers could be isolated was to cleave the graphite onto an oxidized Si wafer, which could then be scanned using an optical microscope to observe the deposited graphene.[43] This is an important reason to explain the fact that, in ensuing studies, SiO_2 has been frequently used for the observation and investigation of graphene,[44−47] in addition to its role as the usual dielectric substrate utilized in device applications. It has been shown that the visibility of graphene appears to depend strongly on both the thickness of the SiO_2 substrate and the wavelength of the light.[43] That is to say, although in theory graphene can be isolated for any thickness of SiO_2, it has been claimed that 300 and 100 nm are the most suitable for visual detection. In practice, as has already been reflected in the relevant references above, a Si wafer with a 300 nm SiO_2 layer on top has been widely used to support graphene. However, the mobility of graphene on SiO_2 at low and room temperatures is limited by scattering, due to either the extrinsic charged impurities in the substrate, which are the dominant factor limiting the mobility for a certain temperature (e.g., 400 K), or the intrinsic temperature-dependent resistivity.[48] If the charged impurity scattering is reduced, room-temperature mobility, limited by the extrinsic scattering due to SiO_2 phonons, could be significantly improved. With optimal fabrication of the SiO_2 substrates, which is still a challenge at this stage, the mobility of graphene under regular working conditions should be approaching the limit, and therefore, this in turn should enhance the application of graphene. Alternatively, it is possible to suspend the graphene sheet(s)[49−51] on top of SiO_2 either to avoid contact with the substrate[52] or to tune the tension of graphene.[53] Experimental results have demonstrated that the morphology of the substrate plays a crucial role in the extrinsic strain-induced disorder in graphene and its effect on transport properties.[54] In contrast, the high mobilities obtained for suspended graphene samples relative to nonsuspended samples are attributed to the absence of impurities caused by substrate effects.[2,55] The use of controlled substrate morphologies thus gives rise to a potential approach to controlling the impact of atomic-scale defects on the nanoscale transport properties of graphene. Nevertheless, in spite of the extrinsic scattering caused in graphene through the contact with SiO_2 substrates, modified SiO_2/Si substrates can provide decent charge carrier mobilities for graphene.[52] Also, it has been experimentally shown that graphene sheets exfoliated on SiO_2 still conduct heat rather efficiently, considerably better than common thin-film electronic materials.[56] Thus, SiO_2 holds an important position in producing functional devices where graphene needs to rest on Si with an insulating layer. Hence, it is briefly discussed here even though conventionally SiO_2 is not categorized as a semiconductor.

2.3. Silicon Carbide (SiC) and Graphene

SiC demonstrates many technical advantages as an excellent member of the group IV semiconductors. Among its various crystalline forms, the hexagonal 4H- and 6H-SiC polytypes have wide energy band gaps of 3.3 and 3.0 eV, respectively.[57]

DOI: 10.1021/cr400607y
Chem. Rev. 2015, 115, 8294−8343

However, although it was shown already in the 1970s[58] that an ultrathin graphitic film (similar to few-layer graphene) could grow on SiC, production of single-layer graphene on 4H-SiC[59] and 6H-SiC[60] has only been reported recently. Clearly, progress was limited by the fact that, as mentioned earlier, single-layer graphene sheets were only officially discovered in 2004. However, one thing that is worth mentioning here is that graphene grown on SiC shows epitaxial characteristics, and these are quite different from those of mechanically exfoliated graphene. The basic mechanism for growing epitaxial graphene on SiC is simply to heat the substrate (in vacuum or an inert atmosphere) to temperatures typically in the 1200−1800 °C range.[57] Under these circumstances, Si atoms desorb from the surface (shown along the arrows in Figure 4a), and the remaining C atoms rearrange to form graphene sheets. Basically, the epitaxial graphene is grown on either the 0001 (Si-terminated) or 000$\bar{1}$ (C-terminated) faces of 4H- and 6H-SiC when crystals are heated in ultrahigh vacuum (UHV). It is even possible to grow graphene under moderate vacuum conditions using an oven with a controlled background gas.[61]

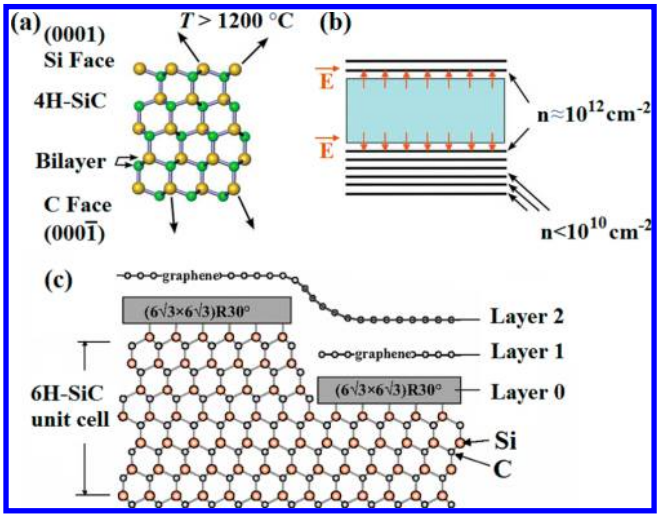

Figure 4. Schematic structure of SiC and growth of epitaxial graphene. (a) 4H-SiC. Yellow and green spheres represent Si and C atoms, respectively. At elevated temperatures, Si atoms evaporate (arrows), leaving a C-rich surface that forms graphene sheets. (b) At a typical growth temperature, few graphene layers are formed on the Si-terminated face (top), with substantially more on the C-terminated face (bottom). (c) Epitaxial graphene (EG) on 6H-SiC (0001) (Si-terminated face): layer 0, carbon-rich buffer; layer 1, first layer with essentially a graphene electronic structure; layer 2, second graphene layer. Images a and b reprinted with permission from ref 57. Copyright 2010 Cambridge University Press. Image c reprinted with permission from ref 62. Copyright 2008 American Physical Society.

It is, however, necessary to be aware that the growth of graphene films on Si-terminated surfaces is fairly different from that on C-terminated surfaces. For a given temperature, as is frequently applicable under UHV, the graphene films grow faster on C surfaces than on Si surfaces.[57] Figure 4b shows that, at a typical growth temperature, very few graphene layers are formed on the Si-face, while many more are formed on the C-face. On one hand, for thin layers, the graphene thickness can be estimated by calculating the ratio of the measured Auger electron intensities of the Si (at 92 eV) and C (at 271 eV) peaks,[12,61] respectively, on the basis of the Auger electron spectroscopy (AES) analysis of energetic electrons emitted from the excited atoms by an impinging electron beam (3 keV incident energy).[63] On the other hand, the thickness of multilayered graphene films can be measured via conventional ellipsometry.[61,64] In any case, scanning tunneling microscopy (STM) is frequently used to display the characteristic graphene images, and surface X-ray reflectivity and low-energy electron diffraction are the processes of choice for probing rotation or distortion of domains, if required.[57] Figure 4c shows a structure of EG/SiC after growth on 6H-SiC (0001) containing a step. The feature that graphene growth fits both the Si-terminated and C-terminated surfaces of SiC indicates that the graphene layer close to the SiC interface is electron-doped typically at a capacity of 10^{12} cm^2 V^{-1} s^{-1} due to the electric field E at the interfaces.[57] Furthermore, the overlayers approach charge neutrality quickly and turn out to be essentially undoped. This is attributed to the fact that the charge density decay length (the charge screening length) is assumed to be approximately the distance of the layer of graphite[62] or one graphene layer.[65] It has been shown experimentally that the growth of graphene on Si-faces is slow and terminates after a relatively short time at high temperatures.[61] However, growth on C-faces can cause thick layers to form (from ∼5 up to 100 layers). Also, the interaction between the first C plane and the SiC surface is comparatively much weaker on C-faces than on the Si-faces of the substrate.[66] This is an important contributing factor to the relatively free rotation of large graphene sheets with respect to each other, during the graphitization, and the lock-in, on average, to preferred orientations on the C-faces of SiC substrates.[61] Therefore, it is worth noting that epitaxial graphene grown on a substrate shows characteristics different from those of exfoliated graphene deposited onto a substrate. The mechanically exfoliated graphene has to be one layer only to keep its form and shape, while epitaxial graphene is more complex and generally shows a multilayered structure, especially on the C-face. Furthermore, it is essential to realize that epitaxial graphene is not simply ultrathin graphite, although it consists of stacked graphene sheets, because only the first layer of graphene at the interface is highly charged and the succeeding layers show rather lower charges.

Also, since mechanically exfoliated graphene flakes lack precise and scalable control over the structures, which is most undesirable in electronic devices, epitaxial growth of graphene on substrates has attracted increasing attention.[67] Following the pioneering work of Forbeaux et al. in demonstrating that millimeter-sized bulklike single-crystalline graphite could be formed as epitaxial thin films on a 6H-SiC (0001) wafer by thermal annealing in a vacuum,[68] Berger et al. produced ultrathin epitaxial graphite films.[12] These were typically composed of three graphene sheets, made through thermal decomposition on the Si-terminated surface of 6H-SiC. Transport measurements were performed at a temperature of 4 K on the "few-layer graphene" samples obtained, and the results suggested that the quantum Hall effect could be observed at lower temperatures, at higher fields, or in ultrathin graphite films of only slightly higher mobility. Thus, the practical feasibility of electronic device applications based on nanopatterned epitaxial graphene has been demonstrated, and hence has boosted the development of research in the field.

Recently, research has been directed at tackling the challenge of the scalable integration of graphene into a practical circuit. Lin et al. fabricated field-effect transistors (FETs) on a 2 in. graphene wafer, as shown in Figure 5a.[69] The wafer was epitaxially formed on the Si-face of 4H-SiC (0001) in a UHV

DOI: 10.1021/cr400607y
Chem. Rev. 2015, 115, 8294−8343

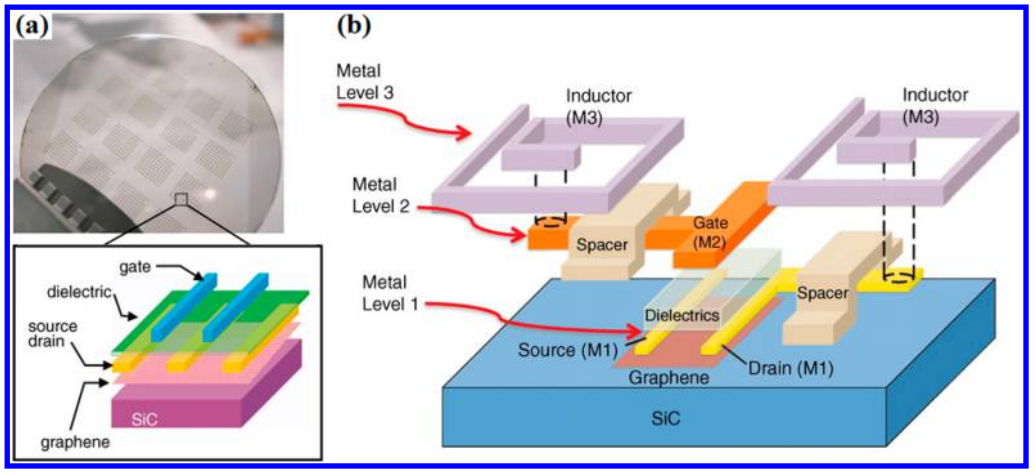

Figure 5. (a) Image of devices fabricated on a 2 in. graphene wafer and schematic cross-sectional view of a top-gated graphene FET. (b) Schematic illustration of a graphene mixer circuit. The critical design aspects include a top-gated graphene transistor and two inductors connected to the gate and the drain of the graphene FET. Image a reprinted with permission from ref 69. Copyright 2010 American Association for the Advancement of Science (AAAS). Image b reprinted with permission from ref 70. Copyright 2011 AAAS.

chamber through thermal annealing at 1450 °C. The graphene grown exhibited an electron carrier density of ~3×10^{12} cm^{-2}, and the Hall-effect mobility was between 1000 and 1500 cm^2 V^{-1} s^{-1}, which enabled the transistors to be operated at high frequencies, up to 100 GHz. They further developed wafer-scalable processes to fabricate arrays of graphene analogue circuits which individually consisted of one graphene transistor and two inductors and were compactly integrated onto single SiC substrates.[70] This is schematically shown in Figure 5b. The integrated circuit was verified as capable of operating as a broad-band radio frequency mixer at frequencies up to 10 GHz. It exhibited remarkable thermal stability with little reduction in performance (less than 1 dB) between 300 and 400 K. Such integration techniques are expected to develop further to bridge the technological gap between a single device and a practical graphene circuit on a wafer scale. In addition, the integration process of graphene devices mentioned above was shown to be possibly applicable to CVD graphene. This would of course, if successful, extend the possibility of producing high-quality uniform graphene layers on large SiC or some other semi-insulating substrates. The CVD growth of epitaxial graphene on SiC is achievable with a certain thickness and direction. This avoids the disadvantage of the growth on metals caused by the limitation that electronic applications require graphene to rest on an insulating substrate. As for the sublimed graphene, the atomic step edges of SiC substrates[71] as well as the defects present on the SiC surface, where Si sublimation starts, especially at dislocations, are most likely to get the graphene pinned to the SiC surface at many randomly distributed points.[72] The edges prohibit the formation of a homogeneous graphene monolayer and its larger extension, although graphene layers can still be continuous.[73] In the case of the CVD process, the nucleation sites of graphene layers seem to be connected with atomic steps on the SiC surfaces, thus enabling "step-flow" epitaxy.[72] Provided that the thermal treatment of the substrate prior to the growth is sufficient, this could open up another possible approach to the production of decent-quality epitaxial graphene on semi-insulating SiC for device applications.

3. GROUP II–VI SEMICONDUCTORS AND GRAPHENE

It is generally accepted that the relationships between the band gap energy and the size of semiconductor particles (quantum dots) show that any decrease in particle size results in an increase of the band gap due to quantum confinement.[74,75] This is also true for many group II–VI semiconductors, such as ZnS and CdS; the result is a shift of the absorption threshold when the size of the quantum dots (QDs) is adjusted.[76] Thus, the unique optical and electronic properties arising from such a quantum confinement of electrons make the group II–VI semiconductors potentially useful for a range of applications. Commonly adopted group II–VI semiconductors such as ZnO and ZnS exhibit relatively wide band gaps. When they are combined, either respectively or collectively, with graphene, whose potential applications, despite excellent electrical and optical characteristics, are restricted because of its zero gap,[14−16] the hybrid nanostructures formed should offer more adaptable functions with improved performance compared to the individual materials.

3.1. Zinc Oxide (ZnO) and Graphene

ZnO is a wide band gap (3.2–3.4 eV) semiconductor that possesses an energy-band structure and physical properties similar to those of TiO_2. It has, however, higher electronic mobilities, 205–300 cm^2 V^{-1} s^{-1} for bulk ZnO and 1000 cm^2 V^{-1} s^{-1} for single nanowires, which should prove favorable for electron transport.[77] It has been reported in a wide range of forms, nanowires, nanorods, and nanotubes, acting as a constituent in a range of functional nanodevices. An additional advantage is that ZnO can be fabricated in a transparent form,[78] and therefore is potentially useful for optoelectronics applications.[79,80] When ZnO is used in graphene composites, it creates an opportunity for an enhancement of the properties of both materials and hence their feasibility for use in various devices.

Kim et al. managed to grow nanoneedle and nanowall ZnO structures on few-layered graphene sheets.[81] These graphene sheets were mechanically exfoliated and then transferred onto SiO_2/Si substrates, using a metal–organic vapor-phase epitaxy (MOVPE) method without the need for a catalyst. The authors demonstrated that the aspect ratio and density of the nanostructures, which could be aligned either in rows or

DOI: 10.1021/cr400607y
Chem. Rev. 2015, 115, 8294–8343

vertically (presumably due to the enhanced nucleation at the graphene step edges), strongly depended on the growth temperature. Also, the optical qualities of the resulting ZnO nanostructures on the graphene layers were investigated using photoluminescence (PL) spectroscopy performed at 17−200 K. PL is the spontaneous emission of light, which is selective and extremely sensitive to discrete electronic states, from the sample under optical excitation.[82] The intensity of the PL signal provides information regarding the quality of the surfaces and interfaces. To ensure high PL intensity and spectral resolution, PL measurements are generally performed at relatively low temperatures as the fraction of radiative recombination of excitons is considerably higher than that of the nonradiative recombination of excitons. When it comes down to high-quality ZnO nanorods, in a typical PL spectrum, sharp peaks in the vicinity of band edges at 3.359−3.376 eV have been observed.[83] It was, therefore, suggested that high-quality ZnO nanostructures were able to be grown on graphene layers.[81] This conclusion was reached as a result of spectral analyses (as mentioned above and in Kim et al.'s work[81]) of the observed free exciton PL peak at 3.376 eV in the spectra of the ZnO nanostructures grown on the graphene layers. Meanwhile, no C-related defect peak occurring at 3.356 eV due to the C−O cluster (acceptor) exciton emission[84,85] was observed. Accordingly, as in the case of the grouping of 2-dimensional graphene and 1-dimensional ZnO, the compatibility of growing ZnO on graphene layers has been greatly exploited to construct well-aligned 3-dimensional nanostructures. Such structures impart a substantial contribution toward integrating multifunctional attributes into a relevant device.

Indeed, the 1-dimensional materials for their part provide a significant enhancement in mechanical flexibility and optical transparency, while their single-crystalline structures hold promise for high-performance devices. In addition, it has been observed that 2-dimensional graphene thin layers also show optical transparency.[87,88] Therefore, when judiciously assembled, the hybrid structures are likely to simultaneously exhibit outstanding electrical conductivity, optical transparency, and mechanical flexibility. This has been demonstrated through the research work of Lee et al.[86] They formed regular arrays of ZnO nanorods on few-layered graphene films, as schematically shown in Figure 6. The key steps in the overall fabrication process included the synthesis of graphene, grown using CVD methods on Ni-coated SiO_2/Si substrates, then transfer of the graphene onto new substrates, and finally low-temperature (within 80−180 °C) selective growth of ZnO nanorods on the graphene. The growth was performed using two approaches: using holes in the graphene as a growth mask and using seed patterns on the graphene. Poly(methyl methacrylate) (PMMA) layers were coated on top of graphene to minimize the mechanical fracture during the transfer. Afterward, it was removed through dissolution or etching. Using similar synthetic conditions, it is possible that graphene can be used as the transparent flexible electrode in hybrid ZnO−graphene structures. Such 1-dimensional ZnO nanostructures can be configured as transparent and flexible to perform as the functional components in optoelectronic devices. If they are constructed in tubular structure form, then these 1-dimenional ZnO nanostructures, due to the larger specific surface area and higher porosity, are expected to offer higher performance, relative to ZnO nanorods, in PL and relevant applications such as solar cells and sensors. Recently, Xu et al. electrodeposited single-crystal ZnO nanotube arrays directly onto a single-layer

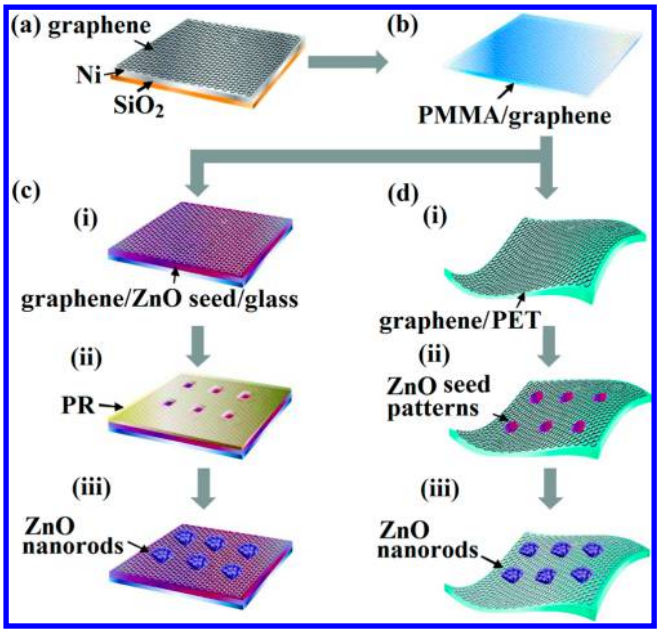

Figure 6. Schematic representation of the fabrication process used to obtain the hybrid architectures of ZnO nanorods and graphene. (a) CVD synthesis of graphene. (b) Free-standing PMMA/graphene by selective etching of the underlying SiO_2 and Ni layers. (c) Growth of a ZnO nanorod array using holes in graphene as a growth mask involves the following: (i) graphene transfer to a glass substrate coated with a textured ZnO seeding layer, (ii) patterning a regular array of holes in graphene by photography and dry etching, and (iii) selective growth of ZnO nanorods via the holes in the photoresist/graphene growth mask. (d) Growth of a ZnO nanorod array using seed patterns on graphene involves the following: (i) graphene transfer to a plastic substrate, (ii) defining an array of ZnO seed patterns, and (iii) selective growth of ZnO nanorods. Reprinted from ref 86. Copyright 2009 American Chemical Society.

graphene electrode.[89] The latter was grown on a Cu foil through CVD and subsequently transferred to a glass slide by virtue of a PMMA coating. The transmittance of the nanotubes thus obtained on the graphene/glass electrode was above 75% over the entire visible range.

Since, as discussed above, planar graphene is capable of remaining transparent at room temperature, and maintaining high carrier mobility approaching 15 000 $cm^2 V^{-1} s^{-1}$,[91,92] it is a potential built-in "window electrode" for optoelectronic devices.[93] In light of the high mechanical elasticity of graphene (corresponding to a Young's modulus, E, of around 1.0 TPa for the bulk graphite, assuming an effective graphene thickness of 0.335 nm),[4] it is possible to realize rollable transparent piezoelectric energy-harvesting devices using CVD-grown graphene as the transparent electrodes on flexible polymer substrates.[90] This is shown in Figure 7 where the ZnO nanorods on the transferred graphene were synthesized at a relatively low temperature of 95 °C using the aqueous solution method. Given the smooth surface morphology and the atomic structure of graphene, vertical growth of well-aligned 1-dimensional ZnO nanorods was initiated. Following similar strategies, PDMS too can be used to prepare mechanically flexible, electroconductive, and optically transparent substrates that are suitable for graphene to grow vertical ZnO nanowires.[78] In this case, graphene was produced through the chemical exfoliation of natural graphite, namely, the modified Hummers method, which includes sonication, subsequent

DOI: 10.1021/cr400607y
Chem. Rev. 2015, 115, 8294−8343

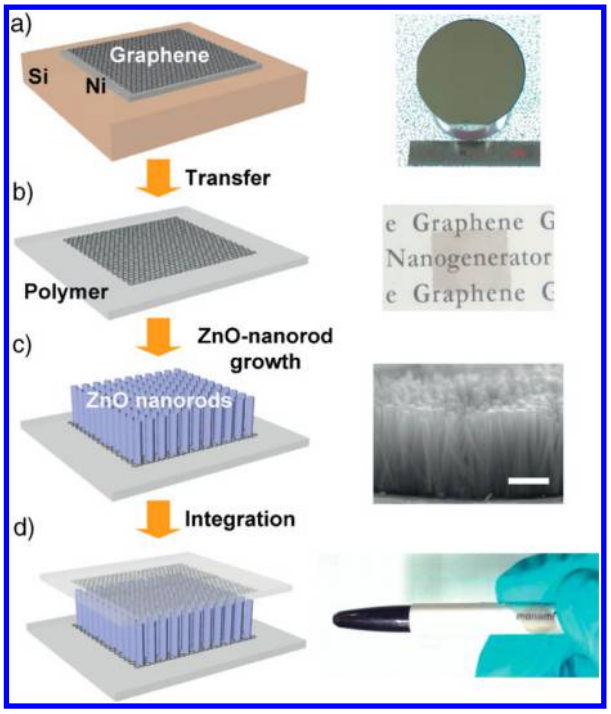

Figure 7. Graphene-based rollable transparent nanostructure. (a) Graphene sheet prepared through CVD on a 4 ft Ni-coated SiO_2/Si wafer. (b) Transparent graphene sheet transferred to a flexible polymer substrate. (c) ZnO nanorods on the transferred graphene sheet. (d) Integrated rollable graphene-based nanostructure. Reprinted with permission from ref 90. Copyright 2010 John Wiley and Sons.

dialysis, and reduction.[94,95] Generally, depositing 1-dimensional ZnO nanostructures on 2-dimensional graphene exhibits reasonable temperature compatibility and mechanical flexibility.[96] The integration of vertical ZnO nanorods/nanowires/nanotubes and graphene is advantageous in overcoming the limitation of hard flat substrates for the purpose of making flexible multifunctional devices.

Nevertheless, while it is viable to fabricate functional components of ZnO on graphene layers, it is extremely important that the dimensions, distributions, and morphologies of the nanostructures, which preferably should be directly grown on the substrates without degrading the electrical properties of graphene, be controlled. In fact, when the ZnO nanostructures are fabricated through hydrothermal methods on few-layered graphene, whether the resulting forms are nanorods, nanodisks, nanoflowers, or others clearly depends on the growth temperature, molar concentration, and pH of the nutrient solution.[97] Particularly, for 3-dimensional heterogeneous nanostructures, the morphology of ZnO on the graphene layers fabricated via CVD has been shown to be highly dependent on the growth temperature.[98] However, it is still possible, to some extent, to orient low-dimensional ZnO nanostructures on graphene-related materials with the assistance of catalysts. For example, Au catalysts, acting as nucleation sites, have been used to assist the alignment of vertical ZnO nanostructures, from pure nanowires to pure nanowalls.[99] These were directly grown on graphene, while the length of the ZnO structures was found to increase with the growth time. Once the low-dimensional nanostructure on 2-dimensional graphene is well controlled, it can serve as a template for diverse applications in optoelectronics, electronics, and photovoltaics. Specifically, precise control of the position of the individual ZnO nanostructures on graphene is a great advantage for flexible transparent display applications. Randomly formed ZnO nanostructures on graphene are avoided to a large extent by controlling the nucleation sites. This clearly offers a practical manipulation of the individual nanostructure. It has been experimentally demonstrated that 1-dimensional ZnO nanostructures can be selectively grown on mechanically exfoliated graphene (on Si substrates with SiO_2 layers of 300 nm on the top).[100] This is achieved by using conventional e-beam lithography and metal−organic vapor-phase epitaxy (MOVPE). Here the preferred ZnO nucleation sites are found at the step edges of the graphene because of their locally higher chemical reactivity.

Also, as previously indicated, single-layer graphene films show fairly good field emission properties, with a large field-enhancement factor of ~3700, a low turn-on field, E_{to}, of 2.3 V μm^{-1} at 10 $\mu A\ cm^{-2}$, and a low threshold field, E_{thr}, of 5.2 V μm^{-1} at 10 mA cm^{-2}.[102] These results are based on randomly oriented graphene sheets with a lot of sharp edges almost normal to the substrate because of the stiffness. Since a large amount of emission sites are needed for enhanced emission to switch on at low field values,[103] it is believed that these edges of single-layer graphene act as active emission sites.[22] More recently, Pandey et al. reported a dramatic increase in the maximum current density of morphologically disordered graphene with respect to planar graphene by a factor of 500.[23] The turn-on electrical field, on the other hand, remained similar (2.26 V μm^{-1}) to that of the single-layer graphene mentioned above. The incorporation of morphological disorder in graphene was found to involve additional edges and defects, which in turn created more emission sites. However, the randomly distributed graphene sheets or edges on the substrates are not extremely desired in those devices or systems demanding a series of stable performances in field emission properties. ZnO-based nanostructures with high surface to volume ratios, such as ZnO nanowires, are also considered credible candidates for field emission applications because of their chemical stability, as well as their oxidation resistance. This is especially true when they are well aligned on the substrates.[104,105] Now that graphene is a promising material for field emission applications because of its low aspect ratio, chemical stability, and excellent electrical conductivity, the ZnO nanowires or nanorods after incorporation can further magnify the high electric enhancement of graphene sheets, and act as additional emission sites.[106] In fact, the turn-on field for heterogeneous nanostructures in a previously mentioned work reported by Kim et al. is as low as 2.0 V μm^{-1} (at 10 $\mu A\ cm^{-2}$).[78] This is due to the decent mechanical and electrical contact between the vertical ZnO nanowires and the graphene film. Another type of investigation into the field emission properties of these heterogeneous nanostructures is related to the growth of graphene on ZnO. Zheng et al. directly grew graphene sheets (GSs) with "pyramid-like" morphologies, using plasma-enhanced chemical vapor deposition (PECVD), on ZnO nanowires coated with Ni catalyst nanoparticles with the view to overcoming the limit of planar morphological features on field enhancement.[101] This is shown in Figure 8. The GSs with small radii and high densities were attributed to the additional emission sites, which led to the enhanced local field on the ZnO nanowire surfaces. The ZnO−GS structure was observed to have a turn-on field of 1.3 V μm^{-1}, substantially lower than that (2.5 V μm^{-1}) of the reference pure ZnO, for extracting the current density of 1 $\mu A\ cm^{-2}$. Also, it had a

DOI: 10.1021/cr400607y
Chem. Rev. 2015, 115, 8294−8343

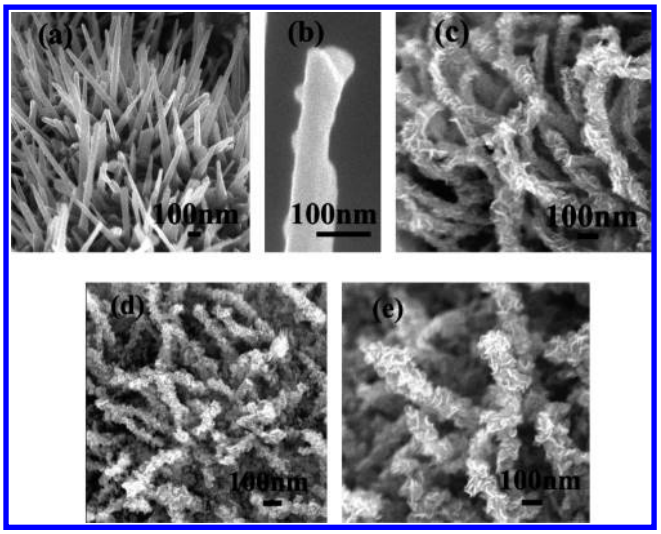

Figure 8. (a) SEM image of as-grown ZnO nanowires. (b) SEM image of ZnO nanowires coated for 5 s with Ni. (c–e) SEM images of ZnO–GSs grown for 2 min (c), 5 min (d), and 10 min (e) after 3 s of coating. Reprinted from ref 101. Copyright 2009 American Chemical Society.

threshold field of 5.7 V μm^{-1} for producing a current density of 1 mA cm^{-2}, while pure ZnO nanowires needed a threshold field of 7 V μm^{-1} for producing a much smaller current density (less than 0.4 mA cm^{-2}). This implies that the hybrid material of GSs on ZnO nanowires is a potential candidate for field emission devices.

Further to these heterogeneous nanostructures consisting of graphene on top of ZnO, they can also be used to adjust the band gap of graphene. It has been demonstrated that graphene nanomesh, comprising single- or few-layered graphene punched with a high-density array of nanoscaled holes, can gain enough band gap for a sufficient gate response and on/off ratio in a large sheet of graphene to create a semiconductor thin film.[108] One possible way to fabricate graphene nanomesh is to use ZnO as the metal oxide semiconductor photocatalyst because of its photocatalytic activity toward carbonaceous materials.[109] Akhavan investigated the local photodegradation of GO sheets at the tip of ZnO nanorods to produce the semiconducting graphene nanomesh.[110] Their work involved physically attaching ZnO nanorod arrays with diameters of 140 nm and lengths of <1 μm, which had been hydrothermally grown and then vertically aligned, onto chemically exfoliated GO sheets (~0.9 nm thick) to cause pores for graphene nanomesh through a photodegradation process. The graphene nanomesh thus obtained was afterward reduced by hydrazine and, without any doping, presented p-type semiconducting behavior, and demonstrated an energy gap of ~1.2 eV between the valence band and the Fermi level. When the nanomesh is, however, made of ZnO, rather than graphene, the performances of the heterogeneous structures as semiconductors could also be expected to be enhanced. It was noticed that back-gated field-effect transistors formed by using periodic ZnO nanomesh on single-layer graphene exhibited tunable electronic properties.[111] They featured both n- and p-type characteristics as a result of controlling the thickness of the ZnO nanomesh layer. This indicates that single-layer graphene is sensitive to the surrounding environment and its electronic properties can be significantly changed by tuning the interface and surface effects.

Even for graphene QDs, their properties can vary widely according to the synthesis process. Since the graphene QDs' band gap depends on the size and shape of the sp^2 domains, it is possible, therefore, to align the band gap of the composite of ZnO nanowires infiltrated with graphene QDs.[112] While the infiltrating contact mode and the high surface area to volume ratio of graphene QDs collectively increase the contact between graphene and ZnO, the properties of the heterogeneous structures can also be modulated through small-area contact. Kim et al. investigated the characteristics of semiconducting ZnO nanowires grown directly onto a metallic multilayer graphene film (~20 layers, 6–6.5 nm), which was fabricated using CVD with Ni catalysts and transferred onto the Si wafer (with a SiO_2 layer).[113] The ZnO nanowires were horizontal and singly grown from high-surface-energy points on the graphene surfaces. They connected the graphene sheets which were employed as the catalyst for the nanowire growth and the Al electrodes. It turned out that the nanoscale contact of the semiconducting ZnO nanowire with the multilayer graphene exhibited near-ohmic conductance with low contact resistances. Similarly, the combination of single horizontal ZnO nanowires and graphene sheets potentially improves the performance of UV photodetectors. Fu et al. fabricated a "sandwich" structure of graphene/ZnO nanowire/graphene for use in UV photodetectors.[107] This is schematically represented in Figure 9.

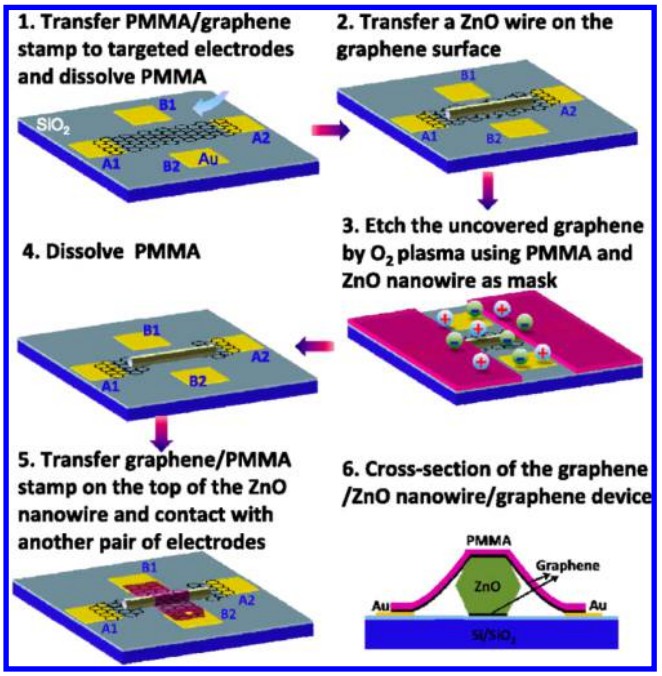

Figure 9. Schematic diagrams of the fabrication processes for the graphene/ZnO nanowire/graphene vertical sandwich device (1–5) and the cross-section of the UV detector based on the graphene/ZnO nanowire/graphene sandwich structure (6). Reprinted with permission from ref 107. Copyright 2012 AIP Publishing LLC.

Schottky contacts were formed at the interfaces between the ZnO nanowire and the top and bottom graphene layers in the sandwich structure. This gave rise to the corresponding photocurrent generation and recovery process upon UV illumination of the device: electron–hole pairs are generated [$h\nu \rightarrow e^{-1} + h^{+}$] and separated quickly by the local electric field at the Schottky barrier region, reducing the electron–hole recombination rates and increasing the carrier lifetime. This,

DOI: 10.1021/cr400607y
Chem. Rev. 2015, 115, 8294–8343

meanwhile, contributed to the increase in the free carrier density. The increased carrier density lifted the Fermi energy and thus reduced the work function of ZnO, resulting in the reduction of the Schottky barrier height and width between ZnO and graphene.[107] These cooperative effects are invoked to account for the improved photoresponsivity in the as-prepared sandwich structure relative to traditional ZnO nanowires.[114] The photocurrent rising time is found to be shorter than 0.7 s in air, the recovery speed about 0.5 s, and the photocurrent on/off ratio of the UV detector up to 8×10^2 under a bias of 3 V. Clearly, the combination of graphene sheets and horizontal ZnO nanowires, apart from the previously mentioned vertical ones, provides an alternative pathway to fabricating heterogeneous nanostructures for integrated optoelectronic devices.

ZnO has also been frequently presented in the form of particles with confined sizes which demonstrate unique physical properties.[117,118] The anchoring of ZnO nanoparticles onto graphene sheets is another effective strategy for the construction of heterogeneous nanostructures. Actually, apart from enhancing field emission factors (with low turn-on and threshold fields),[119] ZnO nanoparticle-decorated graphene provides even more unique characteristics. In Williams and Kamat's quest to explore the interaction between GO and ZnO nanoparticles, they probed the ZnO emission to monitor the electron transfer between semiconductor nanoparticles and the GO sheets.[115] This is shown schematically in Figure 10a. The GO sheets prepared using the Hummers method were suspended in ethanol to interact with the excited ZnO nanoparticles under UV irradiation and subsequently underwent photocatalytic reduction. A mechanism has been suggested by the authors to explain the electron transfer from the excited ZnO nanoparticles to the GO sheets that leads to the production of chemically reduced graphene oxide (RGO). It follows the mechanism previously proposed for ZnO nanoparticles transferring photogenerated electrons to CNTs,[120] which is a valid approach since graphene sheets are analogous to unrolled 2-dimensional CNTs. The mechanism is shown below:

$$\mathrm{ZnO} + h\nu \rightarrow \mathrm{ZnO(h + e)} \xrightarrow{\mathrm{C_2H_5OH}} \mathrm{ZnO(e)} + {}^{\bullet}\mathrm{C_2H_4OH} + \mathrm{H^+} \quad (1)$$

$$\mathrm{ZnO(e)} + \mathrm{GO} \rightarrow \mathrm{ZnO} + \mathrm{RGO} \quad (2)$$

where $h\nu$ stands for the energy of the photon. Under this type of electron transfer mechanism, semiconductor nanoparticles anchored onto a graphene scaffold make it possible to prevent charge recombination, and thus to improve the photoinduced charge separation.[121] Further studies have shown that ZnO nanoparticles on the surface of the RGO sheets also exhibit enhanced photocurrent and photocatalytic performances under UV illumination.[116,122,123] This is attributed to the suppression of recombination of the charge carriers because of the interaction between ZnO and RGO. In addition, the ZnO nanoparticles effectively decorated onto the graphene prevent the sheets from forming agglomerated structures that would cause a dramatic decrease in the specific surface area of the graphene.[124,125] The charge transfer, enhanced photocurrent, and photocatalytic activity by RGO–ZnO composites are summarized in Figure 10b. The figure shows that the photogenerated electron–hole pairs of UV-excited ZnO separate at the interfaces of the ZnO and RGO. The electrons transport along the RGO sheets with high electrical conductivity from the inner region to the external circuit and thus produce the photocurrent. When the density and morphology of the ZnO nanoparticles (or QDs) change, different activities will be triggered.[126] The ZnO QDs which are seeded to grow nanorods on the highly conductive graphene will thus provide a platform to fabricate the visible-blind UV sensors.[127] Alternatively, when exposed to a reducing gas, such as formaldehyde, the coadsorption and mutual interaction between the gas and the adsorbed oxygen (by ZnO) result in oxidation at the surface.[128,129] During this, the released electrons from the gas transfer to the ZnO nanoparticles (or QDs) and further onto the graphene substrate, and this changes the conductivity of the composite. To increase the contact between the graphene and the ZnO of the heterogeneous structure to a higher level, it is even possible to wrap the ZnO QDs with graphene sheets. Son et al. synthesized emissive quasi-core–shell QDs consisting of ZnO cores wrapped in the shells of single-layer graphene.[16] This is graphically summarized in Figure 11. They reported that the strain introduced by the curvature, resulting from the bending of the graphene surrounding the ZnO QDs, opened an electronic band gap of 250 meV in the graphene, and more importantly, the wavelength of excitonic emission of the ZnO QDs could be modulated with the graphene in the form of a consolidated core–shell structure.

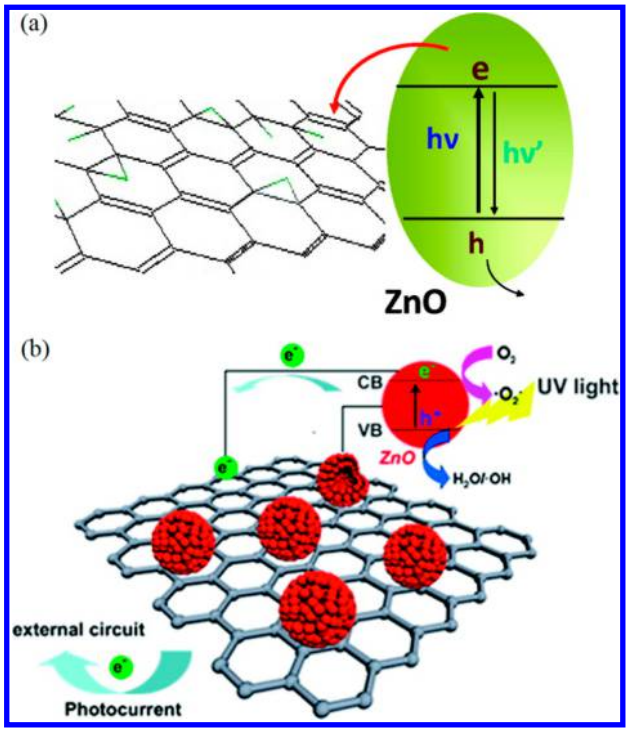

Figure 10. (a) Excited-state interaction between ZnO and graphene oxide (GO). (b) Schematic illustration of enhanced photocurrent density and photocatalytic activity for RGO–ZnO composites. Image a reprinted from ref 115. Copyright 2009 American Chemical Society. Image b reprinted from ref 116. Copyright 2012 American Chemical Society.

From the hitherto discussed heterogeneous nanostructures of graphene and ZnO, it is worth noting that the 2-dimensional nanosheets have been mostly combined with either the 0-dimensional nanoparticles or 1-dimensional nanowires (or nanorods) to enhance the optoelectronic properties. Considering the effects and improvements discussed above, it would

DOI: 10.1021/cr400607y
Chem. Rev. 2015, 115, 8294–8343

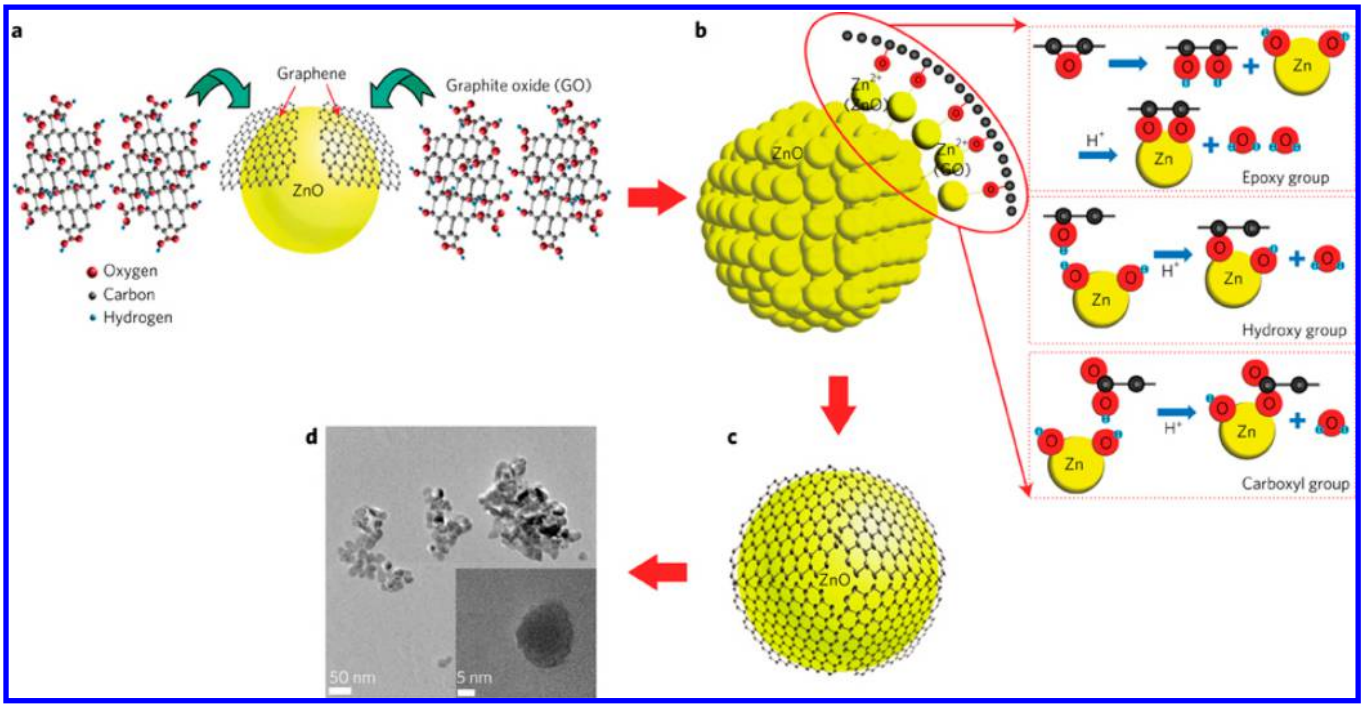

Figure 11. Chemical synthesis process for the ZnO−graphene quasi-QDs. (a) Schematic of chemical exfoliation of graphene sheets from GO. (b) Synthesis of ZnO−graphene QDs from GO and zinc acetate dihydrate. The QDs are synthesized via chemical reaction between three kinds of functional groups (carboxyl (−COOH), hydroxy (−OH), and epoxy (−O−)) of GO and Zn^{2+}. The magnified image shows chemical bonding between the functional groups and Zn^{2+}. (c) Schematic of graphene-covered ZnO QDs. (d) TEM image corresponding to (c). Inset in (d): enlarged HRTEM image of a ZnO−graphene QD. Reprinted with permission from ref 16. Copyright 2012 Macmillan Publishers Ltd.

be interesting to see the added enhancement, if any, created by combining all three types of nanostructures. In Yoo et al.'s work, using a solution-based process, a multidimensionally heterogeneous material consisting of 0-dimensional Ag nanoparticles, 1-dimensional ZnO nanorods, and 2-dimensional graphene sheets was constructed.[130] ZnO nanorods were grown using a hydrothermal method on chemically converted graphene, which had been prepared via a modified Hummers method, and then Ag nanoparticles were sprayed onto the ZnO−graphene composite. It was established that, for the heterostructured sample, the photoinduced electron transfer was doubled by the transfer of electrons from ZnO to Ag, and to graphene, which would then further transfer the electrons to Ag. Hence, it was argued that the recombination of photoinduced electrons and holes of the heterogeneous nanostructure was even suppressed, resulting in enhanced photocatalytic activity.

3.2. Zinc Sulfide (ZnS) and Graphene

ZnS is known as one of the earliest studied semiconductors.[131] Its structure and properties are comparable to those of the more popular and widely used ZnO, yet there are certain properties pertaining to ZnS that are quite unique and advantageous relative to those pertaining to ZnO. For example, ZnS has larger band gaps of 3.72 and 3.77 eV (for the cubic zinc blende and the hexagonal wurtzite ZnS, respectively) than ZnO.[132] It is, therefore, more suitable for visible-blind UV-light-based devices such as photodetectors and sensors. On the other hand, although low-dimensional ZnS nanostructures with various morphologies and shapes have been successfully synthesized via a variety of techniques, systematic studies on ZnS nanostructure arrays have only been initiated over recent years.[133] The progress on ZnS nanostructures has provided a great platform for researchers to exploit their novel properties and potential applications. Indeed, efforts have already been made to investigate ZnS−graphene nanocomposites.

Similar to ZnO, ZnS shows good photocatalytic properties as a result of the rapid generation of electron−hole pairs by photoexcitation and the highly negative reduction potentials of the excited electrons.[134,135] It is hence reasonable to expect that graphene materials decorated with ZnS should give rise to enhanced properties, such as high catalytic activity. In fact, since the properties of ZnS have much in common with those of ZnO, it is not surprising that ZnS nanomaterials show a close resemblance to ZnO in the way they are practically connected to graphene. Using microwave irradiation, Hu et al. prepared composites of ZnS nanoparticles supported on graphene nanosheets in an aqueous medium.[136] They performed PL measurements at room temperature, which were quenched at the low-intensity surface-defect-related emission. On the occasion that light of sufficient energy is incident on a material, photons are absorbed and electronic excitations are created.[82] These excitations eventually relax, and the electrons return to the ground state (i.e., recombination). The emitted light is PL if radiative relaxation occurs. When the holes are scavenged to make the recombination (return of the relaxed electrons) less efficient in the illuminated semiconductor, quenching of the emission will just continue.[137] In addition, emission quenching has been observed for semiconductor nanostructures anchored onto CNTs, where the structural elements are the same as those of graphene.[120] The results showed enhanced decay rates of emission with increased concentration of CNTs, meaning more semiconductors interacted with the CNTs. The charge transfer interaction was deemed to occur between the semiconductor nanostructures in their excited state and the CNTs. Hence, it was deduced by Hu et al. that, from the

DOI: 10.1021/cr400607y
Chem. Rev. 2015, 115, 8294−8343

obvious quenching observed through fluorescence absorption spectroscopy, there was photoinduced electron transfer between the ZnS nanoparticles and the graphene nanosheets.[136] Furthermore, the nanocomposites of graphene nanosheets and ZnS nanoparticles were observed to be highly photocatalytic, showing greater activity toward the photodegradation of methylene blue than the free ZnS nanoparticles synthesized in the absence of graphene (otherwise synthesized under the same experimental conditions). In photoinduced catalysis, the higher the photocatalytic activity, the more electron−hole pairs the catalyst generates. As the positive holes react with the moisture present in the close vicinity, free radicals, such as hydroxyl radicals ($^{\bullet}OH$), are produced. The hydroxyl radicals are highly reactive as an efficient oxidizing agent, able to undergo secondary reactions after the generation of electron−hole pairs. Some organic compounds can thus be photodegraded in the oxidation process caused by the hydroxyl radicals through the removal of a hydrogen atom, forming water and an alkyl radical.[138] As a result of the improved photocatalysis, it was suggested that the graphene nanosheets, with great charge mobility, acted as 2-dimensional catalyst supports for the corresponding structures (fabricated by Hu et al.) to improve the interfacial electron transfer and restrain the electron−hole pair recombination of the ZnS.[136]

It is also worth noting that quenching of the low-intensity surface-defect-related emission of ZnS−graphene nanocomposites synthesized using various methodologies has been observed. Wang et al. noticed that the PL emission of ZnS QDs was significantly quenched after the integration of ZnS with graphene through solvothermal synthesis.[139] Nethravathia et al. reported that low-intensity surface-defect-related emissions were completely quenched in ZnS−graphene nanocomposites which were produced during the reaction of a mixture of GO layers (made from graphite powder) and metal (zinc) ions with H_2S.[140] As a matter of fact, the quenching effect is demonstrable not only for ZnS−graphene composites, but also for ZnO−graphene composites, which have been previously discussed, as well as CdS−graphene composites, which will be discussed in the following section. A comparison of the quenching effects for different nanocomposites is shown in Table 1. It is clear that, with effective integration of group II−VI semiconductors (ZnO, ZnS, CdS, etc.) and graphene, the electron−hole pairs in excited semiconductor QDs can be efficiently separated through the injection of electrons from the QDs to graphene nanosheets. In terms of PL emissions, there are generally two aspects resulting from the excited semiconductors; namely, band edge emission and the low-intensity emission. This is reflected in the ZnO−graphene nanocomposites previously mentioned in ref 16. The band edge emission usually appears for the semiconductor nanoparticles, whereas the low-intensity emission arises from defects and oxygen vacancies. Depending on the actual structure of the graphene and inorganic semiconductors present and the nature of the connection between them in the hybrid material, either the low-intensity emission or the band edge emission can be investigated to monitor the interfacial electron transfer processes.

In addition, it can be seen from the data in Table 1 that, for a given type of semiconductor, the excitation wavelength decreases as the size of the low-dimensional nanomaterial decreases. This size-dependent property is related to the so-called quantum size or confinement effects which essentially arise from the presence of discrete, atomlike electronic

Table 1. Comparison of the Quenching Effects from Luminescence Measurements for Different Nanocomposites[a]

	synthesis process				band edge emission		low-intensity emission		
nanocomposite	semiconductor	RGO	shape of the semiconductor	excitation wavelength (nm)	quenched wavelength (nm)	extent of quenching (%)	quenched wavelength (nm)	extent of quenching (%)	ref
ZnO−GO	zinc acetate in ethanol	Hummers	nanoparticles (2−7 nm)	315	n.a.	n.a.	~530[b]	>95	115
ZnO−GO	zinc acetate dihydrate in DMF[c]	Hummers	nanoparticles (~10 nm)	350	~380	71	550	>95	16
ZnO−GO	$Zn(Ac)_2{\cdot}2H_2O$ with $LiOH{\cdot}H_2O$	Hummers	nanoparticles (3−5 nm)	340	n.a.	n.a.	BS: ~520[b] (~560)	>95	129
ZnO−GO	zinc acetate dihydrate in alcohol	Hummers	nanorods (100 nm long, 12 nm wide)	365	n.a.	n.a.	~580	~90	143
ZnO−GO	zinc acetate in ethylene glycol	Hummers	nanoparticles (~20 nm)	370	n.a.	n.a.	560−580	>95	121
ZnS−GO	$Zn(CH_3COO)_2$ with DMSO[d]	Hummers	nanoparticles (~10 nm)	280	BS: 327.5 (~361)	n.a.	over 480	>95 (peak)	144
ZnS−GO	$Zn(NO_3)_2$ with H_2S	Hummers	nanoparticles (~8 nm)	280	BS: 365.5 (389.5)	~90	~418, ~484, ~525	>95, >95, >95	140
ZnS−GO	$Zn(Ac)_2{\cdot}2H_2O$ with thioacetamide	Hummers	nanoparticles (3−42 nm)	280	BS: 366.8 (381.6)	30	~470	80 (peak)	136
CdS−GO	$Cd(NO_3)_2$ with H_2S	Hummers	nanoparticles (~10 nm)	355	~426	20	~530	90 (peak)	140
CdS−GO	cadmium acetate with thiourea	Hummers	nanoparticles (~4 nm)	365	n.a.	n.a.	~530	>95	139

[a]BS stands for blue-shifted. RGO stands for reduced graphene oxide (GO). Under the BS wavelengths, shown in the "quenched wavelength" columns (for both band edge emission and low-intensity emission), are the original emission peak wavelengths of the materials without graphene or its derivative. [b]As the concentration of GO is increased, the extent of PL quenching increases. [c]Dimethylformamide. [d]Dimethyl sulfoxide.

DOI: 10.1021/cr400607y
Chem. Rev. 2015, 115, 8294−8343

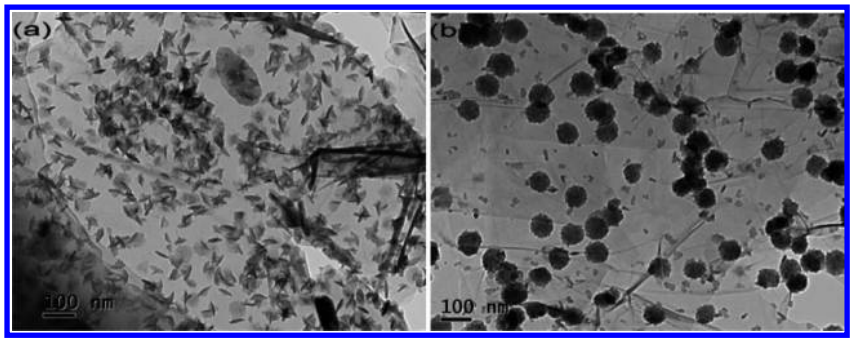

Figure 12. TEM images of ZnS−graphene nanosheets soaked at 180 °C for 12 h with 0.1 M Zn^{2+}: (a) homogeneous QFs on graphene; (b) agglomeration of QDs on graphene. Reprinted from ref 145. Copyright 2012 American Chemical Society.

states.[141] For low-dimensional nanostructures (usually termed nanoclusters, nanocrystals, or quantum dots), these states can be considered as arising from the superposition of bulklike states at each energy level with a concomitant dramatic increase in oscillator strength, which represents the probability of absorption or emission of electromagnetic radiation in transitions between energy levels.[142] Therefore, to excite those semiconductor nanostructures with confinement effects, higher kinetic energy will be required from the individual photons, and this results in slightly shorter excitation wavelengths. Similarly, when the average size of these low-dimensional nanostructures is changed due to substantial attachment to graphene (or RGO), and sufficient electrons are generated so they can diffuse through the regions near the junction between the semiconductor and graphene (for band gap tuning of graphene in addition to the prior photocatalytic reduction of GO),[129] the PL emission of the nanocomposites is found to be blue-shifted relative to that of the semiconductors alone. This is reflected in some of the measurements listed in Table 1. This blue shift of the band edge emission is mainly attributed to the band gap tuning (or opening) of graphene, which in return causes the efficiently interactive hybrid materials to require more energy from the photons of the light sources to be excited than from the inorganic semiconductors alone.

Most studies of ZnS−graphene nanocomposites focus on graphene nanosheets attached with ZnS QDs only. Investigating the effects of other morphologies of ZnS on the nanocomposites would be helpful for making comparisons of the characteristics of these different morphologies and lead to a better understanding of the mechanisms involved. Li et al. prepared ZnS QDs and ZnS quantum flakes (QFs) on RGO nanosheets, using thiourea and zinc chloride, as shown in Figure 12.[145] The molar concentration of reactants was tuned to control the nucleation and growth of the ZnS nanocrystals, which developed from QDs into QFs depending on the reaction time. As expected, the emission spectra were found to depend on the morphology of the ZnS particles. The QFs made the ZnS−graphene composites exhibit a better photovoltaic response than the QDs alone did. This was attributed to the 2-dimensional nanostructure absorbing light irradiation when attached onto the graphene surfaces. Also, since 1-dimensional single-crystalline ZnS nanostructures provide high electron mobility, low-voltage operation, and decent efficiency,[146] ZnS nanowires grown on 2-dimensional graphene have great potential for applications in optoelectronic devices. Although the low-intensity surface-defect-related emission of ZnS−graphene composites can be partially quenched, as described above, it is still possible to generate emission peaks, arising from the surface states, at some wavelengths. Therefore, it is viable that heterogeneous ZnS−graphene structures will yet find a use in field emission displays. In this regard, Kim et al. observed that ZnS nanowires (NWs) grown on multilayered graphene films (MGFs) showed blue-green (503 nm) emissions.[147] However, when doped with Te ions, even without any external catalyst, blue emission (440 nm) was seen. This demonstrates the feasibility of using MGFs, even on their own, as catalysts for hybrid ZnS−graphene devices, as shown in Figure 13.

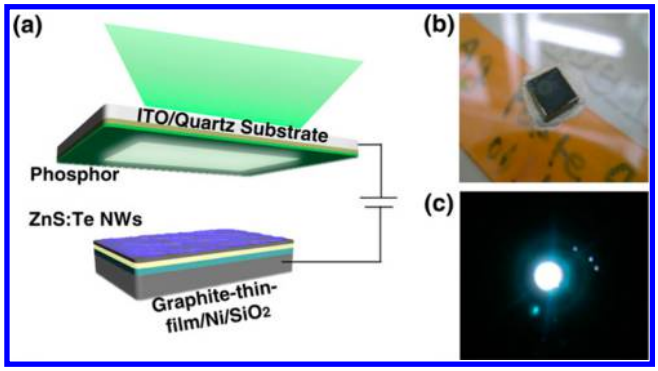

Figure 13. (a) Cross-sectional view of the field-emitting structure employing a nanowire/MGF cathode and a green phosphor/ITO anode. (b) Optical image of a ZnS/Te nanowire/MGF substrate (10 mm × 10 mm). (c) Optical image of the green-light-emitting region. Reprinted with permission from ref 147. Copyright 2010 IOP Publishing.

3.3. Cadmium Sulfide (CdS) and Graphene

Compared to its wide band gap counterparts, CdS is a competitive candidate for making photocatalysts with the remarkable property of being photodegradable in water and air.[148] CdS has a sufficiently negative flat-band potential, which is advantageous for the donation and transferral of electrons.[149−151] Its relatively narrow band gap of 2.42 eV can be used to efficiently absorb visible light.[152] As a result, CdS makes attractive photocatalytic materials for the conversion of solar energy into chemical energy under visible light irradiation. However, prolonged irradiation of CdS suspensions leads to decomposition into Cd and S ions,[153] thus reducing its chemical stability. Also, when CdS is in the form of nanoparticles, aggregation is likely to occur.[154−156] This in turn will result in a reduced surface area and thus a higher recombination rate of the photoinduced electron−hole pairs.

DOI: 10.1021/cr400607y
Chem. Rev. 2015, 115, 8294−8343

Extensive studies have been carried out with a view to improving the efficiency of CdS photocatalytic activity.[157−160] In practice, graphene can be utilized as a nanoscale building block and efficient charge carrier transport channel to facilitate CdS. This is similar to the role played by graphene matrixes in improving the efficiency of the photocatalysts as described in previous sections for ZnO and ZnS. For example, Cao et al. developed CdS−graphene nanocomposites directly from GO in dimethyl sulfoxide (DMSO).[161] This enhanced the stability of the CdS and prevented the aggregation of both graphene and CdS. An ultrafast electron transfer process, with a time constant of about 5 ps, was detected using time-resolved fluorescence spectroscopy, and this was ascribed to the electron transfer from excited CdS QDs (10 nm) to the single-layer graphene matrix. Regarding the application of CdS−graphene to photocatalytic H_2 production, Li et al. investigated the influence of graphene on the properties of CdS clusters (3 nm particles).[162] The materials were prepared using a solvothermal method in which GO served as the support and cadmium acetate ($CdAc_2$) served as the precursor for CdS. It was reported that a high photocatalytic H_2 production rate, driven by a visible light source ($\lambda \geq 420$ nm), of 1.12 mmol h^{-1}, which was about 4.87 times higher than that of pure CdS nanoparticles, was achieved using the CdS-cluster-decorated graphene nanosheets as photocatalysts. Pt was also loaded onto the surface of the photocatalyst through the use of a $H_2PtCl_6 \cdot 6H_2O$ aqueous solution as a cocatalyst. This was believed to reduce the overpotential in the production of H_2 from water,[163] and suppress the fast backward reaction (recombination of hydrogen and oxygen into water).[164] The authors proposed that, under visible light irradiation, the CdS semiconductor electrons would be excited from the valence band to the conduction band and then most likely transferred in one of three ways as schematically shown in Figure 14: (1) to Pt deposited on the surface of the CdS clusters; (2) to C atoms on the graphene sheets; (3) to Pt located on the graphene nanosheets. Eventually, the electrons reacted with the adsorbed H^+ ions to form H_2.

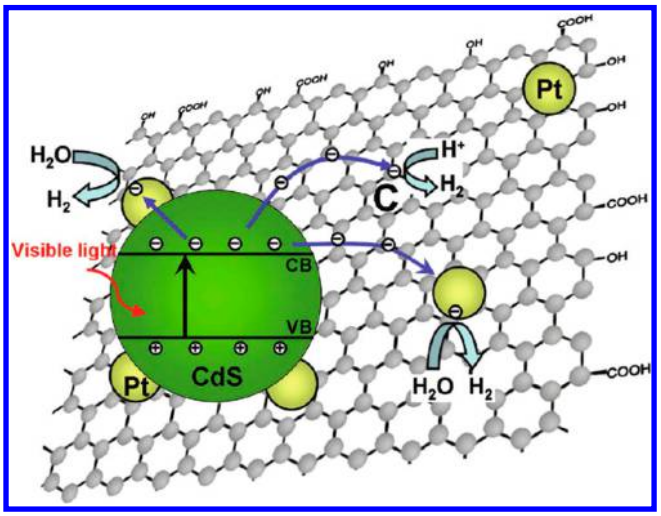

Figure 14. Schematic illustration of the charge separation and transfer in the CdS−graphene system under visible light. The photoexcited electrons transfer from the conduction band of CdS, not only to the located Pt, but also to the C atoms on the graphene sheets, which are accessible to protons that readily transform into H_2. Reprinted from ref 162. Copyright 2011 American Chemical Society.

Further to this work, Jia et al. used N-doped graphene (N-graphene) nanosheets, which were prepared from natural graphite powder and then annealed with NH_3, to form nanocomposites with CdS nanocrystals (nanoparticles).[165] The intended use of the N-graphene nanosheets was as an electron transfer channel for the purpose of reducing the recombination of the photogenerated electrons−holes. As a result of the fact that the size of the CdS nanoparticles in these samples was in the range of 50−300 nm, the highest H_2 evolution rate of the CdS−N-graphene nanocomposites was only 210 μmol h^{-1} under visible light irradiation ($\lambda \geq 420$ nm). Nevertheless, the CdS−N-graphene induced the direct splitting of water into H_2 with improved conversion efficiency relative to pure CdS nanoparticles (more than 5 times higher). On the basis of the above investigations, it was suggested by Zhang et al. that the photocatalytic activities of CdS−graphene nanocomposites could be used for organic transformations.[166] Using a hydrothermal approach, they synthesized a series of CdS−graphene nanocomposites. During the process, the formation of CdS nanoparticles (200 nm) and the reduction of GO occurred simultaneously. Photocatalytic tests showed that the resulting CdS−graphene nanocomposites were able to serve as a visible-light-driven photocatalyst (irradiation source, $\lambda > 420$ nm) for the selective oxidation of alcohols to aldehydes. It was argued that, under visible light irradiation, the alcohol molecules absorbed onto the nanocomposites were oxidized by the holes generated in the valence band. These in turn would produce alcohol radical cations and react with molecular oxygen or superoxide radicals to yield the aldehyde product. On the other hand, Liu et al. evaluated the photocatalytic performance of CdS−RGO nanocomposites through the photocatalytic reduction of Cr(VI).[167] The CdS−RGO composites were found to exhibit enhanced photocatalytic performance in the reduction of Cr(VI), under visible light irradiation ($\lambda > 400$ nm). A maximum removal rate of 92% compared with that of pure CdS (79%) was observed, and this was attributed to the increased light absorption intensity and the prevention of electron−hole pair recombination.

In addition, as illustrated by the data presented in Table 1, CdS−graphene composites lead to a quenching effect similar to that observed for ZnO−graphene and ZnS−graphene composites. In a previously mentioned work, nanocomposites composed of graphene and nanocrystalline metal sulfide were successfully synthesized by dispersing GO, under constant sonication, into a solution of $Cd(NO_3)_2$, through which H_2S was then bubbled.[140] It was reported that, in the spectrum of the CdS−graphene composites, the band edge emission of CdS was almost identical to that of the free CdS particles (11 nm). In contrast, the emission at about 530 nm was completely quenched due to the interaction between the CdS particles and the graphene sheets, as shown in Figure 15. Another previously mentioned work reported that, after the integration of CdS QDs (3−4 nm) with graphene nanosheets, the PL emission was significantly quenched at a wavelength of about 530 nm, with the effect extending up to 700 nm.[139]

It is also worth mentioning that when CdS is coupled with other types of photocatalysts, such as TiO_2, it is possible to extend the region of absorption and improve the sunlight photocatalytic efficiency. Where TiO_2 is concerned, because of its relatively wide band (3.2 eV), its photocatalytic properties are limited to the 10−400 nm wavelength UV region, which is rather narrow compared with the total solar spectrum. Experimental results show that, with the assistance of graphene,

DOI: 10.1021/cr400607y
Chem. Rev. 2015, 115, 8294−8343

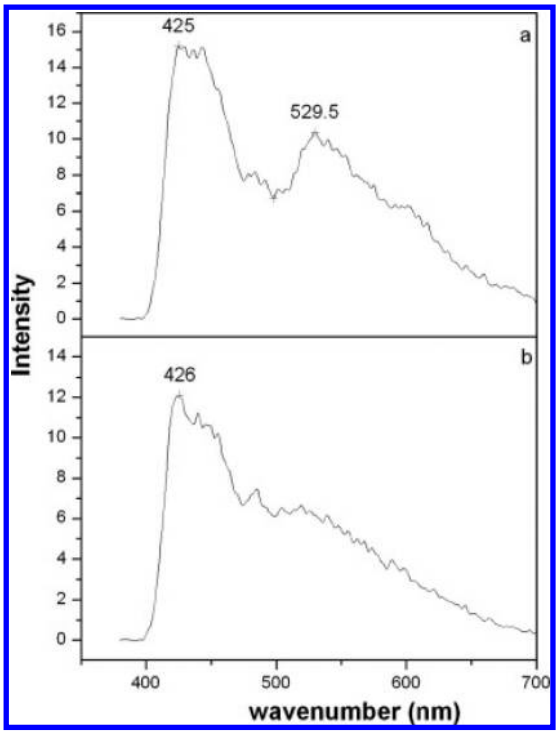

Figure 15. PL spectra of free CdS nanoparticles (a) and the CdS–graphene composite (b) excited at 355 nm. Measurements were performed at ambient temperature (approximately 30 °C). Reprinted with permission from ref 140. Copyright 2009 Elsevier.

the photocatalytic performance of CdS–TiO_2 composites can be enhanced: a maximum degradation efficiency of 99.5% for methyl orange under visible light irradiation, relative to that of pure TiO_2 (43%) and CdS–TiO_2 composites (79.9%), has been achieved.[169] This is ascribed to the increase in specific surface area and the prevention of electron–hole pair recombination. Since the conduction band position of CdS is higher than that of TiO_2, photoexcited electrons from CdS can be efficiently injected into TiO_2.[170] In addition, it has been reported by Santra and Kamat that doping CdS (or CdSe) with optically active transition-metal ions of Mn^{2+} further modifies the electronic and photophysical properties of the CdS–TiO_2 composites.[168] They constructed "QD-sensitized solar cells", with Mn-doped CdS (CdSe) deposited on mesoscopic TiO_2 films as the photoanode. A Cu_2S–GO composite was the electrode and S^{2-}/S the electrolyte. A power conversion efficiency of 5.4% was obtained, under AM 1.5 global filters at an intensity of 100 mW/cm^2 (sunlight). They also proposed a mechanism for this phenomenon where the midgap states created by the Mn-doping would cause electrons to be trapped and screened from charge recombination with holes and/or oxidized polysulfide electrolytes. This is shown in Figure 16.

Apart from the efficient electron transfer to graphene from CdS dots, the use of CdS nanowires as semiconducting channels on graphene for relevant applications has also been reported. Dufaux et al. investigated the photoelectric properties of the interface between graphene sheets.[171] These graphene sheets were mechanically exfoliated from highly oriented pyrolytic graphite and transferred onto Si substrates, and n-doped CdS nanowires, which were synthesized through a solvothermal method. In this system, the graphene sheet was contacted with a CdS nanowire (20 μm in length and 20–80 nm in diameter), and it produced large short-circuit photo-

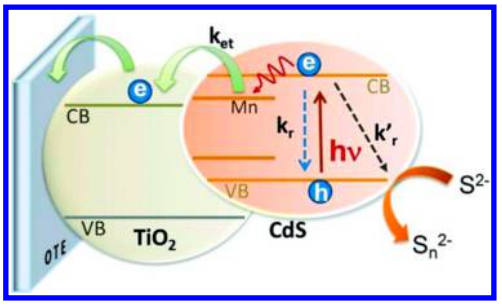

Figure 16. Schematic diagram illustrating the electron transfer (k_{et}) from doped CdS into TiO_2 nanoparticles. k_r and k'_r represent electron recombination with holes and the redox couple, respectively. Reprinted from ref 168. Copyright 2012 American Chemical Society.

currents up to 200 nA, when scanned through the diffraction-limited laser spot of a confocal microscope (intensity 191 kW cm^{-2}). With an applied bias voltage of 0.1 V, Lee et al. obtained an enhanced photocurrent from the CdS–graphene hybrid structure compared with that of the channels based on graphene only.[172] Their system comprised single-crystalline CdS nanowires grown on the Au catalyst patterns of a single-layer graphene sheet (synthesized using a CVD method) in a horizontal tubular furnace. The photocurrent, measured as $I_{max} - I_{dark}$, was up to 2.60×10^{-2} mA, where I_{max} and I_{dark} represent the currents with and without a light source (power density 100 mW cm^{-2}), respectively. The hybrid structure had a much faster operational speed than commercial CdS film-based photodetectors and exhibited large photoresponses. This confirms the feasibility of their strategy in taking advantage of both graphene and semiconducting nanowires for optoelectronic functions.

4. GROUP III–V COMPOUND SEMICONDUCTORS AND GRAPHENE

The group III–V compound semiconductors, such as gallium arsenide (GaAs), boron nitride (BN), gallium nitride (GaN), indium arsenide (InAs), aluminum antimonide (AlSb), and indium phosphide (InP) and their ternary and quaternary alloys, are comprised of elements of columns III and V. Many group III–V semiconductor compounds have been widely used to produce high-speed electronic devices and optoelectronic devices. Their high electrical mobilities and direct band gaps are the attributes that make these semiconductors useful for applications.[173–176] Worth noting is the fact that the industry manufacturing III–V semiconductor integrated circuits is fairly well established for a wide range of applications, including smart phones, cellular base stations, fiber-optic systems, wireless local-area networks, satellite communications, radar, radioastronomy, and defense systems.[177] Recently, widespread research into graphene has boosted the profile of some of the III–V compound semiconductors, particularly those of GaN, BN, and GaAs. They will be discussed in this section.

4.1. Boron Nitride (BN) and Graphene

Boron nitride is a wide band gap semiconductor with a direct band gap of between 5.8 and 6.0 eV.[178] This enables it to be used as a dielectric layer in electronic devices. Its nanostructures consist of diverse 1-dimensional or 2-dimensional morphologies, such as BN nanotubes (BNNTs), BN nanoribbons (BNNRs), and BN nanosheets (BNNSs).[179] In addition, BN is a structural analogue of C; it has layered (hexagonal, h-BN), cubic, and tubular structures, which are similar to C's

DOI: 10.1021/cr400607y
Chem. Rev. 2015, 115, 8294–8343

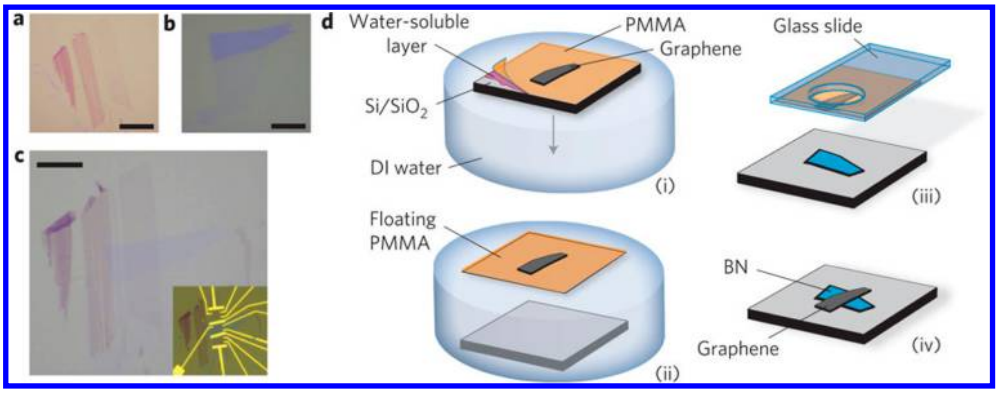

Figure 17. Mechanical transfer process. (a–c) Optical images of graphene (a) and h-BN (b) before and (c) after transfer. Scale bars indicate 10 μm. Inset: electrical contacts. (d) Schematic illustration of the transfer process used to fabricate graphene on BN devices. Reprinted with permission from ref 187. Copyright 2010 Macmillan Publishers Ltd.

graphite, diamond, and CNT phases. Specifically, h-BN consists of sp^2-bonded 2-dimensional layers with alternating boron and nitrogen atoms in a honeycomb arrangement.[179,180] The boron and nitrogen atoms are bound by strong covalent bonds within each layer of h-BN, whereas the layers themselves are held together by relatively weak van der Waals forces. Therefore, the h-BN layers can be mechanically exfoliated from bulk source materials to form thin BN sheets.[181,182] Also, BNNSs do not absorb light in the visible region of the electromagnetic spectrum, and hence are called "white graphene".[183] Nevertheless, although h-BN and graphite (graphene) are both hexagonally structured materials, their electronic properties are rather different. In contrast to the semimetallic nature of graphite, BN possesses high chemical and thermal stability due to its wide band gap.[184] As a result of this property, BN can be used to complement and improve graphene-based devices.

From our discussion of graphene structures related to group II–VI compound semiconductors, it is clear that some morphologically disordered graphene nanosheets on substrates exhibit additional edges and defects. These are needed for constructing the emission sites. The atomic monolayer consisting of hybridized phases of h-BN and graphene is another type of structure that provides a platform to attune physical properties in graphene-based structures. With this in mind, Ajayan's team synthesized atomic layers of h-BN and graphene (h-BNC) materials, which consisted of hybridized, randomly distributed domains of h-BN and C phases.[185] The final products were the result of using a thermal catalytic CVD synthetic method. It involved simultaneously supplying C (methane) and BN (ammonia–borane) sources to deposit 2-dimensional monolayers of h-BNC. The h-BNC samples obtained had a percolating graphene network embedded with BN domains. This caused two optical band gaps ranging between 1.5 and 4.5 eV with the C content distinct from those of pristine graphene, doped graphene, or h-BN. However, since any disorder in the morphology affects the physics of the electrons in graphene and its transport properties,[186] it is likely the performance of substrate-supported graphene, when presented in a disordered way, will be diminished on many occasions relative to that of suspended graphene. Therefore, h-BN is a more promising substrate for the support of graphene as it is capable of retaining most of the graphene quality. This is due to its atomically smooth surface, which is to a large extent prevented from dangling bonds and charge traps. Dean et al. reported the fabrication and characterization of exfoliated mono- and bilayered graphene devices on single-crystal h-BN substrates, by using a mechanical transfer process, as outlined in Figure 17.[187] The h-BN layers were exfoliated from ultrapure h-BN single crystals that were grown from barium boron nitride under high pressure and temperature. The graphene was exfoliated separately onto a polymer stack consisting of a water-soluble layer and PMMA. Measurements showed that the graphene devices on the h-BN substrates had high mobilities and carrier inhomogeneities almost an order of magnitude better than those on SiO_2.

Following this discovery of improved device performances, Xue et al. used scanning tunneling microscopy (STM) to investigate how graphene would conform to h-BN.[188] To carry out STM measurements, they prepared graphene on h-BN (exfoliated from h-BN single crystals) devices, which included a graphene flake on a few-layered h-BN flake with gold electrodes for the electrical contact (Figure 18a). A comparison in height distribution (Figure 18d) showed that the surface corrugations

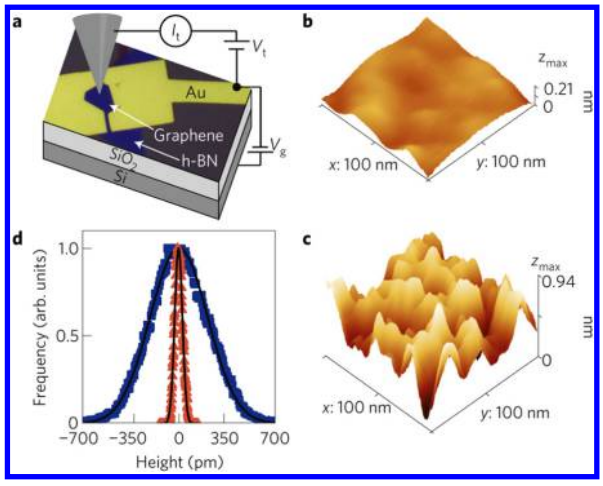

Figure 18. Schematic device setup and topography comparison of graphene on h-BN and SiO_2. (a) Mechanically exfoliated monolayer graphene flake with h-BN underneath and gold electrodes contacting it above. The wiring of the STM tip and back gate voltage is indicated. (b) STM topographic image of monolayer graphene on h-BN showing the underlying surface corrugations. (c) STM topographic image of monolayer graphene on SiO_2 showing markedly increased corrugations. (d) Histogram of the height distributions for graphene on SiO_2 (blue squares) and graphene on h-BN (red triangles) along with Gaussian fits. Reprinted with permission from ref 188. Copyright 2011 Macmillan Publishers Ltd.

DOI: 10.1021/cr400607y
Chem. Rev. 2015, 115, 8294–8343

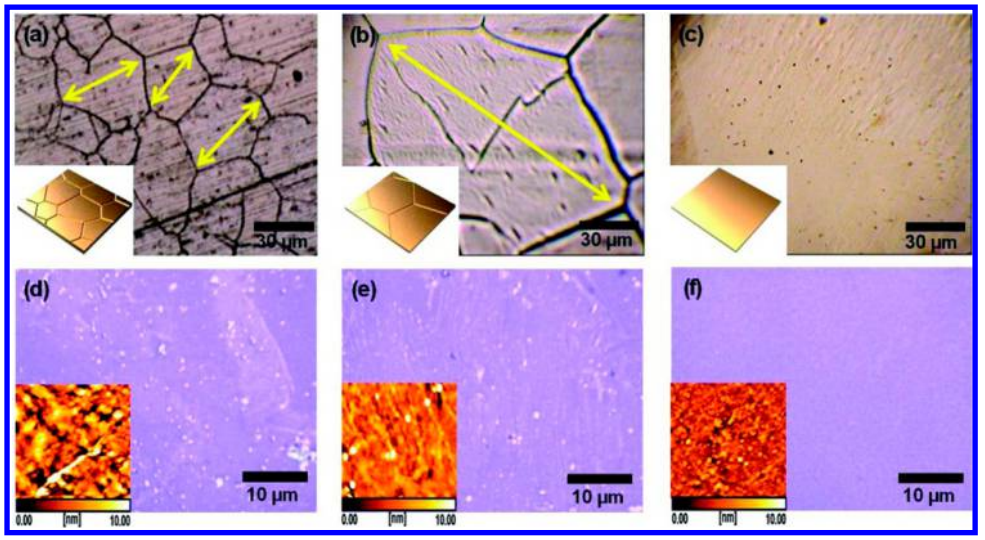

Figure 19. Optical images of Cu foils prepared (a) in pristine condition, (b) by thermal annealing (TA) at 1020 °C for 2 h, and (c) by TA (1020 °C for 2 h)/chemical polishing (CP). The inset images in (a)−(c) show the schematic illustrations of the morphology-controlled Cu foils. Optical images show surface morphologies of h-BN nanosheets transferred onto SiO_2/Si substrates after the growth of the h-BN nanosheets on (d) pristine Cu foil, (e) TA-treated Cu foil, and (f) TA/CP-treated Cu foil. The inset images in (d)−(f) show the corresponding AFM images (scan area 1 × 1 μm^2). Reprinted from ref 192. Copyright 2012 American Chemical Society.

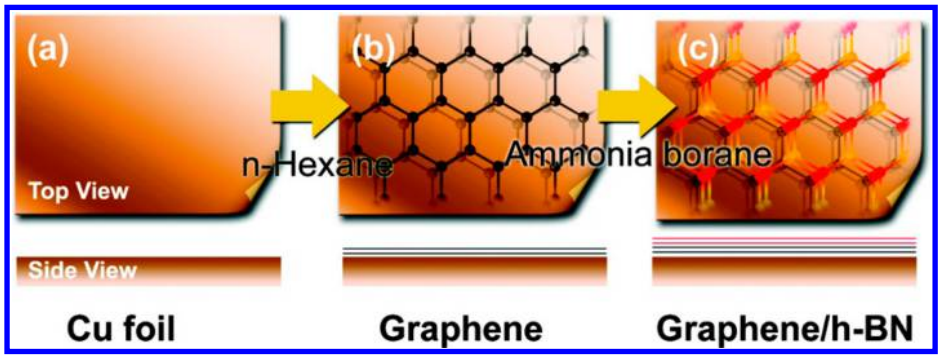

Figure 20. Schematic showing the preparation of a G/BN stacked film. (a) The Cu foil is cleaned and prepared as the growth substrate. (b) A high-quality and large-area graphene film is grown via a CVD process with *n*-hexane as a liquid C source at a temperature of 950 °C. (c) Some graphene is transferred onto SiO_2 substrates for further characterizations, and the rest is loaded into another furnace for the growth of an h-BN film on top. Reprinted from ref 195. Copyright 2011 American Chemical Society.

were much larger for graphene on SiO_2 (Figure 18c) than on h-BN (Figure 18b). This was attributed to h-BN's planar nature for graphene to conform. Further to this, to study the scattering processes specific to CVD graphene, Gannett et al. compared the transport data for CVD graphene on SiO_2 and h-BN.[189] In their experiment, large high-purity h-BN crystals synthesized using high-pressure techniques were tape exfoliated onto Si substrates with 300 nm of oxide and prepatterned Cr/Au alignment marks. A high mobility up to 37 000 $cm^2\ V^{-1}\ s^{-1}$ was obtained, without considering the short-range scattering effect. It has been argued since that the barrier to the scalable high-mobility CVD graphene is not the growth technique but rather the choice of the substrate that minimizes carrier scattering. Indeed, as the ultraflat 2-dimensional structure of h-BN provides a smooth substrate for graphene to sit on, Wang et al. worked out a BN/graphene/BN radio frequency (RF) field-effect transistor (FET), which had h-BN as both the substrate and the gate dielectric with bilayer graphene as the channel material.[190] The mobility (15 000 $cm^2\ V^{-1}\ s^{-1}$) and carrier velocity (3.5×10^7 cm s^{-1}) of the BN/graphene/BN structure were measured and found to be higher than the mobility of the SiO_2 substrates (1500−2000 $cm^2\ V^{-1}\ s^{-1}$) and the carrier velocity of Al_2O_3 gate dielectrics (2.5×10^7 cm s^{-1}), respectively. For multilayered heterostructures of graphene and BN, in which mono- and bilayered graphene crystals are individually contacted and interlaid between atomically thin h-BN crystals, it has been made possible that the interface between graphene and h-BN does not contain more than a small fraction of a monolayer of adsorbates.[191] That is to say, the interface can be atomically sharp, and the contamination (hydrocarbons) inevitably present on top of the 2-dimensional crystals and trapped during their assembly is more likely to be segregated.

For practical applications, h-BN monolayers produced through the micromechanical cleavage of a bulk h-BN crystal may be limited to certain sizes and techniques. To realize large-area h-BN layers with high quality, Lee et al. adopted a CVD process, in which Cu foils acted as the catalyst.[192] Taking into consideration that the quality of the thin film grown on a metallic substrate through surface adsorption would be affected by the surface morphology, as is the case for graphene grown on Cu foils,[193,194] they introduced thermal annealing (TA) or thermal annealing/chemical polishing (CP) to control the surface morphology of the foil. Microscopic data revealed that

DOI: 10.1021/cr400607y
Chem. Rev. 2015, 115, 8294−8343

the number of impurity particles in the h-BN nanosheets grown on the treated Cu foil decreased, relative to that in the h-BN nanosheets grown on the pristine Cu foil, as shown in Figure 19a–c. Afterward, the h-BN nanosheets were transferred onto SiO_2 (300 nm thick)/Si wafers, which also led to a corresponding decrease in surface roughness, as shown in Figure 19d–f. An FET based on graphene was fabricated utilizing the transferred h-BN nanosheets as a buffer layer on the SiO_2 gate dielectric. It was found that this morphological control of the Cu catalyst also improved the crystallinity of h-BN, and therefore led to a higher (2 times) mobility than that obtained without using the h-BN nanosheets.

Having noticed that both graphene and BN layers could be grown of their precursors independently using CVD on metallic substrates, Ajayan and co-workers also demonstrated a large-area growth sequence for graphene/h-BN (G/h-BN) stacked structures. They achieved this by combining the separate CVD growth processes used for graphene and h-BN, as illustrated in Figure 20.[195] First, the graphene film was grown on a Cu foil using a liquid C source (*n*-hexane), and then the h-BN film was grown with an ammonia–borane mixture (NH_3–BH_3) under optimized parameters. After being transferred onto the substrates, it was observed that the G/h-BN film was relatively uniform and continuous, which was useful for further characterization and device fabrication. On the other hand, direct graphene growth on h-BN without any underlying metallic catalyst layer would be of interest when the additional steps of either transferring the graphene film onto a Si wafer or removing the metallic catalyst under high temperature are not desirable. Ding et al. demonstrated the CVD growth, from CH_4, of few-layer graphene on h-BN single-crystal flakes without any assistance of metallic catalysts.[196] The film deposition was carried out at 1000 °C, and the number of layers was tuned by adjusting the growth time and the CH_4 flow rate. These studies again identify that the semiconductor BN, with excellent dielectric properties, matches very well with graphene, proving it is one of the effective candidates for promoting graphene growth.

4.2. Gallium Arsenide (GaAs) and Graphene

Some of the III–V compounds, GaAs in particular, crystallize in a zinc blende structure where, under normal pressures, the two face-centered cubic lattices of the diamond structure are occupied by Ga and As, respectively.[197] GaAs is of a medium gray appearance, and with moderate difficulty can be polished using mechanical methods.[198] Many of the band structure parameters for GaAs are known with a greater precision than for other semiconductor compounds.[176] This is especially reflected in the band gap energy of GaAs, which is 1.519 eV, at low temperatures approaching 0 K, and 1.424 eV, at 297 K.[198] Because of its direct band gap, GaAs can be used to emit light efficiently. Traditionally, it has been exploited as an electronic material or a device medium in compound-semiconductor-related areas. Recent progress in making GaAs nanoscaled structures has shown that it can also be used to enable high-speed transportation in electronically or optically active devices.[174,199,200]

The reader will have surmised from our discussions throughout that graphene layers have been frequently located on SiO_2/Si substrates to be identified using Raman spectroscopy.[201,202] This is due to the early reported studies of graphene which generally adopted mechanical exfoliation. When graphene nanosheets are placed on top of the Si wafer with an oxide layer (e.g., 300 nm thick), by using an optical microscope it has been demonstrated that graphene exhibits decent visibility.[10,92] Any deviation in the thickness of the oxide layer will usually greatly affect the visibility of the graphene, because the optical contrast between the substrate and graphene depends on the thickness of the substrate for a certain wavelength.[43] For example, only a 5% difference in SiO_2 thickness (315 nm instead of the standard 300 nm) makes single-layer graphene completely invisible.[1] To expand the use of Raman spectroscopy, which is a convenient technique for identifying and counting graphene layers, as a nanometrology tool for graphene and graphene-based devices, Calizo et al. investigated the influence of substrates on the room-temperature Raman scattering spectrum from micromechanically cleaved graphene.[203,204] It was however discovered that the G peak recorded for graphene on the n-type (100) GaAs substrate was essentially in the same location (positioned at 1580 cm^{-1}) and of the same shape as that for graphene layers on Si/SiO_2 (300 nm).

Therefore, considering the use of GaAs for ultrafast electronics and optoelectronics, one would expect that combining graphene and GaAs should prove advantageous and lead to additional opportunities, provided both materials are easily visible together. Ahlers and co-workers claimed that a tailored GaAs–aluminum arsenide (AlAs) multilayer structure, with a special sequence of GaAs and AlAs layers, should make mechanically exfoliated graphene just as visible on GaAs as on Si/SiO_2.[205] They prepared mono-, bi-, and multilayers of graphene on GaAs–AlAs substrates, which had three double layers of AlAs on GaAs, and performed the contrast analysis through a standard microscope objective with a numerical aperture of 0.9 (NA0.9), using a green filter with a rectangular passband from 530 to 570 nm. The wavelength of minimum reflectivity and hence maximum contrast was determined by adjusting the thickness of the GaAs and AlAs layers, which in this case was 36 nm. Taking into account the advantage of the surface quality of the GaAs, they also investigated the electronic and magnetotransport properties of the combined material of exfoliated graphene on GaAs–AlAs substrates.[206] Tunability of the carrier density was achieved by using a Si-doped (300 nm) GaAs substrate as the back gate, whereby the GaAs–AlAs multilayer provided the optical visibility as well as the insulating barrier between the back gate and the graphene. On the other hand, a different approach reported the growth of graphene on GaAs–AlAs. It was based on the formation of graphitic C using molecular-beam epitaxy (MBE).[207] The graphitization involved growing highly C-doped GaAs on AlAs, which was then thermally etched in situ (reflection high-energy electron diffraction, RHEED), leaving behind C atoms on the surface, presumably due to their low vapor pressure. Also, the demonstrated visibility of graphene on the GaAs-based material could potentially even increase the possibility of integrating the CVD graphene and GaAs–$Al_xGa_{1-x}As$ heterostructure into a hybrid FET.[208]

Further to this, Peters et al. attempted to enhance the visibility of graphene on GaAs-based substrates by spin-coating PMMA resist on micromechanically cleaved graphene.[209] A PMMA coating layer with an optimum thickness had already been proven effective for intensifying the contrast of single-layer graphene on many substrates.[210] Subsequently, they noticed that single-layer graphene sheets became visible in an optical microscope when the thickness of the PMMA layer was well-defined. Apart from this relatively precise thickness

DOI: 10.1021/cr400607y
Chem. Rev. 2015, 115, 8294–8343

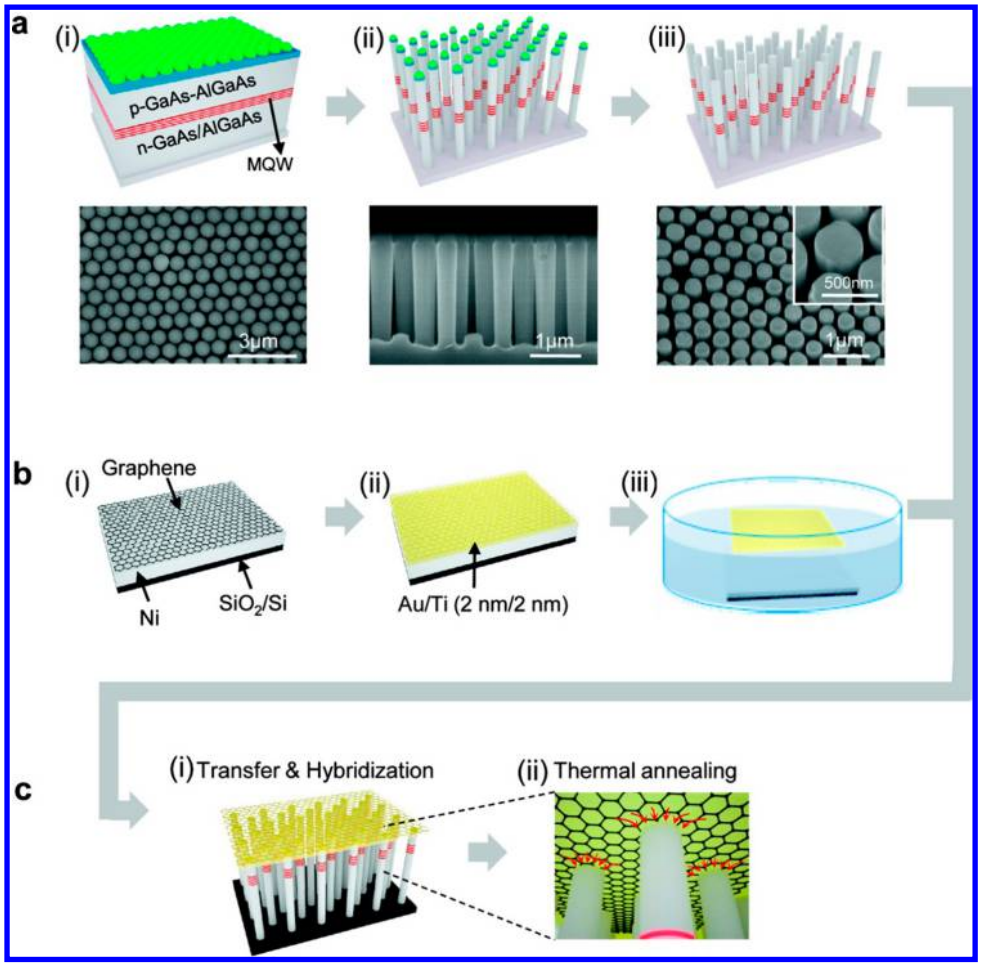

Figure 21. Schematic illustration of the key steps for fabricating PSL−Gr/M architectures. (a) Steps for fabricating vertical PSL arrays: (i) self-assembly of SiO_2 spheres on PMMA-coated semiconductor epilayers, (ii) ICP etching to produce the PSL array, and (iii) removal of SiO_2 spheres and PMMA layers with sonication in acetone. SEM images of the samples at each step appear at the bottom. (b) Steps for fabricating free-standing sheets of Gr/M: (i) graphene synthesis, (ii) metal layer deposition, and (iii) separation of the Gr/M sheet from the substrate. (c) Integration of the PSL array and Gr/M followed by thermal annealing. Reprinted from ref 213. Copyright 2010 American Chemical Society.

control, the advantage of the PMMA overlayer, which is a commonly used resist for e-beam lithography, rests also on the fact that it can be used to pattern graphene.[211] To study the influence of this characteristic on the morphology of graphene, Stöberl et al. spun the PMMA resist onto mechanically exfoliated graphene flakes on the GaAs substrates.[212] They used either optical microscopy or SEM to identify suitable flakes. Subsequently, further analyses of the graphene morphology using AFM strongly indicated that the graphene sheets followed the texture of the sustaining substrates, independent of doping, polarity, and roughness.

Lee et al. reported a type of device that combined vertical arrays of 1-dimensional pillar-superlattice (PSL) structures with 2-dimensional graphene sheets for producing LEDs.[213] Here graphene was mounted directly on the PSL to form a suspended structure, as schematically illustrated in Figure 21. The vertical array of PSL structures was fabricated from group III−V epitaxial semiconductor layers by combining colloidal nanosphere assemblies and deep inductively coupled plasma (ICP) etching techniques. The epitaxial semiconductor layers included $Al_{0.25}In_{0.5}Ga_{0.25}P/Ga_{0.6}In_{0.4}P$ (6 nm/6 nm) multi-quantum well (MQW) structures sandwiched in p-type contact−spreader−cladding layers and n-type cladding−spreader−contact layers grown on GaAs substrates. It was argued that thermal annealing of the graphene/metal (Gr/M) contact to GaAs would induce diffusion of metal atoms from the top graphene layers to the p-GaAs contact layers. This should improve the electrical contact properties and, thus, enhance the carrier injection to the PSLs for light emission. On the other hand, Munshi et al. used an atomic model to explore possible epitaxial growth configurations applicable to conventional semiconductors.[214] Using the self-catalyzed vapor−liquid−solid technique by means of MBE, they demonstrated the growth of vertically aligned GaAs nanowires on graphite and few-layer graphene.

4.3. Gallium Nitride (GaN) and Graphene

GaN-based devices include LEDs, laser diodes, and UV detectors, with respect to photonics, as well as microwave power and ultra-high-power switches in the case of electronics.[215] It has been well established that the equilibrium crystal structure of the III−V nitrides is the wurtzite 2H polytype.[216] In contrast, GaN (and InN) can also crystallize in a metastable zinc blende 3C structure.[216] As a matter of fact, the crystal structure of GaN is strongly influenced by both the nature of the material and the orientation of the substrate.[217] In general, the wurtzite materials grow on hexagonal substrates, whereas zinc blende can be grown on cubic substrates. This is due to the fact that both wurtzite and zinc blende crystal

DOI: 10.1021/cr400607y
Chem. Rev. 2015, 115, 8294−8343

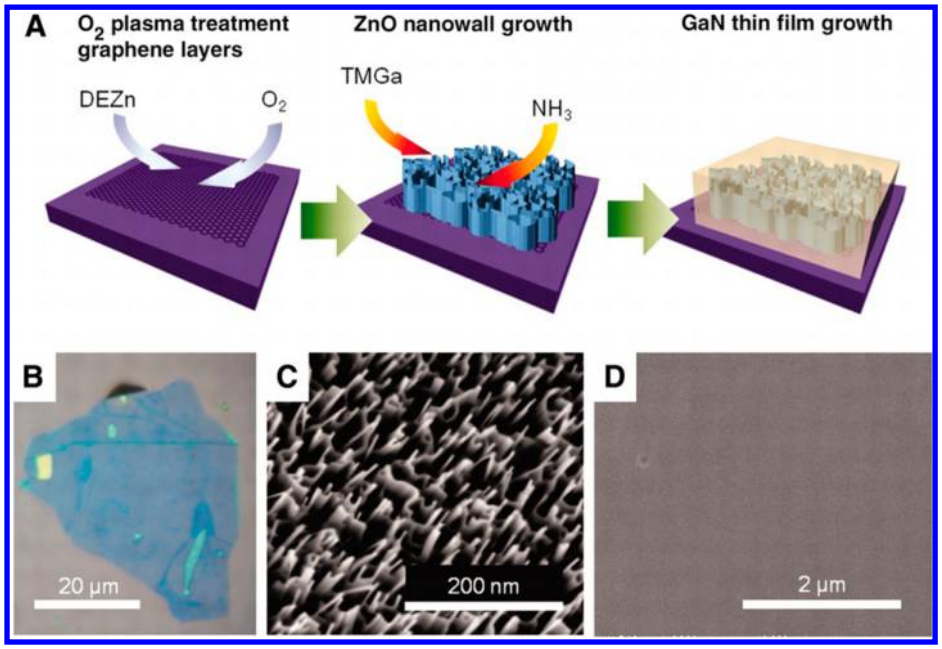

Figure 22. (A) Schematic illustrations of the fabrication processes for epitaxial GaN thin films. (B) Optical microscopic image of oxygen-plasma-treated graphene layers. (C) and (D) are SEM images of the ZnO nanowalls grown on plasma-treated graphene layers (C) and the GaN thin film grown on ZnO nanowalls on plasma-treated graphene layers (D). Reprinted with permission from ref 219. Copyright 2010 American Asssociation for the Advancement of Science.

structures are interpenetrating sublattices of the group III and V elements in which every atom is tetragonally coordinated with four atoms of the opposite species. The crystal structures differ only in their stacking sequence along the (111) axis. Growth on a (111) plane does not act as a template for the zinc blende growth, and the equilibrium wurtzite structure is obtained.[217] The wurtzite polytypes of GaN have a direct band gap of about 3.4 eV, which means they are capable of high-power and high-temperature operations. Indeed, like SiC, GaN has both a high electron saturation velocity and a large breakdown field, and this, combined with high thermal conductivity, makes it an excellent candidate for devices operating under extreme conditions.

However, in spite of some notable advances in graphene research, currently, the practical implementation of graphene into GaN-based devices, for the purpose of improving their mechanical and optoelectronic properties, remains a challenge. One critical obstacle to the integration of graphene with GaN is that direct epitaxial growth, which is an established way of producing high-quality GaN,[218] of nitride on graphene materials is extremely difficult. Chung et al. observed that, in their attempts to grow epitaxial nitride thin films on mechanically exfoliated graphene, mirror-smooth epitaxial GaN thin films could not be grown on pristine graphene layers.[219] This was attributed to the lack of chemical reactivity. Fortunately, the results showed that although GaN nucleation did not occur on the basal plane of pristine graphene, GaN islands could be grown readily along the naturally formed step edges. Thus, as shown in Figure 22, they created more step edges by treating the graphene surface with oxygen plasma, which made the surface rough, and then grew high-density ZnO nanowalls along the step edges formed on the treated graphene layers.[81] A catalyst-free metal−organic vapor-phase epitaxy (MOVPE) process was used. It was proposed that the GaN layers were heteroepitaxially grown on the ZnO nanowalls because both GaN and ZnO have a wurtzite crystal structure with small lattice misfits that are within 2%. As an intermediate layer for GaN growth, the high-density ZnO nanowalls play a critical role under such conditions. This is due to the fact that the crystallinity and the morphology of the GaN depend to a large extent on the density and the quality of the nanowalls. More recently, following this same strategy of growing an intermediate layer of ZnO on CVD graphene, Chung et al. also realized the growth of GaN on amorphous SiO_2 substrates.[220] In this case, there was no epitaxial relationship with GaN either. Although the nitride thin films grown were not single crystals, it was observed that the surface morphology of the nitride thin films was flat and uniform with a high *c*-axis orientation. This model was utilized by the authors to further fabricate LEDs, which reportedly exhibited strong light emission that could be seen with the unaided eye under room illumination.

This technique of growing high-quality inorganic semiconductor thin films indirectly on amorphous substrates led to the creative inspiration for the fabrication of LEDs on large-area noncrystalline solid substrates. Consequently, research on the direct epitaxial growth of GaN-based blue LEDs has been motivated at an even more advanced level. For example, Han et al. investigated the direct epitaxial growth of GaN on RGO, which acted as a buffer layer for the overgrowth.[221] The RGO pattern was produced using a combination of photolithography and spray-coating methods on sapphire substrates. Afterward, undoped GaN was grown from a previously deposited GaN nucleation layer on the RGO pattern, under high temperatures and low pressures. Trimethylgallium and ammonia were used as the gallium and nitrogen sources, respectively. Since RGO generally shows high thermal conductivity and rapid heat-dissipating ability,[222,223] it was shown that the LED chip with embedded RGO outperformed its conventional counterpart by emitting bright light (about 33% enhancement in the light output power) with a relatively low junction temperature (up to 25% reduction) and thermal resistance (up to 30% reduction). Overall, this work has demonstrated that the embedded RGO

DOI: 10.1021/cr400607y
Chem. Rev. 2015, 115, 8294−8343

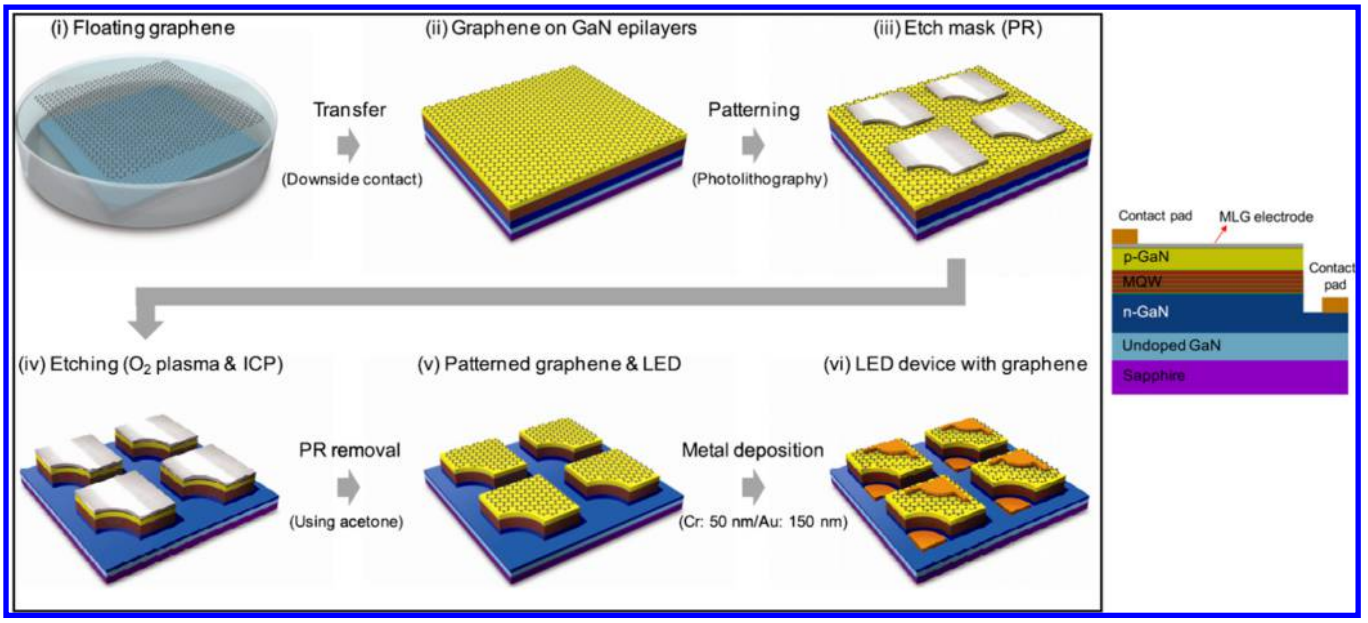

Figure 23. Batch fabrication for GaN-based LEDs with patterned MLG electrodes: (i) an MLG film floats after etching of the Ni substrate with $FeCl_3$, (ii) the MLG film is transferred onto GaN-based LED epilayers, (iii) patterned PR etch masks are formed by photolithography, (iv) etching of the MLG film and the GaN LED epilayers is performed, (v) the PR is removed, and (vi) metal electrodes are deposited to complete the device fabrication. PR = photoresist, and MQW = multiquantum well. Reprinted with permission from ref 224. Copyright 2010 IOP Publishing.

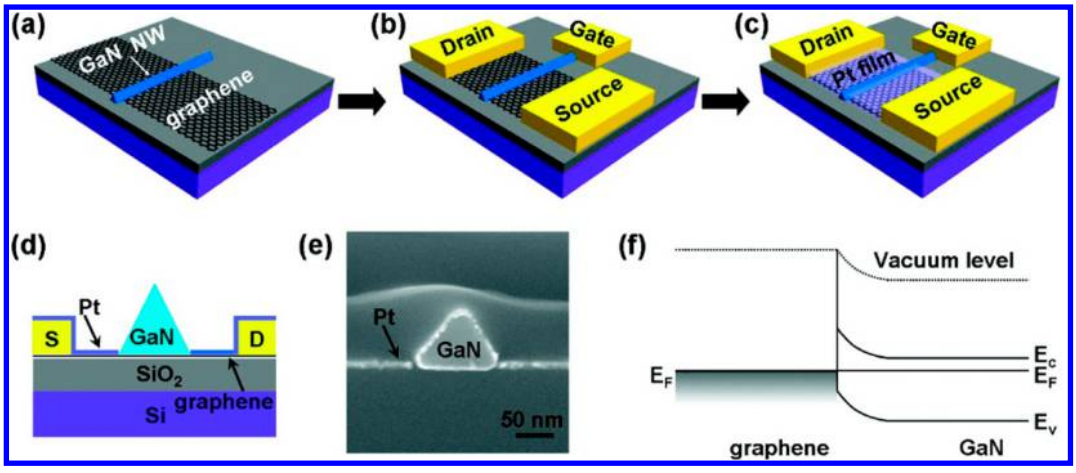

Figure 24. Schematic illustration of the fabrication process of the top-gated graphene transistor with a GaN nanowire as the self-aligned top gate. (a) A GaN nanowire is aligned on top of the graphene. (b) The external source, drain, and top-gate electrodes are fabricated using electron beam lithography. (c) Deposition of a 10 nm Pt film to form the source and drain electrodes self-aligned with the nanowire gate. (d) Schematic illustration of the cross-section of the device. (e) SEM image of the cross-section of the GaN nanowire/graphene device, illustrating well-separated source and drain electrodes due to the nanowire shadow effect. (f) Schematic energy band diagrams of a single GaN nanowire on graphene. EF, EC, and EV are Fermi level, conduction band, and valence band, respectively. Reprinted from ref 233. Copyright 2010 American Chemical Society.

pattern not only aids the growth of single-crystal high-quality GaN, but also acts as a heat-dissipating layer.

To develop graphene on a practical scale applicable to optoelectronic devices, Jo et al. employed multilayer graphene (MLG) films, which were CVD-synthesized on Ni, as transparent electrodes in GaN-based blue LEDs.[224] Figure 23 shows the fabrication process of the LED devices with MLG electrodes. The authors observed that the MLG electrodes on the GaN LED devices presented intense EL spectra and a sheet resistance of ~620 Ω/□ with a transparency of more than 85% in the 400−800 nm wavelength range. This implies that the MLG electrodes effectively operate as a transparent current-spreading layer. Therefore, it was suggested that CVD-synthesized graphene could advance conventional GaN LEDs, and even promote the applications of graphene-based thin films as transparent electrodes for optoelectronic devices. This aim has led to further important work in this field. Kim et al. produced graphene-based transparent conductive electrodes as the current-spreading layer in UV GaN LEDs.[225,226] Their graphene source deposited onto the surface of the UV LED was either mechanically exfoliated or transferred from Cu substrates (after the CVD). Caldwell et al. reported a dry transfer technique using Nitto Denko Revalpha thermal release tape, which enabled the transfer of epitaxial graphene (squared, up to 16 mm on one side) from the C-face SiC "donor" substrate onto various "handle" substrates, including both p-type and n-type GaN substrates.[227] It is expected that this transfer technology will enable epitaxial graphene films to be compatible

DOI: 10.1021/cr400607y
Chem. Rev. 2015, 115, 8294−8343

with GaN substrates for use as optically transparent contacts in optoelectronic applications. However, further improvement in the thickness and uniformity of the C-face epitaxial graphene films would make the process even more reliable. The fact that the use of bare graphene as a window electrode in p-type GaN would pose intrinsic limitations for current injection due to its work function (~4.5 eV), which is smaller than that of p-type GaN (7.5 eV), inspired Lee et al. to insert thin Ni/Au between graphene and p-type GaN to reduce the contact resistance of the GaN LED.[228] Their measurements showed that the contact resistance was reduced from ~5.5 to ~0.6 Ω/cm^{-2}, while the optical transmittance exceeded 78% for visible light. As a result, the GaN LEDs incorporated with metal/graphene electrodes gave rise to current spreading and injection into the p-type GaN layer. This led to a 3-fold enhancement in the electroluminescent intensity, compared with that generated from graphene alone, as well as a strong uniform blue light emission. Chandramohan et al. inserted a Au layer between multilayer graphene and p-GaN to decrease their work function difference. This improved the electrical coupling between graphene and p-GaN and the forward voltage of the GaN-based LED consisting of MQW structures.[229] Choe et al. focused on the role of Au nanoparticles, rather than an entire continuous interlayer, for decorating multilayer graphene electrodes for use in GaN-based optoelectronic devices.[230] Thus, they improved the electrical conductivity and modified the work function of the graphene films. Alternatively, Seo et al. applied ITO nanodot nodes onto the surface of the p-type GaN layer to combine it with graphene, which was directly deposited as the transparent electrode in InGaN/GaN MQW LEDs, with the view to optimizing the electro-optic characteristics in the UV region.[231,232]

Since GaN is a suitable candidate for high-temperature and high-power applications, integration of GaN and graphene has also led to the development of new types of transistors. Liao et al. reported the fabrication of graphene transistors with a sub-100 nm channel length using a highly doped n-type GaN nanowire as the local gate.[233] Figure 24 illustrates the fabrication approach of these graphene transistors. Highly n-doped GaN nanowires were synthesized using a metal−organic chemical vapor deposition (MOCVD) method and transferred on top of the graphene, which was mechanically peeled onto a doped p-type Si substrate with a 300 nm thick thermal SiO_2 layer. Following this, e-beam lithography and metallization (Ti/Au, 50 nm/50 nm) were performed to define the external source, drain, and gate electrodes. A thin layer of Pt (10 nm) was then deposited on top of the graphene across the GaN nanowire in which the GaN nanowire separated the Pt film into two isolated regions that formed the self-aligned source and drain electrodes next to the nanowire gate. In this device, the contact between graphene and the GaN nanowire created a Schottky-like barrier which prevented significant charge leakage between the graphene channel and the GaN nanowire gate. The interface depletion layer in the GaN nanowire functioned as a "semi-high-k" gate dielectric ($k \approx 10$), and the GaN nanowire itself functioned as the local gate. It was conceived that the triangle cross-section of the GaN nanowire with a flat side surface would allow a seamless contact between the nanowire gate and the graphene to ensure the critical gate coupling for producing high transconductance. By using GaN nanowires of optimized sizes as the local gate, terahertz operation is likely to be achieved even in smaller transistors.

5. OXIDE SEMICONDUCTORS AND GRAPHENE

Oxide semiconductors have been thoroughly investigated for their inherent features utilizable in transparent electrodes.[234,235] These advantages are mainly related to their durability, high carrier density (n-type), compatibility with plastic substrates, fairly wide band gaps, and colorability.[236] Progress in the growth techniques for thin oxide films has increased the competence of the oxide semiconductors against conventional compound semiconductors. Therefore, oxide semiconductors have the potential to develop new functionalities for novel optoelectronic devices that are hard to realize with previously established semiconductor technologies. Many studies have emerged on the integration of oxide semiconductors and graphene for realizing higher performances or new features. In this context, two typical oxide semiconductors, TiO_2 and ITO, will be discussed in this section.

5.1. Titanium Dioxide (TiO_2) and Graphene

TiO_2 is frequently studied because it is abundant, low-cost, and, to some extent, environmentally benign as well as being an efficient and stable photocatalyst.[237] Its effectiveness has also been demonstrated in nanostructure and conductive coatings.[238−240] Basically, there are three main types of TiO_2 structures: rutile, anatase, and brookite. Zhang and Banfield pointed out that, for ultrafine TiO_2 particles, anatase is the most stable phase when the particle size is less than 11 nm, brookite is the most stable phase when the particle size is between 11 and 35 nm, and rutile is the most stable phase when the particle size is greater than 35 nm.[241] Accordingly, it is widely acknowledged that the thermodynamic phase stability of TiO_2 depends on the particle size when the particles are ultrafine, although the environment of the particles can play an important role in fixing the phase.[242,243] The rutile and anatase phases of TiO_2 have attracted a lot of attention, since they are related to the most practically oriented work. The band gap energies for rutile TiO_2 and anatase TiO_2 are estimated to be 3.0 and 3.2 eV, respectively.[242] This means TiO_2 can only be excited under irradiation of UV light at wavelengths of less than 380 nm,[244] which of course covers only ~5% of the solar spectrum.[245] With regard to photocatalytic performance, it was proposed to link the application of graphene materials with TiO_2, thus giving rise to the primary research area of TiO_2−graphene composites.

In an early work of the TiO_2−graphene composite nanostructures by Kamat and co-workers, they reported successfully carrying out the UV-induced photocatalytic reduction of GO.[246] Since charge separation takes place upon UV irradiation of the TiO_2 colloids in ethanol (alcohol), they suggested that the holes were scavenged to produce ethoxy radicals, thus causing the electrons to accumulate within the TiO_2 particles (reaction 3). The accumulated electrons would serve to interact with the GO sheets and then reduce certain functional groups (reaction 4).

$$TiO_2 + h\nu \rightarrow TiO_2(h + e) \xrightarrow{C_2H_5OH} TiO_2(e) + {}^{\bullet}C_2H_4OH + H^+ \quad (3)$$

$$TiO_2(e) + GO \rightarrow TiO_2 + RGO \quad (4)$$

They added GO, which was prepared using the Hummers method, into the TiO_2 colloidal suspension, and performed subsequent sonication for 30 min to finally produce the dispersion of GO sheets coated with TiO_2 nanoparticles (2−7

DOI: 10.1021/cr400607y
Chem. Rev. 2015, 115, 8294−8343

nm), as schematically shown in Figure 25. UV irradiation was carried out using an Oriel 450 W xenon arc lamp. The change

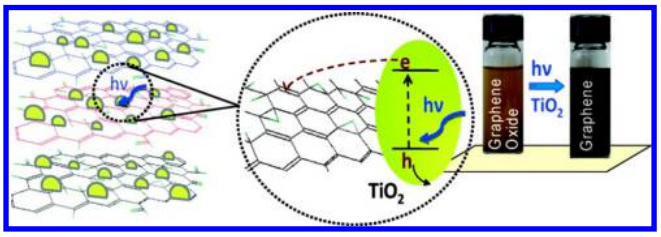

Figure 25. TiO_2–graphene composites and their response under UV excitation, with color change of the TiO_2 nanoparticles and GO before and after UV irradiation. Reprinted from ref 246. Copyright 2008 American Chemical Society.

in color from brown to black indicated the reduction of GO resulting from partial restoration of the π network within the carbonaceous structure.[247−249] In other words, the suspended GO in ethanol becomes chemically reduced as it accepts electrons from UV-irradiated TiO_2. Also, as a result of this particular work, it was suggested that the direct interaction between the TiO_2 particles and the graphene sheets would hinder the collapse of the exfoliated sheets of graphene. Recalling the features of typical group II–VI semiconductors previously discussed in this review, it is clear that the TiO_2 characteristics show great similarities with respect to photocatalysis. Taking into account the reduction of GO by photoexcited TiO_2, the Kamat group further investigated the ability of RGO to act as a 2-dimensional support to store and shuttle electrons. This work was based on their previous investigations into C materials, including CNTs, that are analogous to graphene.[250−252] They anchored TiO_2 and Ag nanoparticles at separate sites of a graphene sheet, and demonstrated that photogenerated electrons from UV-irradiated TiO_2 (~3 nm) were transported across RGO to convert Ag ions into Ag.[253] Also, the photocurrent generation of the TiO_2–RGO films was probed by depositing them as photoanodes onto an optically transparent electrode.[254] After irradiation by the UV light, the excited TiO_2 electrons were collected by the electrode. This resulted in a significant enhancement of the photocurrent (more than 90%) relative to that of the counterparts made from pure TiO_2 films. Such an effect was attributed to graphene's electron-accepting ability. Since graphene's zero-field conductivity (within the limits of the vanishing charge carrier concentration), σ_{min}, does not disappear, but instead exhibits values of the order of 4 e^2/h (close to the conductivity quantum e^2/h),[1,92,255] it is clear that graphene's electron-conducting ability is distinctively different from that of many other materials. It has also been demonstrated that the conductivity of graphene nanosheets is sufficient for antistatic applications. Even the conductivity (~7200 S m^{-1}) of relatively thick graphene paper at room temperature is comparable to that of chemically modified single-walled CNT paper.[87] In addition, this role of graphene

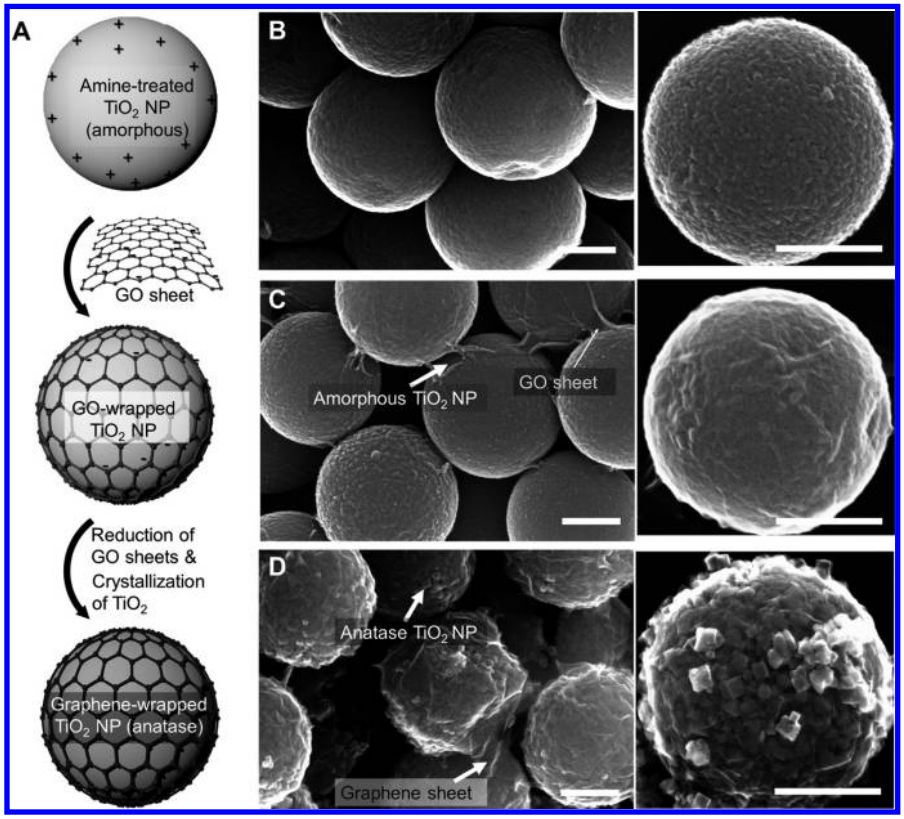

Figure 26. Synthesis steps for graphene-wrapped anatase TiO_2 nanoparticles (NPs) and corresponding SEM images. (A) Synthesis steps of graphene-wrapped TiO_2 nanoparticles. The surface of amorphous TiO_2 nanoparticles was modified by APTMS and then wrapped by GO nanosheets via electrostatic interaction. Graphene-wrapped anatase TiO_2 nanoparticles were synthesized through one-step hydrothermal GO reduction and TiO_2 crystallization. (B) SEM images of bare amorphous TiO_2 nanoparticles prepared by the sol–gel method. (C) SEM images of GO-wrapped amorphous TiO_2 nanoparticles. The weight ratio of GO to TiO_2 was 0.02:1. (D) SEM images of graphene-wrapped anatase TiO_2 nanoparticles. The scale bar represents 200 nm. Reprinted with permission from ref 266. Copyright 2012 John Wiley and Sons.

DOI: 10.1021/cr400607y
Chem. Rev. 2015, 115, 8294–8343

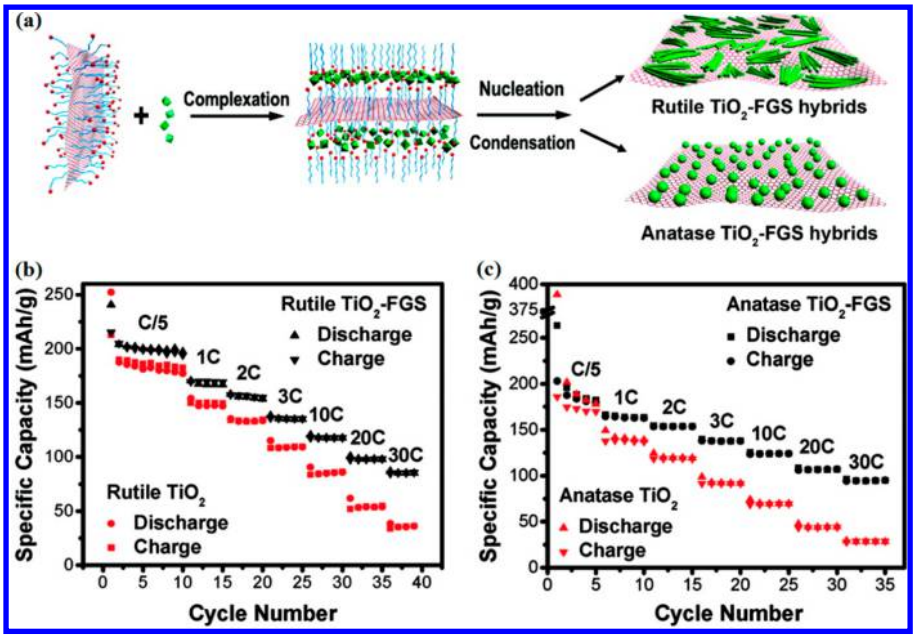

Figure 27. (a) Anionic sulfate surfactant-mediated stabilization of graphene and growth of self-assembled TiO_2–FGS hybrid nanostructures. (b) Specific capacity of the control rutile TiO_2 and the rutile TiO_2–FGS hybrids at different charge–discharge rates. (c) Specific capacity of the control anatase TiO_2 and the anatase TiO_2–FGS hybrids at different charge–discharge rates. Reprinted from ref 258. Copyright 2009 American Chemical Society.

acting as an active conductor or a conductive additive is reflected in the work performed by other groups on graphene–TiO_2 composites. For example, Zhang et al. demonstrated that the TiO_2–graphene system based on commercially available P25 nanoparticles and GO showed a better performance in the photodegradation of methylene blue than either P25 alone or the composites of P25–CNT.[256] Presumably, this was due to the excited electrons transferring more efficiently through TiO_2 to graphene.[257] Another relevant case showed that the use of graphene in hybrid nanostructures enhanced Li ion insertion/extraction kinetics in TiO_2.[258] This will be illustrated in Figure 27 and discussed in more detail below.

The role of graphene-based nanostructures in taking advantage of the photocatalytic activity of semiconductor nanoparticles has been employed in an ensuing range of studies exploring the properties of TiO_2–graphene composites. Akhavan et al. deposited GO platelets on anatase TiO_2 thin films, which induced photocatalytic reduction of the GO platelets with UV–vis light when the composites were immersed in ethanol.[259] The composite films were then utilized as nanocomposite photocatalysts for the degradation of *Escherichia coli* bacteria in an aqueous solution under solar irradiation. On such occasions, the photocatalytic and bactericidal activities of the TiO_2-based materials were improved by graphene with an increase in the electron transfer rate.[239,260,261] Noting that metal oxide semiconductors decompose carbonaceous bonds in the photocatalytic process,[109,262] the authors also physically attached TiO_2 nanoparticles (~15 nm), using Kamat's method, to chemically synthesized single-layer GO nanosheets, which were deposited between Au electrodes. The aim was to examine in more detail the behavior of the TiO_2–GO composite when exposed to UV irradiation.[263] The photocatalytic reduction was nearly completed after UV irradiation for 2 h and resulted in a significant increase in the graphitized sp^2 structure over the disorders in the GO. However, since the C content decreased in the local oxidation between the graphene and the photocatalyst, as a result of the UV irradiation, degradation of the reduced sheets appeared after the photocatalytic reduction. Thus, it was suggested that longer photocatalytic processes would cause a high increase in the resistivity, because of the photodegradation of RGO sheets. When TiO_2–graphene composites were synthesized using tetrabutyl titanate and GO with the assistance of calcination, the calcination atmosphere was shown to affect the photocatalytic activity.[264] A particularly decent performance was observed for those samples calcined in a nitrogen atmosphere. This was attributed to the existence of oxygen vacancies generated from the TiO_2 lattice during the calcination process.[265] These oxygen vacancies were supposed to act as electron traps for the photocatalytic reaction.

Alternatively, coating TiO_2 with graphene-related materials has also been shown to lead to enhanced photocatalytic activity. Early studies have demonstrated that graphite-coated TiO_2 composites show higher photocatalytic activity than the common TiO_2 photocatalyst (Degussa P25).[267,268] On the basis of this, Zhang et al. fabricated TiO_2–C core–shell structures through a hydrothermal method, using commercial TiO_2 and glucose as the starting materials.[269] They further graphitized the carbonaceous cages by calcination in a tube furnace at 800 °C in N_2. The surface hybridization of TiO_2 with graphite-like C layers a few nanometers thick yielded an efficient separation of electron–hole pairs under UV irradiation. This is because of the high migration efficiency of photoinduced electrons at the TiO_2–C interface. Recently, Lee et al. prepared graphene–anatase TiO_2 hybrid nanoparticles by wrapping amorphous TiO_2 nanoparticles with GO, followed by GO reduction and TiO_2 crystallization via a hydrothermal treatment.[266] The synthesis steps are shown in Figure 26. The GO-wrapped amorphous TiO_2 nanoparticles were made by coassembling positively charged TiO_2 nanoparticles with negatively charged GO nanosheets, which were reduced during the process. Presumably, due to the direct interaction between

DOI: 10.1021/cr400607y
Chem. Rev. 2015, 115, 8294–8343

the C and Ti atoms on the nanoparticle surface during the hydrothermal treatment, the TiO_2−graphene nanoparticles exhibited a red shift of the band edge and a reduction of the band gap (2.80 eV). This allowed more absorption of visible light and transfer of photogenerated electrons, and thus enhanced the photocatalytic activity under visible light. Incidentally, the band gaps of the samples were determined using the Kubelka−Munk function versus light energy (i.e., the relationship of $[\alpha h\nu]^{1/2}$ versus photon energy, where α is the adsorption coefficient), corresponding to the absorption spectra.[270] Since the combination of GO and TiO_2 nanoparticles in a core−shell structure maximizes the interfacial contact between them, the photocatalytic activity has great potential to exceed that of the TiO_2 nanoparticles loaded onto a larger graphene sheet.[271] Indeed, it was pointed out that the band gap of the TiO_2 nanoparticles (6−8 nm) attached onto single-layer GO sheets had to be even narrower than 2.43 eV to surpass the TiO_2−GO counterpart of P25 TiO_2 in visible light photocatalytic performances.[272]

Apart from the photocatalytic characteristic that attracts the most attention for TiO_2−graphene composites, TiO_2 has also shown active electrochemical performance that can be modified with graphene. Wang et al. have demonstrated that nanostructured TiO_2−graphene hybrid materials are better in terms of Li ion insertion/extraction kinetics than TiO_2.[258] Anionic sodium dodecyl sulfate (SDS) surfactants, which can adsorb onto graphene to form functionalized graphene sheets (FGSs) that highly disperse and interact with the oxide precursor,[273] were used to assist the stabilization of graphene in aqueous solutions and facilitate the self-assembly of in situ grown nanocrystalline TiO_2 (either rutile nanorods or anatase nanoparticles) with graphene, as shown in Figure 27a. Measurements revealed that, with the incorporation of FGSs, the specific capacity of TiO_2 in the hybrids increased for all tested charge/discharge rates compared with that of the control (pure) TiO_2, as shown in parts b and c of Figure 27. The cycle life of a rechargeable cell is a measure of the loss of capacity as the cell is fully charged and discharged numerous times.[274] Usually, it is characterized in percent loss over a number of cycles. For a battery that consists of one or more electrically connected rechargeable cells, the cycle life is related to the number of discharge−charge cycles the battery can undergo before it fails to meet certain performance criteria (battery failure) under specific charge and discharge conditions, such as temperature and humidity.[275,276] In this context, discharge is defined as an operation in which a battery delivers electrical energy to an external load and charge is an operation in which the battery is restored to its original charged condition by reversal of the current flow. That is to say, the charge−discharge process refers to the cycle of electricity passing through a rechargeable battery from a charger and afterward releasing it into the external electrical load. Since graphene has excellent electronic conductivity, the improved capacity at high charge−discharge rates is attributed to the increased electrode conductivity in the presence of the percolated graphene network embedded with TiO_2 electrodes. The FGSs used in this study of TiO_2−graphene hybrid materials[258] were prepared through thermal exfoliation of graphite oxide, during which the dried graphite oxide was rapidly heated (>2000 °C/min, up to 1050 °C) and split into individual sheets through the thermal expansion of evolved gases. These gases included to a large extent CO_2 generated from the decomposition of the oxygen-containing groups of the graphite oxide.[277] Because of the elimination of oxygen from the functional groups and any residual water during the rapid heating, an increase in the C/O ratio leads to the reduced GO state.[278] This also allows the C/O ratio to be tuned within a certain range, and thus, its conductivity can be increased to higher values. Similarly, thermal reduction was performed on the TiO_2−GO materials prepared via the hydrolysis of TiF_4 in the presence of an aqueous dispersion of GO, which led to the formation of anatase/rutile TiO_2−RGO.[279] However, in the photocatalytic chemical reduction the TiO_2 was shown to retain the anatase phase in the TiO_2−RGO composites. In fact, heating at high temperatures (up to 1100 °C) prompted the reduction of GO via restoration of the sp^2 structure,[280] and the TiO_2 in the composites was shown to have undergone a partial phase transformation from anatase to rutile. The onset temperature of the transition from anatase to rutile was determined to be between 700 and 750 °C.

The self-assembly approach mentioned in the paragraph above is relatively easy to perform, making it a potential pathway for the high-efficiency production of TiO_2−graphene composites. Further to this, a self-assembly process of TiO_2−graphene can also be performed using TiO_2 nanorods and GO sheets at the water/toluene two-phase interface. This is a result of the fact that the TiO_2 nanorods are prone to leave the organic phase after adhering to the GO sheets due to the coordination between the phenolic hydroxyls on GO and the TiO_2.[281] This means that the surfactants assisting the connection of TiO_2 and graphene during the assembly are replaceable with the two-phase process to furnish an alternative approach. In addition, direct growth of TiO_2 nanocrystals on GO sheets to prepare TiO_2−graphene composites has been reported in a two-step method.[282] Here, TiO_2 was coated onto GO sheets by hydrolysis and then crystallized into anatase nanocrystals by a hydrothermal treatment. The TiO_2 nanocrystals directly grown on graphene appeared to exhibit strong interactions with the underlying GO sheets since sonication did not lead to their dissociation from the sheets. This also triggered a 3-fold enhancement in the kinetics of the degradation reaction, under UV irradiation, of rhodamine B ($C_{28}H_{31}ClN_2O_3$) over P25. It is thus indicated that the photocatalytic performance of the TiO_2−graphene composites was improved because the strong coupling facilitated interfacial charge transfer (GO as an electron acceptor) and inhibited electron−hole recombination.[283]

Similar photocatalytic performances can be observed for composites based on graphene and another oxide semiconductor, Fe_2O_3, which is one of the simplest oxides. Natural Fe_2O_3 mainly occurs in two polymorphic forms: cubic γ-Fe_2O_3 and rhombohedral α-Fe_2O_3.[285] The α-Fe_2O_3 form (hematite) is the most stable iron oxide compound material, and has also been used as a photocatalyst.[286] Compared with TiO_2, α-Fe_2O_3 has a smaller band gap of ∼2.2 eV, which facilitates the optical absorption in the range of visible light.[287,288] However, α-Fe_2O_3 usually exhibits a weak performance in photocatalysis due to its short excited-state lifetime (∼10 ps), low mobility (less than 1 $cm^2\ V^{-1}\ s^{-1}$), and short hole diffusion length (2−4 nm), which can all significantly limit its efficiency in charge separation and collection.[289−292] It has been demonstrated recently that α-Fe_2O_3−graphene composites with well-defined distributions exhibit improved photocatalytic efficiencies over pure α-Fe_2O_3.[284] Comprising 2-dimensional α-Fe_2O_3 hexagonal nanoplates (∼200 nm) that are covered by reduced graphene oxide (RGO), as shown in Figure 28, the aforementioned composites

DOI: 10.1021/cr400607y
Chem. Rev. 2015, 115, 8294−8343

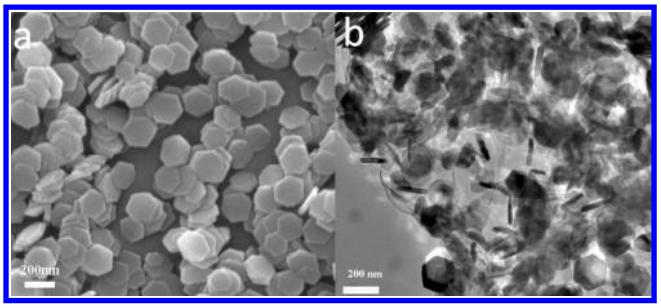

Figure 28. SEM image (a) of α-Fe_2O_3 hexagonal nanoplates and TEM image (b) of α-Fe_2O_3–RGO composites. Reprinted with permission from ref 284. Copyright 2014 John Wiley and Sons.

are synthesized through template-free hydrothermal methods. With such a combination of α-Fe_2O_3 and graphene, a record high photocatalytic activity for α-Fe_2O_3 in degrading rhodamine B (98% for the composites and only 66% for the pure α-Fe_2O_3 within 20 min of irradiation) has been achieved for the first time. The photocatalytic performances of the composites indicate enhanced electron transfer rates and prolonged lifetime of the photogenerated charge carriers. The role of graphene for α-Fe_2O_3, therefore, in terms of photocatalysis is believed to be similar to that for TiO_2, as previously discussed. This is despite their different band gap energies.

5.2. Indium Tin Oxide (ITO) and Graphene

Over the past decade, the substitution of ITO by graphene-based materials in transparent electrodes has been strongly supported by extensive research because of the superior transmittance and conductivity characteristics of graphene.[93,247,293,294] ITO for its part is a wide band gap semiconductor (3.5–4.3 eV) which shows high transmission in the visible and near-infrared regions of the electromagnetic spectrum.[295] Typical compositions of ITO are a solid solution of indium(III) and tin(IV) oxides, with In_2O_3 weighing 90% and SnO_2 weighing 10%. An ITO thin film sustains its chemical stability under a wide range of temperatures,[296,297] and can thus be used in harsh environments. Due to these unique properties, before ITO is completely superseded by graphene, if ever, it still shows considerable potential for producing hybrid materials with graphene, either to improve the quality of ITO or to support graphene.

Hong et al. fabricated composite films consisting of graphene and a prefabricated polymer, poly(styrenesulfonate)-doped poly(3,4-(ethylenedioxy)thiophene) (PEDOT–PSS), by spin-coating the aqueous mixture of 1-pyrenebutyrate (PB^-)-stabilized graphene and PEDOT–PSS on ITO at room temperature.[298] Since PEDOT–PSS is a conducting polymer with strong film-forming ability,[299,300] the composite films exhibited high electrocatalytic activity as counter electrodes. They catalyzed the reduction of I_2 to I^- after electron injection[301,302] in dye-sensitized solar cells (DSSCs), plus they exhibited high transmittance (>80%) at visible wavelengths. In such a working scheme, ITO acts as the substrate, without any thermal treatment, for the working electrodes (graphene/PEDOT–PSS), which show better performances than the commonly used catalytic electrode (Pt) or the polymer used alone. Similarly, graphene prepared from natural graphite with *p*-phenylenediamine (PPD) as the reducing reagent also exhibited high conductivity on ITO (about 150 S cm^{-1}): it was 6 orders of magnitude higher than that of GO and 4 orders of magnitude higher than that in the normal plane of the film.[303] This was due to the weak contact among the oriented graphene monolayers absorbing the residual PPD oxidation product. The role of ITO as a transparent conducting electrode can be further attuned by using graphene material when it is deposited on top of the ITO as the electron-blocking and hole-transporting layer. Li et al. used chemically derived GO on ITO anodes to decrease the recombination of electrons and holes and the leakage current for organic photovoltaics.[304] Poly(3-hexylthiophene) (P3HT) and fullerene derivative phenyl-C61-butyric acid methyl ester (PCBM) blends were placed on top of the graphene to provide sites for charge separation and bicontinuous pathways for efficient carrier transport at the interfaces of the acceptor nanostructures and the donor polymer matrix. It was reported that this resulted in high efficiency of the organic photovoltaics comparable to that of the devices fabricated with PEDOT–PSS as the hole-transporting layer. The incorporation of GO between the P3HT–PCBM layer and the ITO for the purpose of constructing the photovoltaic device structure is shown in Figure 29a. The corresponding energy levels of the components are shown in Figure 29b. It is worth noting that the injection of holes into the valence band of GO should be favored.

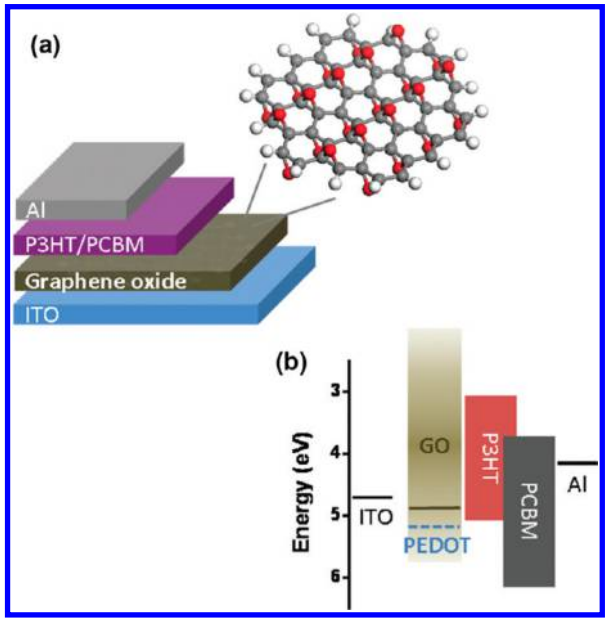

Figure 29. (a) Schematic drawing of the photovoltaic device structure consisting of the following: ITO/GO/P3HT–PCBM/Al. (b) Energy level diagrams of the bottom electrode ITO, the interlayer materials [(PEDOT–PSS, GO), P3HT (donor), and PCBM (acceptor)], and the top electrode Al. Reprinted from ref 304. Copyright 2010 American Chemical Society.

Also worth noting is the fact that when ITO is used as a working electrode, it can assist the reduction of GO through electrochemical methods. Liu et al. showed that a GO film (prepared using the Hummers method) deposited onto an ITO substrate using electrophoresis was electrochemically reduced in situ.[305] This was achieved by an electrochemical workstation involving a conventional three-electrode electrochemical system which consisted of a graphene film-coated ITO slide as the working electrode, a Pt wire as the counter electrode, and a Ag/AgCl reference electrode in saturated KCl solution. Before electrochemical reduction, the GO sheets, while undergoing the electrophoresis process, migrated toward the ITO anode under

DOI: 10.1021/cr400607y
Chem. Rev. 2015, 115, 8294–8343

a constant potential, where they eventually formed the GO film. Using a similar strategy, Feng et al. prepared a graphene/polyaniline (PANI) composite film using GO and aniline as the starting materials.[306] The main objective was accomplished through the electrochemical synthesis in a three-electrode system, with the ITO (or glass carbon electrode) as the working electrode, Pt as the counter electrode, and a saturated calomel electrode as the reference electrode. Since the GO/aniline suspension was cast onto ITO by spin-coating, the size of the film could be controlled by exploiting the area of the ITO. In addition, Zhuang et al. demonstrated that, as a result of the electrochemical reduction of functionalized GO deposited on ITO, electrons propagated with less scattering, thus giving rise to increased conductivity ($\sim 10^2$ S m^{-1}) of the composite material at room temperature.[307] Additionally, Das et al. noticed that the Raman spectra of mechanically exfoliated graphene on conducting ITO plates showed a lowering (a red shift) of the G mode frequency by ~6 cm^{-1}, compared to that (~1580 cm^{-1}) of bulk, highly oriented pyrolitic graphite (HOPG).[308] A softening (~20 cm^{-1}) in the 2D mode of the single- and few-layered graphene on ITO, compared to graphene on SiO_2 (~2682 cm^{-1}), was also observed. Since both the G and 2D bands are related to the physics of quantum electrodynamics, it was only estimated that the lowering of the frequency implies that, when deposited onto the conducting ITO substrate, the unit cell constant of the graphene layer was altered. On the other hand, there was a blue shift (~8 cm^{-1}) of the G peak position for single-layer graphene on the SiO_2/Si substrate due to charge impurities. Nevertheless, what was demonstrated is the possibility that the Raman spectra of graphene on the conducting ITO plate as well as on the SiO_2/Si substrate will shift with the number of graphene layers.

On the basis of the above discussions regarding the use of ITO as a supporting substrate for graphene, there are indications that the combination of ITO and graphene can also be used to support other materials, such as metal particles, to improve their activity and performance. As a matter of fact, metal oxides, such as for ITO, have adequate stabilities in oxidizing environments.[310,311] This further supports the feasibility of using ITO in supporting metal particles, when electrochemical processes are involved. To minimize the instability that may be caused by the high surface area and any coarsening in long-term operations, Kou et al. synthesized ITO nanocrystals (10–12 nm) directly onto functionalized graphene sheets (thermally exfoliated),[278] triggering the formation of ITO–graphene hybrids. This is shown in Figure 30a,b. The ITO–graphene hybrids were then deposited with Pt nanoparticles (~2 nm) to form the Pt–ITO–graphene triple-junction structures (see Figure 30c–f).[309] Investigations showed that the Pt nanoparticles were preferentially located at the junctions between the ITO and the graphene. These Pt–ITO–graphene triple junctions were found to be more thermodynamically favorable than isolated Pt and ITO clusters on the graphene sheets. This conclusion is supported by the authors' periodic density functional theory calculations, which provided information on the interfacial binding. The strong interactions improved the activity and stability of the Pt nanoparticles on the ITO–graphene hybrid, which in turn led to higher activity than that of other C counterparts such as Pt–CNT hybrids. With such strong stability and activity, the Pt–ITO–graphene may even prove a promising electrocatalytic material for oxygen reduction, not to mention that the graphene substrate would also be very resistant to oxidation.

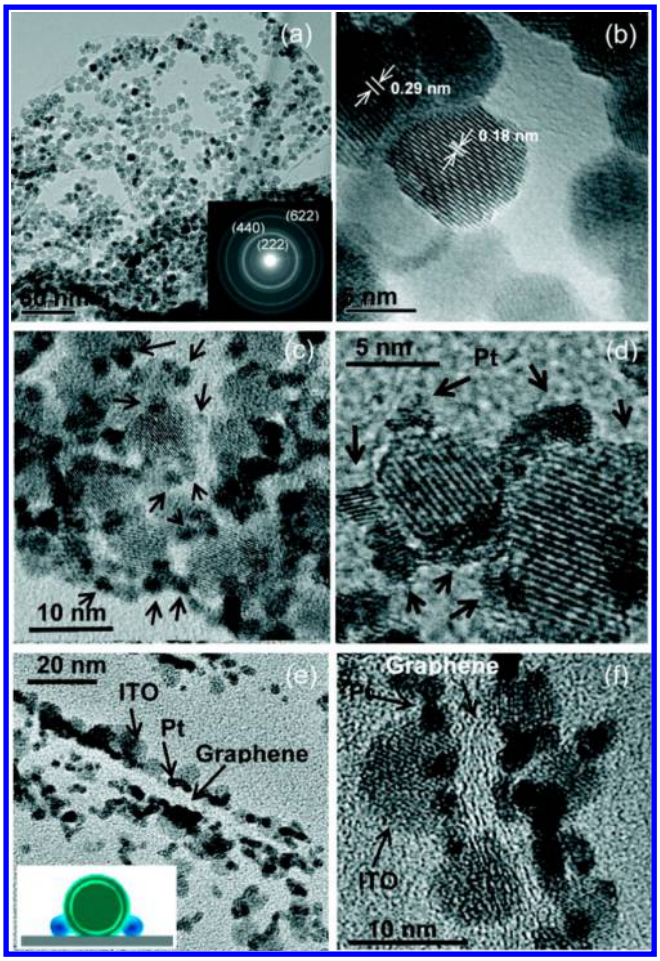

Figure 30. TEM images of ITO nanoparticles (NPs) on graphene sheets (a, b), TEM images of Pt–ITO–graphene (c, d), and cross-sectional TEM images of Pt–ITO–graphene (e, f). Inset: schematic structure of a Pt–ITO–graphene nanocomposite. Reprinted from ref 309. Copyright 2011 American Chemical Society.

6. INTERPLAY BETWEEN INORGANIC SEMICONDUCTORS AND GRAPHENE

From the above sections, readers have hopefully noted that the way graphene and inorganic semiconductors are associated is fairly dependent not only on the nature of the semiconductor group, but also on the end purpose of the association and ultimately the application. It leads to a subtle interplay between graphene and the inorganic semiconductor. This can be framed from two aspects. First, so far, about 4–5 principal methods for graphene production have been reported. In addition, there are several other methods that are either less accessible or infrequently used. It is well-established that the form of the graphene will vary in accordance with the synthesis method. This in turn, of course, further affects the chemical and physical characteristics of the graphene produced. A typical example mentioned earlier in this review is the fact that graphene epitaxially grown from SiC is different, in terms of its interlayer structures and the operating conditions during the production, from mechanically exfoliated graphene. Another example is the visibility of graphene, which depends on the number of graphene layers deposited onto a particular substrate. Nevertheless, this does not necessarily mean that multilayered graphene is preferable, however good its visibility, to single-layer graphene. Second, what can be confidently stated is that,

DOI: 10.1021/cr400607y
Chem. Rev. 2015, 115, 8294–8343

since the nanostructures of inorganic semiconductors for use in solid-state electronics exist in various phases and dimensions, the structure as well as the synthesis method of the graphene will need to match the inorganic semiconductor involved, both physically and chemically. This is necessary to make the hybrid material achieve or improve a particular function. It is essential, therefore, to examine the effect of the synthesis techniques on both the graphene and the inorganic semiconductors. This is in addition to the intense efforts needed to improve the industrial processing routes for efficient combination. On the basis of this, not only the interplay between conjugated graphene and inorganic semiconductors, but also the optimization of the arrangement for the combination needs to addressed.

6.1. Synthesis of Graphene

6.1.1. Mechanical Exfoliation or Cleavage. It was only after reports of mechanically exfoliated graphene appeared that the massive production of single-layer graphene was initiated. Such mechanical exfoliation techniques involve repeatedly cleaving a graphite crystal, on the top of which small square mesas are prepared using an oxygen plasma.[10] Highly oriented pyrolytic graphite (HOPG) sheets, which are commercially available, are frequently used as the starting material. To cleave the mesas off the HOPG sample and then facilitate the peeling of graphite flakes off the mesas using Scotch tape, one has to press the mesa-structured surface onto a photoresist and apply a thermal treatment. Thin flakes consisting of single- or few-layered graphene left in the photoresist can then be released in acetone, and subsequently captured onto Si wafers with the SiO_2 layer on the top.

One of the disadvantages of the mechanical exfoliation is that, due to the fact that the graphene solutions in acetone are more than likely to be mixed with both single- and few-layered graphene sheets, to obtain a single-layer graphene sheet, success depends on a fortuitous encounter. Also, manual peeling-off of graphite is repetitive labor-intensive work. However, an advantage is that mechanical exfoliation is easy to perform in that it does not require any special environment or apparatus. The captured graphene sheet on the SiO_2/Si substrate can be tuned for better contrast. In fact, despite the low production of mechanical exfoliation, many graphene properties have been evaluated using the mechanically exfoliated graphene (Figure 31).[312] Because of the high quality of the original single-crystal graphite source, the graphene produced using mechanical exfoliation retains high electrical and mechanical properties.[313]

Figure 31. Mechanical exfoliation of graphene using Scotch tape from HOPG. Reprinted with permission from ref 312. Copyright 2011 Elsevier.

Nevertheless, clearly this approach is not suitable for the large-scale production of graphene, and hence, it is necessary to look into other options. Alternative strategies, including, among others, the epitaxial growth of graphene layers on SiC through sublimation and the direct growth of graphene (needing transfer afterward) onto metallic substrates through CVD, have already been noted in discussions in the previous sections.

6.1.2. Epitaxial Growth. Some early reported research work on graphite formation demonstrated that heating either the C-face or the Si-face on 6H-SiC (0001) and $(000\bar{1})$ surfaces to temperatures between 1000 and 1500 °C in ultrahigh vacuum (UHV) caused sufficient sublimation of the Si to leave behind a C-rich surface.[58] It is clear that graphene-like structures formed on the two polarized surfaces are adequately distinguishable. In addition to the fact that graphene growth on the Si-face is much slower compared with that on the C-face, Si-face graphene is epitaxial with an orientational phase rotated 30° relative to the SiC lattice, while the C-face film can have multiple orientational phases.[314] The orientational disorder in C-face grown graphene sheets under UHV limits their appeal for most studies on structure, growth, or electronics. However, it has been demonstrated that preparing the epitaxial growth in an evacuated radio frequency (RF) induction furnace, rather than in UHV, improves the quality of the graphene-based films grown on the C-face of 4H-SiC.[11] In the furnace environment, the minimum graphitization temperature is 1420 °C, which is somewhat higher than the minimum graphitization temperature required to grow graphene in UHV on C-face SiC.[315] The graphitization performed for 5−8 min in the furnace under a pressure of 3×10^{-5} Torr produces 4−13 graphene layers. In fact, the graphene film thickness can be adjusted by controlling both the growth temperature and the growth time. The coherent domains for the furnace-induced C-face graphite are more than 3 times higher than those for the UHV-induced Si-face graphite. This correlates with the high carrier mobility of up to 27 000 $cm^2\ V^{-1}\ s^{-1}$ measured for the overlapped C-face graphene and the low carrier mobility of ∼1000 $cm^2\ V^{-1}\ s^{-1}$ measured for the Si-face graphite films.[59]

Epitaxial growth leads to the production of graphene-based films on SiC substrates without any transfer process, and this is desirable for the subsequent work of producing semiconductor devices. Kedzierski et al. fabricated arrays consisting of hundreds of epitaxial graphene transistors on a single SiC chip over many square millimeters.[316] The mobility in this case approached 5000 $cm^2\ V^{-1}\ s^{-1}$ and the on/off current ratios up to 7. Since these results corresponded to the C-face graphene films grown in an RF furnace, this indicates that not only is the long-range oriented order achievable in furnace-grown epitaxial graphene on SiC, but also the graphene properties can be sufficiently preserved for the transport in semiconductor devices made from furnace-grown C-face films.

6.1.3. Chemical Vapor Deposition. Subsequent to the success of mechanical exfoliation and epitaxial growth techniques, CVD-based methods have also been introduced for the production of graphene. A CVD process often involves exposing the selected substrate to a gaseous precursor for the purpose of depositing high-purity solid materials, and chemical reactions are normally involved. In the semiconductor industry, it is frequently used to produce thin films. CVD-based methods are widely used in microfabrications to deposit materials in various forms. The formation of "monolayers of graphite", through decomposition of C_2H_2 and C_2H_4 on hot surfaces, dates back to the 1960s.[317] Almost 40 years later, in 2006, the

DOI: 10.1021/cr400607y
Chem. Rev. 2015, 115, 8294−8343

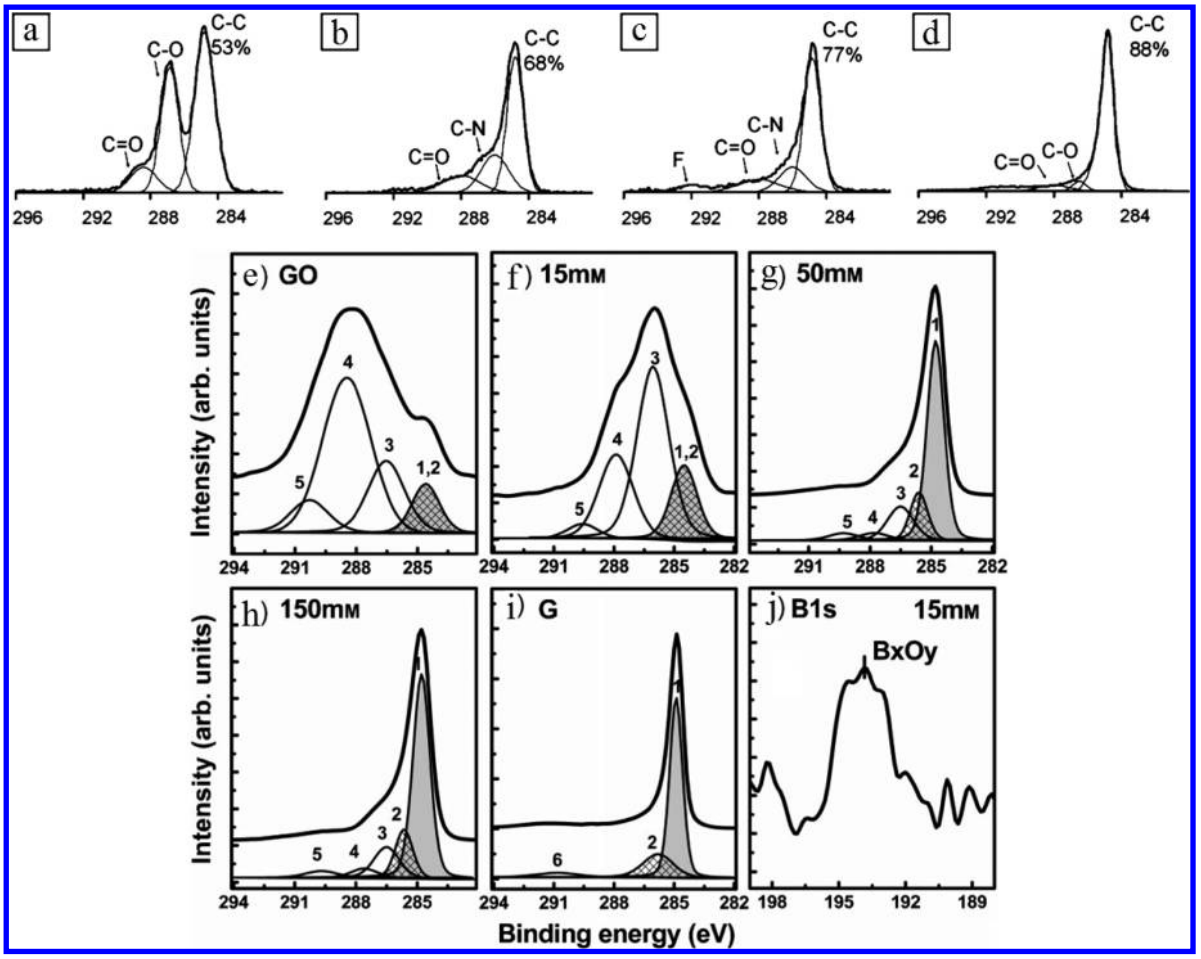

Figure 32. XPS analysis of the effect of different reduction treatments on the GO films. For panels a–d, deconvolution reveals the presence of C–C (~284.8 eV), C–N (~285.7 eV), C–O (~286.2 eV), and C═O (~287.8 eV) species in the film. The percentage of deoxidized carbon (C–C, ~284.5 eV) in each film is indicated in the figure. (a) Nonreduced film. (b) Hydrazine-vapor-treated film. (d) Hydrazine vapor plus annealing at 400 °C. (d) Thermal annealing at 1100 °C in vacuum. The significant C–N signal in panels c and d suggests formation of hydrazone groups during the hydrazine treatment. The F signal at ~292 eV, most evident in panel c, is caused by contamination from the vacuum system. (e) C 1s peak in the XPS spectra of GO. (f–i) RGO obtained using 15 mM (f), 50 mM (g), and 150 mM (h) $NaBH_4$ and (i) graphite. The curves were fitted considering the following contributions: C═C (sp^2, peak 1), C–C (sp^3, peak 2), C–O/C–O–C (hydroxyl and epoxy groups, peak 3), C═O (carbonyl groups, peak 4), O—C═O (carboxyl groups, peak 5), and π–π^* (peak 6). (j) B 1s peak in the XPS spectrum of RGO obtained using 15 mM $NaBH_4$. Images a–d reprinted from ref 247. Copyright 2008 American Chemical Society. Images e–j reprinted with permission from ref 327. Copyright 2009 John Wiley and Sons.

first report on the successful synthesis of few-layer graphene films using CVD was published.[318] A natural hydrocarbon source, camphor, was thereof used to synthesize graphene (from camphor pyrolysis) on Ni substrates. Such graphene films were prone to folding, and the minimum layer number in the films was 20. This study, however, opened up a new processing route for graphene synthesis in spite of the fact that the folding behavior of the film and the overlapping of graphene layers were yet to be solved.[319]

Recent achievements in graphene growth using CVD have confirmed the reproducibility of the graphene production on a relatively large scale and the successful transfer to many other substrates. It was previously discussed that the decomposition of hydrocarbons into graphitic materials through CVD methods can also be well catalyzed on Si and Cu substrates. Some other metallic substrates used to support the graphene synthesis through CVD include those made from Pt and Ru.[320,321] After chemical etching, the metallic substrate is removed from the graphene film(s), which then can be transferred to another substrate. Indeed, judicious transfer procedures from the metallic substrate demonstrate that it is possible to transfer large-area (~cm^2) graphene films, either single-layer or few-layer, onto any arbitrary substrate.[322] This indicates that CVD techniques are most promising for the large-scale production of graphene films. In addition, graphene doping is made possible by introducing a specific gas, for example, NH_3, during the CVD growth.[323] In this case, depending on the doping configuration within the sublattices, the nitrogen atoms alter the physicochemical properties, as well as the tolerance to external stimuli, of the doped graphene.[324] Furthermore, the growth temperature can be lowered even further when a plasma is used to enhance the CVD for the graphene production. Under these circumstances, the electric field direction caused by the plasma sheath will result in the vertical growth of graphene against the substrate surface.[325,326] This creates another possible approach for the mass production of freestanding few-layer graphene by means of plasma-enhanced CVD (PECVD).

6.1.4. Chemical Derivation. In 1958, Hummers and Offeman's work on the preparation of graphite oxide was briefly

DOI: 10.1021/cr400607y
Chem. Rev. 2015, 115, 8294–8343

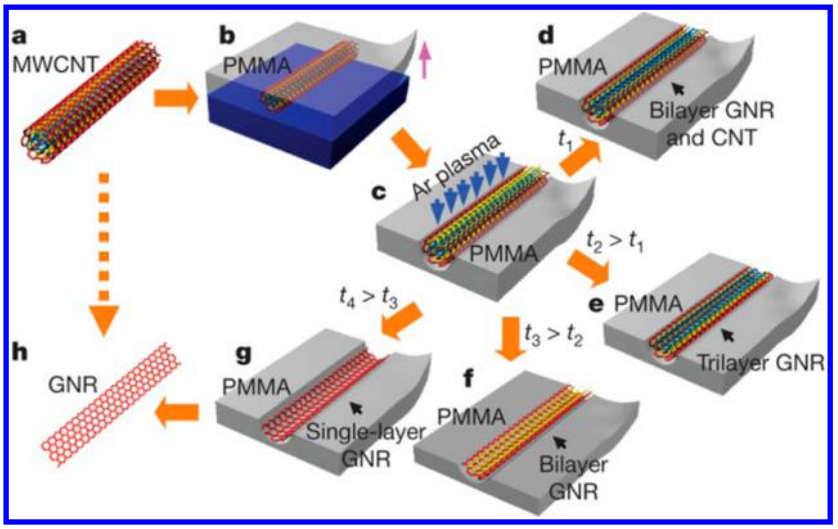

Figure 33. Making GNRs from CNTs. (a) A pristine MWCNT is used as the starting raw material. (b) The MWCNT is deposited on a Si substrate and then coated with a PMMA film. (c) The PMMA–MWCNT film is peeled from the Si substrate, turned over, and exposed to an Ar plasma. (d–g) Several possible products are generated after etching for different times: GNRs with CNT cores are obtained after etching for a short time t_1 (d); tri-, bi-, and monolayer GNRs are produced after etching for times t_2, t_3, and t_4, respectively (e–g) ($t_4 > t_3 > t_2 > t_1$). (h) The PMMA is removed to release the GNR. Reprinted with permission from ref 334. Copyright 2009 Macmillan Publishers Ltd.

reported.[94] They introduced a rapid and relatively safe method compared to its predecessors. The process was completed by treating the graphite with an anhydrous mixture of sulfuric acid, sodium nitrate, and potassium permanganate at temperatures below 45 °C for a couple of hours. Since it did not involve potassium chlorate, which was replaced by potassium permanganate, the constant hazard of explosion was avoided. Recently, with the assistance of X-ray and electron diffraction, the complete oxidation process has been monitored using the total disappearance of the 0.34 nm inter-graphene spacing and the appearance of a new one within the 0.65–0.75 nm range, depending on the water content of the graphite oxide.[278] Subsequently, few-layer or even single-layer graphene can be obtained by decomposing the intercalated graphitic sheets through a thermal expansion process, during which a large amount of gases, mainly CO_2, will be generated in the van der Waals space. The graphite oxide can be further separated by using ultrasonic treatment to form individual GO sheets. Thermal expansion is thus believed to be an essential step for the successful splitting of graphite oxide into single graphene sheets.

Phenol, carbonyl, and epoxy moieties are introduced during the oxidative intercalation, and this accounts for the colloidal stability of the GO suspension.[313] Therefore, as a single-sheet platform, GO has the potential for further chemical derivatization. Its electronic properties are different from those of the individual semimetallic graphene layers obtained through mechanical exfoliation. In fact, the structural defects cause the electronic structure of GO to be semiconductive. To restore the pertinent properties of graphene, chemical reduction of the GO is needed. Typical reduction reagents include hydrazine[328] and sodium borohydrate.[327,329] The color of the well-dispersed RGO in water turns from brown to black. In addition, because of the removal of oxygen atoms, RGO becomes less hydrophilic. However, currently, the complete chemical reduction of GO is not realizable, and the resulting material is only a transitional product between graphene and GO. XPS studies indicate that, on one hand, chemical reduction using hydrazine or thermal annealing (up to 1100 °C) performed subsequent to the splitting does not regenerate the exact graphene structures. This is shown in Figure 32a–d. On the other hand, $NaBH_4$ reduction forms residual hydroxyl functional groups, as shown in Figure 32e–j. As a result, when the original structure of graphene is essential, chemical derivation is ruled out and physical exfoliation should be pursued. Nevertheless, RGO processing is relatively straightforward, and the reasonable conductivity and transparency make the RGO thin films a possible component for transparent conductors in the future.[87,88]

6.1.5. Additional Approaches. Apart from the mechanical peeling of graphite flakes by means of Scotch tape, treating graphite dispersions in a proper liquid solution, with ultrasonication, constitutes another type of physical exfoliation. It was first reported by Hernandez et al. that dispersing graphite into some solvents, such as *N*-methylpyrrolidone (NMP), led to exfoliation of graphene sheets.[330] The exfoliation was ascribed to the strong interaction between graphite and the amides from the solvent. This is similar to the corresponding characteristics of single-walled CNTs in amide solvents.[331] For graphite, the surface energy was defined as the energy per unit area required to overcome the van der Waals forces when peeling two sheets apart. Since the energy balance is expressed as the enthalpy of mixing, a minimal energy cost of exfoliation was expected from solvents the surface energy of which matches that of graphene. For these solvents, it was proposed that the energy required to exfoliate graphene would be balanced by the solvent–graphene interaction, and therefore, the ultrasound and charge transfer between the amide and the graphite would allow the exfoliation to take place. Indeed, the absence of defects or oxides was confirmed by the authors using X-ray photoelectron, infrared, and Raman spectroscopies, thus indicating that the solvent-exfoliated C sheets were genuine graphene. Similarly, crystals of natural graphite were exfoliated by sonication in dimethylformamide (DMF), resulting in a suspension of thin graphitic platelets with a large proportion of single-layer graphene flakes.[332] Centrifugation removed any large thick flakes, leaving the remaining suspensions with mainly well-dispersed graphene and few-layer graphite flakes. It

DOI: 10.1021/cr400607y
Chem. Rev. 2015, 115, 8294–8343

appears that such exfoliation products exhibit features analogous to those from the chemical exfoliation. However, because of the absence of the oxidation step, the liquid-phase (wet) exfoliation does not suffer from the limitation of defects and degradation of electrical properties. The disadvantage of the liquid-phase exfoliation is largely the cost of the solvent. The liquid-phase exfoliation for the production of graphene can nonetheless be accomplished in water, provided that effective surfactants, for example, those made of sodium dodecylbenzenesulfonate (SDBS), are adsorbed onto the individual single-layer graphene to stabilize the dispersion against aggregation.[333] This occurs typically on account of electrostatic (Coulomb) repulsion between the surfactant-coated graphene flakes. For the above-mentioned liquid-phase exfoliations, the graphene suspensions/dispersions need to be deposited with the assistance of a thermal treatment onto the solid substrates to obtain dry graphene. These products, however, will be prone to overlapping of individual flakes or sheets.

Another route adopted to produce functionalized graphene sheets is related to the thermal expansion of graphite oxide. This has been previously mentioned in the discussions of hybrid materials of oxide semiconductors and graphene.[277,278] It begins with treating natural graphite flakes in an oxidizing solution of sulfuric acid, nitric acid, and potassium chlorate, similar to the Hummers method. On completion of the reaction, the mixture is added to excess water, washed with HCl, and then repeatedly washed with water until the pH of the filtrate becomes neutral. The fundamental prerequisites that enable this preparation of single-layer graphene sheets are complete oxidation of the graphite and extremely rapid heating of the graphite oxide. The latter splits the graphite oxide into individual sheets through evolution of CO_2. As the thermal energy evolved from the decomposition of the hydroxyl and epoxide groups of graphite oxide heats the sample, it allows for faster reaction rates and higher internal temperatures. This ensures sufficient rapid pressure buildup for uniform exfoliation. It has also been demonstrated that unfurling CNTs can lead to the production of graphene. Jiao et al. utilized an approach for making graphene nanoribbons (GNRs) by opening multiwalled carbon nanotubes (MWCNTs) through the plasma etching of nanotubes partly embedded in a polymer (PMMA) film. This is shown in Figure 33.[334] Mono-, bi-, and multilayer GNRs and the GNRs with inner CNT cores were produced depending on the diameter and layer number of the starting MWCNTs as well as the etching time. A similar approach for cutting MWCNTs open was performed in a solution-based oxidative process.[335] During this procedure the attachment of permanganate to adjacent C atoms made the nanotubes unravel. It is inevitable that edge scattering due to the restrained size of the nanotubes and the residual oxidized defect sites, which are created in the unfurling methods, will cause inferior electronic characteristics of the graphene products, compared with those of mechanically cleaved large sheets of graphene. Nevertheless, since the shell number and diameter of the starting CNTs can be modulated, this type of method offers a new way of producing graphene with adjustable structures. Indeed, there are alternative methods, including the organization of molecules,[336] for obtaining graphene-based materials. Due to complex procedures as well as low compatibility, these methods are, however, infrequently used for the production of graphene-based hybrid materials with common inorganic semiconductors.

6.2. Association of Inorganic Semiconductors and Graphene in Connection with Synthesis Methods

The association of inorganic semiconductors and graphene is essentially reflected in the way in which they are connected. A reasonable combination is based on the careful consideration of many aspects. These include the synthesis methods for both the graphene and the semiconductors, the particular group of semiconductors and their corresponding properties, the structure of the graphene products, and the intended application of the hybrid material. Achieving a complex function requires the integration of a number of properties, in particular, mechanical robustness, electrical conductivity, and chemical stability. The implementation of high-quality hybrid materials of inorganic semiconductors and graphene depends on the synergic delivery of the above-mentioned properties to a specific objective. For example, it is unwise to use oxidized graphene for chemically and physically demanding applications, whereas the value of freestanding graphene produced at much greater expense will not be fully realized if the hybrid materials are randomly mixed. Therefore, to construct an effectively associated heterogeneous structure, the characteristics of the semiconductor as well as its specific form set a certain constraint on the pattern of the graphene products. The use of graphene itself is such as to support any application of the semiconductors to one or more particular areas.

The single-layer graphene sheets obtained by mechanical exfoliation possess high mechanical strength and electrical conductivity, which are essential for extremely harsh and strict working conditions. This means that the hybrid materials of as-obtained graphene and Si, which is a typical representative of the group IV elemental semiconductors, are particularly attractive. The semiconducting Si normally withstands high temperatures and electric demands without becoming dysfunctional. This facilitates the use of such hybrid materials for building high-power integrated circuits. In the semiconductor industry, pure monocrystalline Si is often employed for the production of Si wafers used in electronics. In a hybrid system based on graphene and Si, a wafer of monocrystalline Si serves as a mechanical support for the graphene. Indeed, to ensure reliable visibility of the hybrid material, single-layer graphene made by mechanical exfoliation must be insulated from the wafer by a thin layer of SiO_2. Under certain conditions, this can be obtained by exposing the element to oxygen. Similar visibility can be observed for substrates employing the group III−V compound semiconductors of GaAs and AlAs. This is possible despite a much lower insulating barrier than that of SiO_2/Si substrates. Arranging a GaAs−AlAs multilayer structure with a manipulated sequence of AlAs and GaAs layers leads to a sizable graphene contrast. Since GaAs has a higher electron mobility than Si, which of course allows GaAs transistors to function at high frequencies, the influence of GaAs on the transport properties of graphene delivered through the interface between GaAs and graphene is more positive. Another group III−V compound semiconductor, BN, is expected to be an even better support for mechanically exfoliated graphene. This is because h-BN, one of its various crystalline forms, is analogous to graphite from a structural perspective. It consists of equal numbers of boron and nitrogen atoms that are sp^2-bonded within 2-dimensional layers. At the atomic scale, the surface of h-BN is smooth, making it a very reliable substrate that does not adversely affect the quality of graphene resting on it. The result, therefore, is a higher mobility of mechanically exfoliated graphene on h-BN substrates than on SiO_2/Si substrates.

DOI: 10.1021/cr400607y
Chem. Rev. 2015, 115, 8294−8343

Besides, for those group III−V semiconductors that can be deposited as a thin film, the purpose of supporting the graphene is not only to serve as a mechanical support. Integration of mechanically exfoliated graphene onto the GaN thin film deposited on a substrate, which is typically made of either sapphire or SiC, can enhance the performances of GaN. It also provides more features for the intended range of device applications. In fact, although wide-band GaN can be grown on mechanically exfoliated graphene, an intermediate layer or structure is needed for growth between GaN and graphene, because of the weak interaction.

In the case of the group II−VI compound semiconductors and metal oxides, the structural forms in which they are found are mostly 0-dimensional and 1-dimensional on the micro- and nanoscales. Hybrid materials based on mechanically exfoliated graphene and these semiconductors tend to be arranged as multidimensionally heterogeneous structures. This in turn may lead to multifunctionality and unique physical properties. The band gaps of frequently utilized group II−VI semiconductors are direct, causing high radioactivity. Because of these wide band gaps, the prototypical II−VI semiconductors in such hybrid materials alleviate the negative zero-gap influence intrinsically associated with mechanically exfoliated graphene. The nucleation of group II−VI semiconductors on the surface of stabilized graphene sheets made by mechanical exfoliation is comparatively active at the step edges. This is similar to the case of group III−V semiconductor GaN. The high mobility of graphene prevents fast recombination of electrons and holes produced out of the radiated II−VI semiconductors that are grown on the graphene surface. The II−VI semiconductors, on the other hand, endow more semiconducting characteristics onto the coupled graphene. This feature is applicable not only to the hybrid materials based on the group II−VI semiconductors and the graphene products made using CVD techniques, but also to their counterparts involving several metal oxides. Under UV light, TiO_2, the naturally occurring oxide semiconductor of titanium, particularly in its anatase form, is a photocatalyst. In the photogenerated catalysis resulting from the hybrid materials of graphene and TiO_2, electron−hole pairs are created in the photocatalytic TiO_2. This generates free radicals that are able to undergo further reactions with the graphene. On the nanoscale, TiO_2 also produces electricity under the influence of light. For heterogeneous structures, with TiO_2 resting on mechanically exfoliated graphene, the electrons generated from the TiO_2 are collected by the graphene, and this enhances the photocurrent. The photoinduced activity of TiO_2 is very close to that of some group II−VI semiconductors, such as ZnO and ZnS. In addition, their band gaps are roughly in the same range, which means that TiO_2 and the relevant group II−VI semiconductors show great compatibility. This allows them to be combined together to make hybrid materials with graphene. The role of the combined oxide semiconductor ITO with respect to the mechanically exfoliated graphene in such hybrid materials is, however, as a solid supporting substrate. Since the conducting ITO substrate shows electrical and constitutional characteristics different from those of the insulating SiO_2 layer on the Si, it subtly prompts distinct evolvement in spectral emissivity of the exfoliated graphene sheet(s) physically propped on top.

It is obvious that the size of mechanically exfoliated graphene is limited by the area of mesas from which the graphitic flakes are obtained. Production of relatively large-scale graphene films has to be either independent of the size of the sources or accomplished using a large substrate. As a result, the graphene films synthesized via CVD methods with hydrocarbon gases, such as CH_4 and C_2H_6, as the C source push the progress toward practical applications. Under suitable temperature and pressure, a low concentration of C in the hydrocarbon source, such as CH_4, leads to the growth of single-layer graphene. Larger hydrocarbon gases with high concentrations of C will lead to the production of multilayer graphene. Apart from the metallic substrates, Ni and Cu, whose atomic structures have high and low solubilities of C,[312] respectively, Si constitutes a typical semiconductor substrate for the CVD growth of graphene. However, unlike the absorption of C atoms into the Ni thin film at high temperatures and the subsequent separation of the graphene layers on fast cooling,[322,337] or the catalytic decomposition of CH_4 by the active Cu surface only with minimal C diffusion into the Cu film,[30] the mechanism for CVD growth of graphene on Si begins with a surface reaction. Despite its limited thickness, native oxide naturally grown on Si decomposes at high temperatures, leaving reactive Si atoms with free dangling bonds on top. The C atoms decomposed from CH_4 are secured by the dangling bonds and accumulate to form graphene. Since Si carbonization, rather than graphene formation, is found in the temperature range from 1000 to about 2500 °C, the simultaneous production of individual graphene and Si phases in an optimized fashion must be triggered at a fairly high temperature but below 1000 °C.[29] It should nevertheless be noted that although the CVD growth of graphene on Si makes a reasonable breakthrough without using any metal catalysts, the fairly high-quality graphene sheets made from metal-catalyzed CVD are mostly compatible with Si wafers as well. However, an additional transfer process from metallic substrates is needed. As pointed out earlier, the number of graphene layers is hard to control under these circumstances. This issue is also relevant to epitaxially grown graphene on SiC. The advantage of hybrid materials based on epitaxial graphene grown out of SiC is that transferral of the graphene can be avoided. Hence, SiC is a frequently employed group IV compound semiconductor. Its endurance under high temperatures (over 2500 °C) and pressure and its chemical inertia make SiC useful for bearing high-quality graphene. Actually, not only does it act as a platform as well as a high-purity resource for the epitaxial growth of graphene, SiC can also be integrated with the graphene grown on it as a substrate into a practical circuit for electronic devices. Long-range orientation of few-layer graphene is also obtainable by judicious choice of the growth environment, which corresponds to the production of few-layer graphene with scalable control. The electron transport properties of the mechanically exfoliated graphene can be adequately preserved in the epitaxial graphene.

For the group II−VI semiconductors, CVD graphene makes up a platform large enough to grow uniform 1-dimensional nanomaterials. The smooth surface morphology of graphene resulting from its atomic structure is a facilitator for the orientation of semiconductor vertical growth. ZnO is the most investigated II−VI semiconductor for this type of structure involving 2-dimensional CVD graphene. In such a heterogeneous structure, CVD graphene serves as the transparent and flexible electrode, while the 1-dimensional ZnO nanostructures yield mechanically flexible electronic components. Those 1-dimenional ZnO nanostructures with larger specific surface areas, such as nanotubes and hollow nanowires, can even improve the optoelectronic performances. The role of graphene as a growth template/platform is similar for the 1-dimensional

DOI: 10.1021/cr400607y
Chem. Rev. 2015, 115, 8294−8343

nanostructure of the oxide semiconductor TiO_2, which not only provides mechanical flexibility but also, in return, imparts photocatalytic activity to the hybrid materials containing CVD graphene. The photoinduced properties are typically reflected in the heterogeneous nanostructures between the 0-dimensional nanostructures of the relevant semiconductors and the chemically exfoliated graphene. On the contrary, the group III−V compound semiconductors are apt substrates for CVD graphene, although the compatibility to grow group III−V compound semiconductors on CVD graphene is somewhat limited, as previously discussed. In this regard, the association of CVD graphene with the III−V semiconductor h-BN, which can be produced via mechanical exfoliation and CVD, is particularly interesting and "natural", because of their analogous structures. On one hand, the high-purity crystals of h-BN obtained by mechanical exfoliation are large enough for CVD graphene to rest on while retaining their high mobility. This indicates that the choice of the substrate is a key issue for achieving scalable high-mobility CVD graphene. On the other hand, since both the graphene and the h-BN layers can be independently grown using CVD on metallic substrates, by combining the CVD growth processes for graphene and h-BN, stacked structures with an adjustable growth sequence of graphene/h-BN layers are realizable.

The characteristic of chemically exfoliated graphene is the double-edged quality: relatively simple fabrication together with inescapable defects. Oxidation of graphite powders, without any complicated synthesis conditions, leads to good yields of the final product. The RGO can be stored in a water-based solution or in the form of powder after drying. This makes it an easier process to handle stacks of graphene sheets or amorphous graphene flakes when they act as a matrix for low-dimensional inorganic semiconductors. For individual Si nanostructures instead of the more conventional wafer form, the mechanical strength and additional conductive paths are commonly needed. In a compact environment where Si nanostructures of large quantity are intensively stimulated, physically distributing GO among the Si nanostructures via mixed dispersions helps to enhance the structural durability and the conductive activity of the Si. Under such circumstances, neither the mechanically exfoliated graphene, with superlative mechanical and electrical properties, nor the CVD graphene with a large area is likely to bring an optimal advantage, because of the complicated procedures, high costs, and limited productivity involved. The situation is similar to that for inorganic semiconductors from other groups where low-dimensional nanostructures, including ZnO, ZnS, CdS, and TiO_2, can be created in large quantities. The II−VI semiconductors and oxide semiconductors concerned are accompanied by photocatalytic activity, which means the partial reduction of GO produced from chemical exfoliation can be further advanced. This is the result of electron transfer to GO from the photoexcited semiconductors. As the band gaps of those photocatalytic semiconductors are moderately different, their sensitivities to absorb light vary in terms of the wavelength range. In practice, for these inorganic semiconductors, the photocatalytic activities are mostly limited to the 300−400 nm UV region. The only exception is CdS, which is active in the visible light region. A graphene block provides an efficient channel for charge transportation, which will reduce the decomposition rate of the photocatalytic semiconductors caused by continuous irradiation. This feature of such photocatalytic semiconductors is focused on the reduction of GO as well as the generation of photocurrent. Thus, it is slightly different from that for mechanical graphene. Applying GO into the hydrothermal reactions that can be used to produce various nanostructures of these photocatalytic semiconductors leads to the simultaneous formation of semiconductor nanostructures and the reduction of GO. It prompts direct interaction between the semiconductors and GO through electron transfer and consolidates the linkage. In practice, this results in the extension of the light absorption to the visible region and the prevention of electron−hole recombination.

The discussions presented above indicate that, in a properly organized hybrid material, apart from receiving mechanical support as well as an electron transport channel, the semiconductors involved for their part may also play various roles. These include acting as the growth substrate, tuning the band gap, and providing further deoxidization for the graphene-related structures. The particular group, the nature as well as the dimensions, of semiconductor(s) determines to some extent the form of the presence of the graphene in the hybrid material and, hence, also the optimal synthesis routes. Taking all these aspects into consideration, clearly the influences between the semiconductors and the associated graphene are, in a way, contradictory, and for the moment not equally weighed. The subtle interplay thus caused between them affects the dimensional characteristics and ultimate use of the hybrid materials. For example, in the case of inorganic semiconductors with indirect band gaps, such as Si and SiC from group IV, the minimum-energy state in the conduction band and the maximum-energy state in the valence band, characterized by the crystal momentum in reciprocal space, are different. This means photons cannot be emitted in the indirect band gap because the electron must pass through an intermediate state and transfer momentum to the crystal lattice, to comply with the conservation of crystal momentum. In terms of light absorption, with the same mechanism, rather it is possible for light to penetrate into an indirect band gap semiconductor much farther before being absorbed than into a direct band gap semiconductor. However, the low band gap of approximately 1.2 eV of Si is in a suitable range where the daylight photons can be absorbed efficiently.[338] This is despite the fact that the indirect band gap gives rise to a weak absorption of about one-third of usable solar photons.[339] Thus, the Si cells present in sufficient thickness (typically in hundreds of micrometers) have been routinely used in solar cells,[340] since exceedingly thin devices would let too much of the light simply pass through. Under such circumstances, a graphene layer deposited on the Si solar cell would enhance the performance in light trapping and charge carrier transportation, especially when a junction is formed. Because solar cells are found to be more efficient in the form of nanowires than in thin films, transferring CVD graphene onto parallel Si nanowire arrays is favored. Si thin films can nonetheless accommodate mechanically exfoliated graphene layers. On the contrary, the indirect band gap of SiC, ranging from 2.2 to 3.3 eV, is comparatively large. This is an essential prerequisite for high-quality heterojunctions incorporating the high-power, high-temperature capabilities of SiC together with the advantages of a wide band gap emitter.[216] The epitaxial graphene grown on either the Si-face or C-face of SiC features stacked layers with 2-dimensional platforms.

The group II−VI semiconductors ZnS, ZnO, and CdS, the group III−V semiconductors GaN and GaAs, and the oxide semiconductor TiO_2 all have direct band gaps. This means that the momentum of electrons and holes is the same in both the

DOI: 10.1021/cr400607y
Chem. Rev. 2015, 115, 8294−8343

Table 2. Representative Characteristics of Hybrid Materials with Different Forms, Dimensions, and End Functions[a]

hybrid material	band gap of the semiconductor (eV)	form (size) of the semiconductor	form of graphene	fraphene synthesis method	heterogeneous structure	purpose and use	ref[b]
Si−graphene	1.2, indirect	oxidized Si wafer	graphene flake(s)	mechanical exfoliation	graphene flake(s) propped on a Si wafer	mechanical support for single-layer graphene	43
		Si NPs, within 30 nm	RGO sheets	chemical derivation (Hummers method)	Si NPs dispersed between RGO sheets	Li ion battery anodes	39
SiC−graphene	2.2−3.3, indirect	6H-SiC substrate	few-layer graphene	epitaxial growth	few-layer (three sheets) graphene grown on the Si-terminated face of a SiC substrate	scalable control of the graphene structure	12
ZnS−graphene	3.7, direct	ZnS NPs, 3−42 nm (aggregation)	RGO sheets	chemical derivation (Hummers method)	ZnS NPs on RGO sheets	photocatalysis (photodegradation) in the UV−vis region	136
ZnO−graphene	3.2, direct	ZnO NRs, 100 nm wide	few-layer graphene	CVD growth (on Ni-coated SiO_2/Si)	ZnO NRs grown on a graphene substrate	transparent conducting electrodes	86
		ZnO NPs, 2−5 nm	GO sheets	chemical derivation (Hummers method)	ZnO NPs on RGO sheets	photocatalysis (reduction of graphene) in the UV−vis region	115
CdS−graphene	2.4, direct	CdS NPs, 3−100 nm (aggregation)	GO sheets	chemical derivation (Hummers method)	CdS NPs on RGO sheets	photocatalysis (H_2 production) in the UV−vis region	162
BN−graphene	5.8−6.0, mainly direct	h-BN substrate, 14 nm thick	single-layer graphene	mechanical exfoliation	graphene on h-BN	graphene devices on an h-BN substrates with enhanced mobilities	187
GaAs−graphene	1.519, direct	GaAs wafer	few-layer graphene	mechanical exfoliation	graphene on GaAs	mechanical support for graphene	203
GaN−graphene	3.4, direct	GaN thin film	few-layer graphene	mechanical exfoliation	GaN epitaxially grown on ZnO-coated graphene	GaN LEDs based on graphene, with strong electroluminescence	219
TiO_2−graphene	3.0−3.2, direct	TiO_2 NPs, 2−7 nm	GO sheets	chemical derivation (Hummers method)	TiO_2 NPs on GO sheets	photocatalysis (reduction of graphene) in the UV−vis region	246
ITO−graphene	4, direct; 3, indirect	ITO substrate	GO sheets	chemical derivation (Hummers method)	GO on ITO	ITO anode for a GO-based working electrode	304

[a]NPs and NRs are short for nanoparticles and nanorods, respectively. [b]References not limited to a specific value of the band gap energies.

DOI: 10.1021/cr400607y
Chem. Rev. 2015, 115, 8294−8343

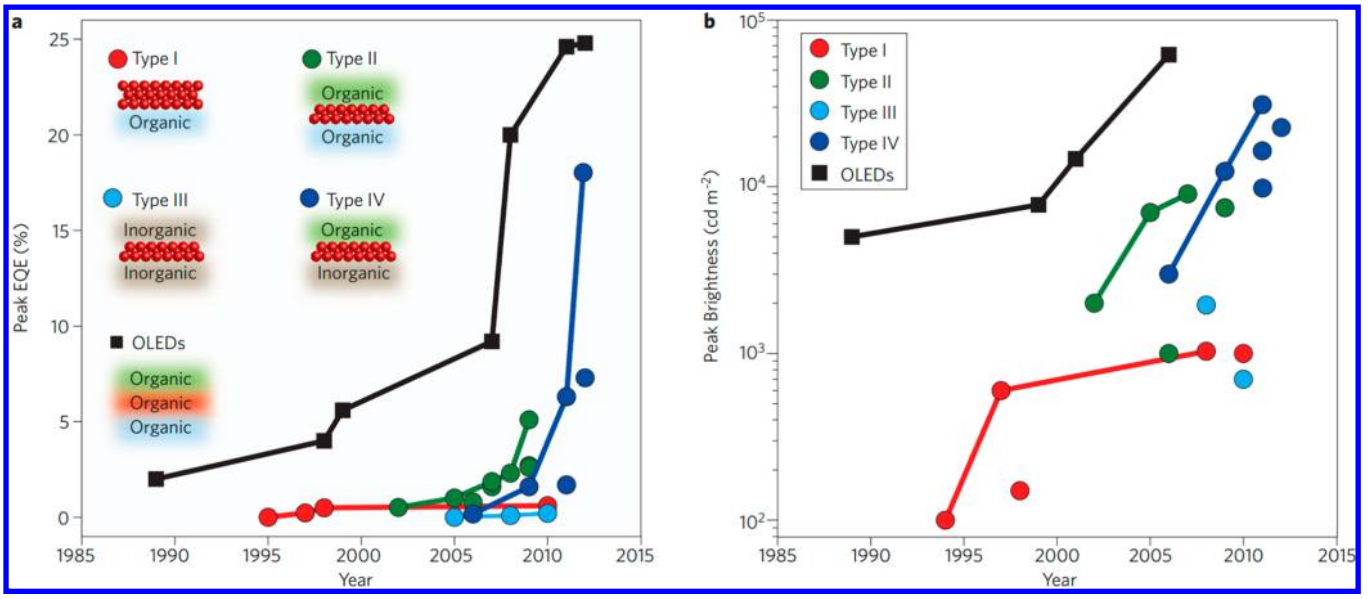

Figure 34. Progression of orange/red-emitting QD-LED performance over time in terms of peak EQE and peak brightness. (a) Peak EQE. (b) Peak brightness. QD-LEDs (a substantial but nonexhaustive selection from the literature) are classified into one of four "types", as described in the text, and are compared with selected orange/red-emitting (phosphorescent) OLEDs. Solid lines connect new record values. Reprinted with permission from ref 349. Copyright 2012 Macmillan Publishers Ltd.

conduction and valence bands for all these semiconductors, and hence, their electrons can directly emit a photon. Light with a photon energy level less than the band gap of the semiconductor with a direct band gap is not easily absorbed and hence passes straight through the semiconductor. The photon from the light with energy greater than the band gap of the semiconductor transmits its energy to the semiconductor electron, and this moves it up into the conduction band, leaving a hole in the valence band. The onset wavelength of the light absorption corresponds to the value of the band gap.[341,342] That is why the decreasing band gaps of ZnS, ZnO, and CdS, which are 3.7, 3.2, and 2.4 eV, respectively, lead to a reversely proportional performance in light absorption from the invisible UV region to the visible region. The light absorption is well reflected through low-dimensional nanomaterials, which can be attached in sufficient quantities with chemically exfoliated graphene to increase the contact and therefore improve the efficiency. In the case of TiO_2, the higher band gaps lead to light absorption in the deeper UV region. For the III−V semiconductors GaAs and GaN, their ultrafast electronic and optoelectronic performances as well as the visible light absorption can be successfully enhanced by graphene. One major difference between GaAs and GaN, when separately combined with graphene, is that GaN does not grow on graphene epitaxially due to the weak chemical reaction. In contrast, for the III−V semiconductor BN, apart from the direct band gap properties previously mentioned in this review, the indirect band gap energies have also been reported.[178,343,344] This indicates the band gaps of BN are in a wide range of 3−7 eV. The oxide semiconductor ITO likewise shows both direct and indirect band gap energies. The indirect band energies are located around 3 eV depending on the carrier concentration, whereas the direct band energies approach 4 eV.[345−347] Wide band gaps bring transparency in the visible part of the spectrum to these semiconductors, and this enables them to act as transparent substrates with graphene. These influences represent, to some extent, the interplay between the graphene and the inorganic semiconductors combined in the hybrid materials. The characteristics of these hybrid materials most typically studied, including the end function, dimension, and form, are listed in Table 2.

6.3. Reciprocal Effects and Subtle Development

Ultimately, one compelling question worth delving deeply into is raised through the discussions in this review. Can the graphene−semiconductor nanocomposites we have described truly become a new class of promising functional materials? As mentioned in previous sections, due to the inherent physical and chemical properties arising from their structural characteristics, graphene and its derivatives possess several unique properties. When it comes down to the micro- and nanoscaled composites that combine graphene and inorganic semiconductors, the electronic, optical, mechanical, and thermal advantages of graphene take precedence in their uniqueness. Indeed, from the point of view of the inorganic semiconductors, the role of graphene in the composites can be considered as either enhancing the semiconductor performance or increasing the overall efficiencies of the systems. Although it is predicted by many that graphene, being a "zero-gap semiconductor", will eventually replace some semiconductors, such as Si, there is much long-term practical development work to be done. Also, it should not be forgotten that the zero-gap feature of graphene, which is a result of the identical environment of the two C atoms in the individual unit of the hexagonal structure,[348] puts a cumbersome limit on realizing its promise as a semiconductor. Therefore, at the present stage it could be more reasonable and practical to combine graphene and inorganic semiconductors than to actually replace the inorganic semiconductors. Their combination will therefore "take advantage of each component for the other"; relevant examples include the tuning of the band gap for graphene and the prevention of the electron−hole pair recombination for semiconductors. Current research progress in the field does not suggest that, in the near future at least, any significant difference will be made that could change the trend in combining graphene and inorganic semiconductors.

DOI: 10.1021/cr400607y
Chem. Rev. 2015, 115, 8294−8343

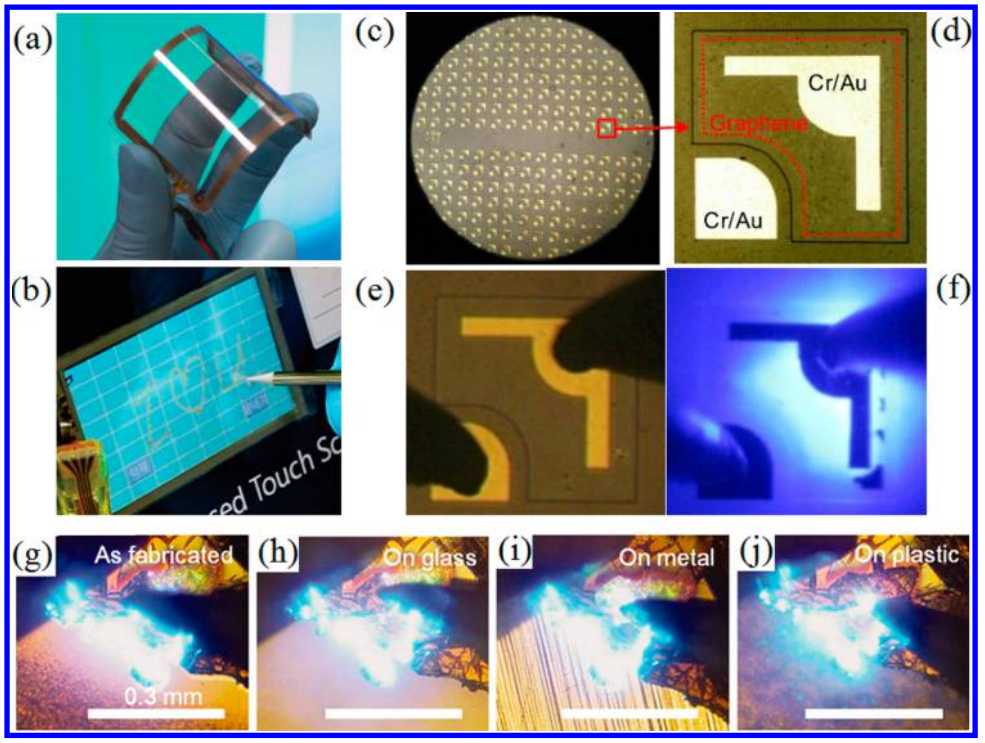

Figure 35. (a) An assembled graphene/PET touch panel showing outstanding flexibility. (b) A graphene-based touch-screen panel connected to a computer with control software. (c) Large-area patterned multiple LED devices and (d) an individual LED. (e, f) LED with tip probes attached (e) before applying the input current and (f) after applying an input current of 100 μA. Images a and b reprinted with permission from ref 293. Copyright 2010 Macmillan Publishers Ltd. Images c–f reprinted with permission from ref 224. Copyright 2010 IOP Publishing. Images g–j reprinted with permission from ref 219. Copyright 2010 American Association for the Advancement of Science.

One emphasis of this review is that the graphene–inorganic semiconductor nanocomposites are supposed to be a good match. On one hand, it has been over 10 years since single-layer graphene became accessible. It is extremely encouraging to see the steady gain in advances in the knowledge of graphene. In addition, a greater range of approaches are being developed to precisely tailor the electronic properties of the C-based substance.[350,351] On the other hand, the size-dependent properties, such as high adsorption and catalytic activity due to the large surface area to volume ratio and quantum confinement, are the main features of the inorganic semiconductors that distinguish their nanomaterials from the corresponding bulk materials. The latter normally have constant physical properties regardless of their size. However, the semiconductor nanomaterials have been going through intense investigation with a view to extending their practical applications. For example, it has taken nearly two decades to reach the point where quantum dots can be effectively involved in producing display devices.[349,352−354] Figure 34 summarizes the progress for the case of orange/red-emitting (almost always CdSe-based) QD-LEDs (quantum dot light-emitting devices) with respect to two criteria: peak external quantum efficiency (EQE) (Figure 34a) and peak brightness (Figure 34b).[349] For solid-state lighting sources and displays, the EQE is the key metric, directly proportional to the power conversion efficiency, and the brightness values are typically in the range of 10^2–10^3 cd m^{-2}. The QD-LEDs presented in Figure 34 are classified into four architectural types: QD-LEDs with polymer charge transport layers (type I), QD-LEDs with organic small-molecule charge transport layers (type II), QD-LEDs with inorganic charge transport layers (type III), and QD-LEDs with hybrid organic–inorganic charge transport layers (type IV). It is shown that, despite the unbalanced development, these four types of devices have evolved chronologically. What is further noticeable is that, for properly adjusted hybrid materials, the increase in both EQE and brightness is steady, with values approaching those of phosphorescent organic LEDs (OLEDs).

The progress for the graphene–inorganic semiconductor nanocomposites has not yet reached that for the nanocomposites based on quantum dots. This is understandable since really graphene development is only in its 11th year. However, it has been clearly demonstrated that the involvement of graphene-based materials enhances the conductivity of quantum dot films, and thus improves the charge collection and transport.[355,356] The graphene produced on large flexible substrates can be transferred onto foreign substrates (e.g., poly(ethylene terephthalate) (PET) substrates) and then used to fabricate transparent electrodes for touch-screen panel devices, as illustrated in parts a and b of Figure 35.[293] This clearly shows the potential of graphene to replace conventional transparent electrodes. Also, as mentioned in earlier sections, graphene materials based on inorganic semiconductors (e.g., GaN) can be used as transparent electrodes for LEDs.[224] Parts c and d of Figure 35 present the optical micrographs of fabricated GaN LEDs (on a centimetric scale). They show multiple devices with patterned multilayer graphene (MLG) electrodes as well as an individual device, respectively. In Figure 35e,f is shown an MLG electrode LED before and after the application of an input current, respectively. Blue light emission is clearly visible, even at a low input current of 100 μA. The MLG electrode GaN LEDs are seen to show light output performance comparable to that of conventional GaN LEDs with ITO. They have the added advantages of preserving better transparency and robustness.

DOI: 10.1021/cr400607y
Chem. Rev. 2015, 115, 8294–8343

Also, the relatively weak bonds between the interlayers of the graphene allow the transfer of thin films grown on graphene substrates onto foreign substrates. From an example demonstrated earlier in this review (in section 4.3), it is noticed that high-quality GaN films grown on substrates composed of graphene layers can be transferred to substrates such as metal, glass, and plastic.[219] The use of layered graphene substrates, for one thing, avoids the use of more conventional sapphire substrates for nitride film growth. These sapphire substrates require sophisticated techniques to be separated from the GaN because of the strong bonding between GaN and sapphire.[357,358] Most importantly, the transferred devices can emit strong, yet fairly uniform blue light visible to the naked eye under normal room illumination. This is shown in the optical microscopy images in parts g–j of Figure 35. The high emission performance is attributed to the uniform current spreading and injection caused by the graphene electrodes, which were preserved from the layered graphene substrates during the transfer. On the other hand, the new substrates coupled with the graphene electrodes after the transfer allow inorganic LEDs to be fabricated in diverse rigid or flexible forms.

Therefore, further engineering of the graphene electrodes to increase the conductivity as well as tuning of the work function to improve the interface matching may even enhance the performance of LEDs based on graphene electrodes and inorganic semiconductors. It is expected that such graphene film improvements will be beneficial for future applications as transparent electrodes in optoelectronic devices. Indeed, the properties of graphene discussed throughout this review all indicate that replacement of traditional electrodes made of noble metals, such as Pt,[359,360] with those made of inexpensive graphene is likely. This is supported by the fact that the structure and morphology of graphene are mechanically advantageous over those of another recently developed competitor for such electrodes, namely, carbon nanotubes (CNTs). As mentioned previously in this review, the CNTs are also an allotrope of carbon. CNTs and graphene are similar in many aspects.[361] The work functions of CNT and graphene nanosheets are closely related (4.5–4.8 eV), and both materials react to the surrounding environment similarly because of the basic structure and nature of the honeycomb C lattice. However, the 1-dimensional tubular structure of CNTs presents one major difference between CNTs and graphene, and hence between the ways these two allotropes of C are integrated with inorganic semiconductors. When it is a question of thin film electrodes, CNTs are generally organized through interweaving, while graphene sheets are formed by stacking. The morphology, roughness, and properties of the thin films are therefore different between CNTs and graphene. In fact, their 2-dimensional structure makes the graphene thin films more reliable in transparency and smoothness than CNTs. This is especially true for some optoelectronic devices, such as LEDs, where surface smoothness is very important. The conductivity of well-made graphene films, typically including those made from CVD graphene, is most likely higher than that of the CNT films. This is due to the sensitive contact resistances between the CNTs, which in turn dominate the electrical transport.[362,363] However, the conductivity of thin films made from graphene oxide (GO) is lower than that of well-aligned CNTs due to the presence of oxygen-related defects. This is despite the advantage of two-dimensional contacts between the graphene sheets over the intermittent point contacts found in the CNTs.

So far, although it might be somewhat presumptuous to declare that graphene itself will certainly turn out to be the promising material of the future, investigations to date strongly suggest that graphene is not only compatible with so many other materials, especially inorganic semiconductors, but also helpful in boosting their performances. In practice, it is the size of graphene which intrinsically determines that it can only exert its full functional capacity with nanomaterials. Compared with the conventional bulk materials, nanomaterials have the advantage of fast device turn-on times and extremely small-scale compactness. This is reflected in the performance enhancement, prompted by the graphene features, of nanoscale inorganic semiconductors for macroscale structures or devices, as discussed in previous sections. Thus, it can be safely stated that nanoscale phenomena eventually act on the macroscale features. Indeed, for practical applications, the nanocomposites consisting of graphene and inorganic semiconductors are likely to frame a bridge between bulk materials and atomic or molecular structures.

Indeed, it is well recognized that graphene can fulfill multiple functions in a wide range of devices, which include transparent conductor windows, photoactive layers, and channels for charge transport.[17] Apart from the above-mentioned display devices, the nanocomposites of inorganic semiconductors and graphene also show encouraging signs of future success in optoelectronics. As previously noted, graphene can be incorporated into nanostructured inorganic semiconductors to enhance the charge transport rate, thus preventing recombination and improving the internal photocurrent efficiency. One further example is shown in Yang et al.'s work where the authors incorporated 2D graphene into nanostructured TiO_2 photoanodes to form graphene bridges in dye-sensitized solar cells.[364] It was demonstrated, from their investigation of electronic and ionic transport processes using electrochemical impedance spectra (EIS), that faster electron transport and lower recombination can be achieved in the graphene-incorporated solar cells. This ultimately led to a photoelectrical conversion efficiency of up to 7%, which is about 39% higher than that of conventional nanocrystalline TiO_2 photoanodes under the same experimental conditions. Consequently, it seems fairly reasonable to assume that photodetectors based on graphene and group IV or group III–V inorganic semiconductors can deal with the charge recombination much better than those based on inorganic semiconductors alone. Since graphene absorbs a significant fraction of the incident light, from the ultraviolet to terahertz range, due to its electronic structure,[365,366] it is even possible to tackle the wavelength limits of absorption for inorganic semiconductors combined with graphene. However, one should bear in mind that the effective functional area of graphene also plays an important role in the charge separation. It has been observed that an internal field can be formed near the electrode–graphene interfaces.[367] Such phenomena are associated with the random electron–hole puddles arising from the impurity centers that are inclined to be charged.[368−371] In a fairly small region (e.g., 200 nm) of current generation, the charge carriers can travel out of the internal field promptly.[372] Hence, most of the electron–hole pairs generated would be outside of the electric field. As a result, charge carrier recombination rather than separation would occur.[17] On this occasion, it is possible that the small effective area of a single layer of graphene can decrease the detection efficiency because the internal field causes the generated charge carriers to have a short lifetime.

DOI: 10.1021/cr400607y
Chem. Rev. 2015, 115, 8294–8343

This, however, raises a further question that is related to the number of graphene layers, when graphene is combined in practice with inorganic semiconductors. From the discussions throughout this review, it is well understood that single-layer graphene is a crystalline allotrope of C with 2-dimensional properties of a periodic array of C atoms. Multilayer graphene, on the other hand, has properties more similar to those of bulk graphite. The cohesion of graphene stacks results from the van der Waals forces, which account for the change in electronic properties of the individual layers.[374−376] However, a high density of rotational faults where adjacent sheets are rotated relative to each other, as observed for multilayer graphene grown on the C-terminated face of 4H-SiC, may lead to decoupling of the adjacent graphene sheets so that their band structure becomes nearly identical to that of isolated graphene.[373] Figure 36 shows the ab initio (first principle)

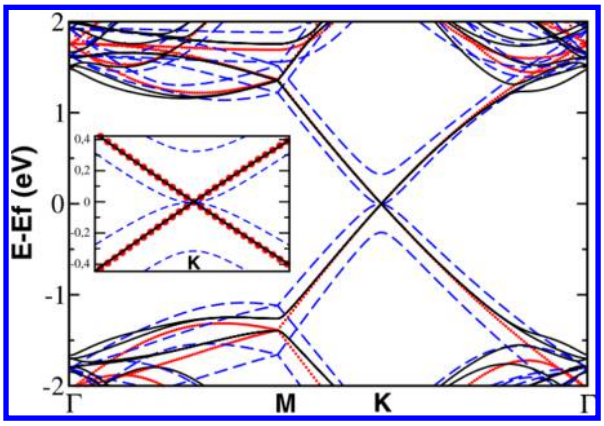

Figure 36. Calculated band structure for three forms of graphene: (i) isolated graphene sheet (dots), (ii) AB (Bernal) stacked graphene bilayer (dashed line), and (iii) $R30/R2^{+}$ fault pair (solid line). The inset shows details of the band structure at the *K*-point. Reprinted with permission from ref 373. Copyright 2008 American Physical Society.

density functional theory calculations comparing the band structures for an isolated graphene sheet, a graphene bilayer with AB (Bernal) stacking, which refers to the structure that half of the atoms in one layer are positioned exactly on top of half of the atoms of the other layer,[377] and a bilayer rotational fault pair. The rotational fault density for the calculation is based on the surface X-ray diffraction (SXRD) and scanning tunneling microscopy (STM) measurements of the C-face films with adjacent layers rotated 30° ($R30$) and 2.20° ($R2^{+}$), respectively. Because the Dirac dispersion at the *K*-point (reciprocal space point) is preserved, the electronic properties of an isolated graphene sheet can thus be maintained.[373] Nonetheless, by virtue of the altered carrier concentrations, the electronic properties of graphene itself, either single-layered or multilayered, deviate from those of graphite.[378] On one hand, single-layer graphene is generally superior in terms of electronic properties and thermal conductivity compared with multilayer graphene. On the other hand, multilayer graphene comes about with less sophisticated processing steps. This characteristic is also similarly applicable to graphene oxide. It has been noticed that multilayer graphene and graphene oxide can improve the performances of many inorganic semiconductors, particularly in the field of battery research[32,39] and charge separation.[115,129,136] However, it should be noted that they do not have the advantage of building structural subtleties on the micro- and nanoscales. Therefore, it is inferred that well-ordered single-layer graphene should be used in sensitive applications in which precise alignment of structures is of primary concern, such as in Schottky contacts[107,233] and analogue circuits.[70] Multilayer graphene and graphene oxide possess adequate function for making hybrid materials with fewer demands for ordering of the structures. In practice, to date it still remains a challenge to avoid structural disorder and retain the functionality concurrently through a fairly simple manufacturing process when graphene-related materials are prepared. Nevertheless, as hopefully established in this review, recent progress has demonstrated the feasibility of successfully making graphene−inorganic semiconductor heterostructures. Also, since graphene has evolved into a versatile platform for the investigation of various phenomena,[374] the shift in focus from studying graphene itself to its use in applications is expected to trigger even more breakthroughs, although possibly not as rapidly as the demands of the relevant industries would like.

7. CONCLUSIONS AND OUTLOOK

Several topics have been discussed in this paper with the view to demonstrating the significant effects of the heterogeneous structures of inorganic semiconductors and graphene with various dimensions. Most of these effects were not even anticipated a decade ago. The effort put into the area is being disseminated across an increasing number of laboratories around the world. It involves many aspects of research, including optoelectronics, physical chemistry, and nanotechnologies, among others. Modern techniques in microscopic and electronic measurements allow us to carry out very sophisticated experiments on atomically thin graphene sheets and ultrasmall semiconductor structures. Meanwhile, progress in this area strongly depends on the chemical constitution and physical organization of the heterogeneous structures. It is true that the topic of this review is directly based on the discovery and development of graphene, which has prompted new phenomena and characteristics related to inorganic semiconductors. It is also true that the effect of the inorganic semiconductors on the end function and form of graphene in the heterogeneous structures is not negligible. General discussions presented here regarding the hybrid materials based on inorganic semiconductors and graphene, on one hand, concern the synthesis, properties, and applications. The specific categories, on the other hand, represent the collective characteristics pertaining to a particular group as well as the unique characteristics associated with the relevant inorganic semiconductors and the graphene together. The way the heterogeneous structures are organized can be relatively straightforward or involve a number of different techniques. This is dependent on the nature of the inorganic semiconductors, the form of the graphene, and the desired end functions.

As supported by the many studies discussed in this review, much notable work has been performed in this field to integrate graphene into electronic devices based on inorganic semiconductors. In summary, although it seems unlikely that commercially applicable graphene-based memory chips and microprocessors will be routinely available in the next decade, great progress is being made. It is expected that graphene, with extremely high charge-carrier mobility, will improve device performance and increase the range of potential functions. However, as pointed out, complex integration of graphene into the inorganic semiconductor-based devices is still challenging. Examples discussed in this paper indicate that delicate control

DOI: 10.1021/cr400607y
Chem. Rev. 2015, 115, 8294−8343

over the fabrication or growth of graphene for the intended application is essential. If commercial production is to succeed, then relevant processes will need to be more explicit, reproducible, and compatible with the materials involved in industry. Clearly, the fabricated systems will also need to be stable during their performance lifetimes. This requires significant improvement over current levels. Nevertheless, where graphene and representative inorganic semiconductors are concerned, it is believed that, as shown in this review, an even broader range of areas for future applications is being steadily developed.

AUTHOR INFORMATION

Corresponding Author

*E-mail: xshfang@fudan.edu.cn.

Notes

The authors declare no competing financial interest.

Biographies

Nan Gao obtained his doctoral degree in engineering and science from The University of Nottingham, United Kingdom, in 2012. Following his postgraduate studies, Dr. Gao started his academic career as a postdoctoral research associate to study the synthesis and characterisation of nanocomposites at Fudan University, China. His research interests mainly include interface phenomena and functional composite materials. Currently, Dr. Gao is a scientist working on functional structures and interface dynamics at the Max-Planck Institute for Polymer Research, Mainz, Germany.

Xiaosheng Fang is currently a professor in the Department of Materials Science, Fudan University, China. He received his Ph.D. degree from the Institute of Solid State Physics, Chinese Academy of Sciences, in 2006 under the supervision of Professor Lide Zhang. Previously, he was a Japan Society for the Promotion of Science (JSPS) postdoctoral fellow at the National Institute for Materials Science (NIMS), Japan, as well as a research scientist at the International Center for Young Scientists (ICYS)—International Center for Materials Nanoarchitectonics (MANA). His current research involves the controlled fabrication, novel properties, and optoelectronic applications of semiconductor nanostructures, especially with a focus on II–VI inorganic semiconductor nanostructure-based optoelectronic devices.

ACKNOWLEDGMENTS

We thank Dr. Linfeng Hu from Fudan University for his kind assistance. This work was supported by the National Postdoctoral Science Foundation of China (Grant 2013M541462), National Natural Science Foundation of China (Grants 51471051 and 51372040), Science and Technology Commission of Shanghai Municipality (Grant 13NM1400300), Shanghai Shu Guang Project (Grant 12SG01), and Programs for Professor of Special Appointment (Eastern Scholar) at Shanghai Institutions of Higher Learning.

ABBREVIATIONS

AFM	atomic force microscopy
BNNR	boron nitride nanoribbon
BNNS	boron nitride nanosheet
BNNT	boron nitride nanotube
BS	blue-shifted
CNT	carbon nanotube
CP	chemical polishing
CVD	chemical vapor deposition
DMF	dimethylformamide
DMSO	dimethyl sulfoxide
DSSC	dye-sensitized solar cell
EELS	electron energy-loss spectroscopy
EG	epitaxial graphene
EIS	electrochemical impedance spectroscopy
EQE	external quantum efficiency
FET	field-effect transistor
FGS	functionalized graphene sheet
GNR	graphene nanoribbon
GO	graphene oxide
GS	graphene sheet
HOPG	highly oriented pyrolitic graphite
HRTEM	high-resolution transmission electron microscopy
ICP	inductively coupled plasma
LED	light-emitting diode
MBE	molecular-beam epitaxy
MLG	multilayer graphene
MOCVD	metal–organic chemical vapor deposition
MOVPE	metal–organic vapor-phase epitaxy
MQW	multiquantum well
MWCNT	multiwalled carbon nanotube
NMP	*N*-methylpyrrolidone
NP	nanoparticle
NW	nanowire
OLED	organic light-emitting diode
P3HT	poly(3-hexylthiophene)
PANI	polyaniline
PB^-	1-pyrenebutyrate
PCBM	phenyl-C61-butyric acid methyl ester
PECVD	plasma-enhanced chemical vapor deposition

DOI: 10.1021/cr400607y
Chem. Rev. 2015, 115, 8294–8343

PEDOT−PSS	poly(styrenesulfonate)-doped poly(3,4-(ethylenedioxy)thiophene)
PET	poly(ethylene terephthalate)
PL	photoluminescence
PMMA	poly(methyl methacrylate)
PPD	*p*-phenylenediamine
PSL	pillar superlattice
QD	quantum dot
QF	quantum flake
RF	radio frequency
RGO	reduced graphene oxide
RHEED	reflection high-energy electron diffraction
SDBS	sodium dodecylbenzenesulfonate
SDS	sodium dodecyl sulfate
SEM	scanning electron microscopy
SOI	silicon-on-insulator
STM	scanning tunneling microscopy
SXRD	surface X-ray diffraction
TA	thermal annealing
TEM	transmission electron microscopy
UHV	ultrahigh vacuum
XRD	X-ray diffraction

REFERENCES

(1) Geim, A. K.; Novoselov, K. S. The rise of graphene. *Nat. Mater.* **2007**, *6*, 183−191.
(2) Bolotin, K. I.; Sikes, K. J.; Jiang, Z.; Klima, M.; Fudenberg, G.; Hone, J.; Kim, P.; Stormer, H. L. Ultrahigh electron mobility in suspended graphene. *Solid State Commun.* **2008**, *146*, 351−355.
(3) Balandin, A. A. Thermal properties of graphene and nanostructured carbon materials. *Nat. Mater.* **2011**, *10*, 569−581.
(4) Lee, C.; Wei, X.; Kysar, J. W.; Hone, J. Measurement of the elastic properties and intrinsic strength of monolayer graphene. *Science* **2008**, *321*, 385−388.
(5) Lee, J. U.; Yoon, D.; Cheong, H. Estimation of Young's modulus of graphene by Raman spectroscopy. *Nano Lett.* **2012**, *12*, 4444−4448.
(6) Fang, X. S.; Bando, Y.; Gautam, U. K.; Ye, C. H.; Golberg, D. Inorganic semiconductor nanostructures and their field-emission applications. *J. Mater. Chem.* **2008**, *18*, 509−522.
(7) Park, W. I.; Lee, C.-H.; Lee, J. M.; Kim, N.-J.; Yi, G.-C. Inorganic nanostructures grown on graphene layers. *Nanoscale* **2011**, *3*, 3522−3533.
(8) Artukovic, E.; Kaempgen, M.; Hecht, D. S.; Roth, S.; GrUner, G. Transparent and flexible carbon nanotube transistors. *Nano Lett.* **2005**, *5*, 757−760.
(9) Zhang, M.; Fang, S. L.; Zakhidov, A. A.; Lee, S. B.; Aliev, A. E.; Williams, C. D.; Atkinson, K. R.; Baughman, R. H. Strong, transparent, multifunctional, carbon nanotube sheets. *Science* **2005**, *309*, 1215−1219.
(10) Novoselov, K. S.; Geim, A. K.; Morozov, S. V.; Jiang, D.; Zhang, Y.; Dubonos, S. V.; Grigorieva, I. V.; Firsov, A. A. Electric field effect in atomically thin carbon films. *Science* **2004**, *306*, 666−669.
(11) Hass, J.; Feng, R.; Li, T.; Li, X.; Zong, Z.; de Heer, W. A.; First, P. N.; Conrad, E. H.; Jeffrey, C. A.; Berger, C. Highly ordered graphene for two dimensional electronics. *Appl. Phys. Lett.* **2006**, *89*, 143106.
(12) Berger, C.; Song, Z. M.; Li, T. B.; Li, X. B.; Ogbazghi, A. Y.; Feng, R.; Dai, Z. T.; Marchenkov, A. N.; Conrad, E. H.; First, P. N.; de Heer, W. A. Ultrathin epitaxial graphite: 2D electron gas properties and a route toward graphene-based nanoelectronics. *J. Phys. Chem. B* **2004**, *108*, 19912−19916.
(13) Hirono, S.; Umemura, S.; Tomita, M.; Kaneko, R. Superhard conductive carbon nanocrystallite films. *Appl. Phys. Lett.* **2002**, *80*, 425−427.
(14) Katsnelson, M. I.; Novoselov, K. S. Graphene: New bridge between condensed matter physics and quantum electrodynamics. *Solid State Commun.* **2007**, *143*, 3−13.
(15) Han, M. Y.; Brant, J. C.; Kim, P. Electron transport in disordered graphene nanoribbons. *Phys. Rev. Lett.* **2010**, *104*, 056801.
(16) Son, D. I.; Kwon, B. W.; Park, D. H.; Seo, W.-S.; Yi, Y.; Angadi, B.; Lee, C.-L.; Choi, W. K. Emissive ZnO-graphene quantum dots for white-light-emitting diodes. *Nat. Nanotechnol.* **2012**, *7*, 465−471.
(17) Bonaccorso, F.; Sun, Z.; Hasan, T.; Ferrari, A. C. Graphene photonics and optoelectronics. *Nat. Photonics* **2010**, *4*, 611−622.
(18) Das Sarma, S.; Adam, S.; Hwang, E. H.; Rossi, E. Electronic transport in two-dimensional graphene. *Rev. Mod. Phys.* **2011**, *83*, 407−470.
(19) Lemme, M. C.; Echtermeyer, T. J.; Baus, M.; Kurz, H. A graphene field-effect device. *IEEE Electron Device Lett.* **2007**, *28*, 282−284.
(20) Chau, R.; Datta, S.; Doczy, M.; Doyle, B.; Jin, J.; Kavalieros, J.; Majumdar, A.; Metz, M.; Radosavljevic, M. Benchmarking nanotechnology for high-performance and low-power logic transistor applications. *IEEE Trans. Nanotechnol.* **2005**, *4*, 153−158.
(21) Kim, K.; Choi, J. Y.; Kim, T.; Cho, S. H.; Chung, H. J. A role for graphene in silicon-based semiconductor devices. *Nature* **2011**, *479*, 338−344.
(22) Eda, G.; Unalan, H. E.; Rupesinghe, N.; Amaratunga, G. A. J.; Chhowalla, M. Field emission from graphene based composite thin films. *Appl. Phys. Lett.* **2008**, *93*, 233502.
(23) Pandey, S.; Rai, P.; Patole, S.; Gunes, F.; Kwon, G. D.; Yoo, J. B.; Nikolaev, P.; Arepalli, S. Improved electron field emission from morphologically disordered monolayer graphene. *Appl. Phys. Lett.* **2012**, *100*, 043104.
(24) Fan, G. F.; Zhu, H. W.; Wang, K. L.; Wei, J. Q.; Li, X. M.; Shu, Q. K.; Guo, N.; Wu, D. H. Graphene/silicon nanowire Schottky junction for enhanced light harvesting. *ACS Appl. Mater. Interfaces* **2011**, *3*, 721−725.
(25) Xie, C.; Lv, P.; Nie, B. A.; Jie, J. S.; Zhang, X. W.; Wang, Z.; Jiang, P.; Hu, Z. Z.; Luo, L. B.; Zhu, Z. F.; Wang, L.; Wu, C. Y. Monolayer graphene film/silicon nanowire array Schottky junction solar cells. *Appl. Phys. Lett.* **2011**, *99*, 133113.
(26) Jeong, H. H.; Kim, J.; Lee, J.; Jeon, S.; Lee, W.; Lee, S. H. Formation of a top electrode on vertical Si nanowire devices using graphene as a supporting layer. *Appl. Phys. Express* **2012**, *5*, 105103.
(27) Yan, Z.; Peng, Z. W.; Sun, Z. Z.; Yao, J.; Zhu, Y.; Liu, Z.; Ajayan, P. M.; Tour, J. M. Growth of bilayer graphene on insulating substrates. *ACS Nano* **2011**, *5*, 8187−8192.
(28) Kumar, S.; Levchenko, I.; Cheng, Q. J.; Shieh, J.; Ostrikov, K. Plasma enables edge-to-center-oriented graphene nanoarrays on Si nanograss. *Appl. Phys. Lett.* **2012**, *100*, 053115.
(29) Hong, G.; Wu, Q.-H.; Ren, J.; Lee, S.-T. Mechanism of non-metal catalytic growth of graphene on silicon. *Appl. Phys. Lett.* **2012**, *100*, 231604.
(30) Li, X.; Cai, W.; Colombo, L.; Ruoff, R. S. Evolution of graphene growth on Ni and Cu by carbon isotope labeling. *Nano Lett.* **2009**, *9*, 4268−4272.
(31) Shang, N. G.; Papakonstantinou, P.; McMullan, M.; Chu, M.; Stamboulis, A.; Potenza, A.; Dhesi, S. S.; Marchetto, H. Catalyst-free efficient growth, orientation and biosensing properties of multilayer graphene nanoflake films with sharp edge planes. *Adv. Funct. Mater.* **2008**, *18*, 3506−3514.
(32) Cho, Y. J.; Kim, H. S.; Im, H.; Myung, Y.; Jung, G. B.; Lee, C. W.; Park, J.; Park, M. H.; Cho, J.; Kang, H. S. Nitrogen-doped graphitic layers deposited on silicon nanowires for efficient lithium-ion battery anodes. *J. Phys. Chem. C* **2011**, *115*, 9451−9457.
(33) Lee, Y. H.; Pan, K. C.; Lin, Y. Y.; Prem Kumar, T.; Fey, G. T. K. Lithium intercalation in graphites precipitated from pig iron melts. *Mater. Chem. Phys.* **2003**, *82*, 750−757.
(34) Kasavajjula, U.; Wang, C.; Appleby, A. J. Nano- and bulk-silicon-based insertion anodes for lithium-ion secondary cells. *J. Power Sources* **2007**, *163*, 1003−1039.
(35) Cui, L.-F.; Ruffo, R.; Chan, C. K.; Peng, H.; Cui, Y. Crystalline-amorphous core-shell silicon nanowires for high capacity and high current battery electrodes. *Nano Lett.* **2009**, *9*, 491−495.

DOI: 10.1021/cr400607y
Chem. Rev. 2015, 115, 8294−8343

(36) Chan, C. K.; Peng, H.; Liu, G.; McIlwrath, K.; Zhang, X. F.; Huggins, R. A.; Cui, Y. High-performance lithium battery anodes using silicon nanowires. *Nat. Nanotechnol.* **2008**, *3*, 31−35.
(37) Cui, L.-F.; Yang, Y.; Hsu, C.-M.; Cui, Y. Carbon-silicon core-shell nanowires as high capacity electrode for lithium ion batteries. *Nano Lett.* **2009**, *9*, 3370−3374.
(38) Kim, H.; Cho, J. Superior lithium electroactive mesoporous Si@carbon core-shell nanowires for lithium battery anode material. *Nano Lett.* **2008**, *8*, 3688−3691.
(39) Lee, J. K.; Smith, K. B.; Hayner, C. M.; Kung, H. H. Silicon nanoparticles-graphene paper composites for Li ion battery anodes. *Chem. Commun.* **2010**, *46*, 2025−2027.
(40) Yang, S. N.; Li, G. R.; Zhu, Q.; Pan, Q. M. Covalent binding of Si nanoparticles to graphene sheets and its influence on lithium storage properties of Si negative electrode. *J. Mater. Chem.* **2012**, *22*, 3420−3425.
(41) Evanoff, K.; Khan, J.; Balandin, A. A.; Magasinski, A.; Ready, W. J.; Fuller, T. F.; Yushin, G. Towards ultrathick battery electrodes: Aligned carbon nanotube - enabled architecture. *Adv. Mater.* **2012**, *24*, 533−537.
(42) Havener, R. W.; Ju, S. Y.; Brown, L.; Wang, Z. H.; Wojcik, M.; Ruiz-Vargas, C. S.; Park, J. High-throughput graphene imaging on arbitrary substrates with widefield raman spectroscopy. *ACS Nano* **2012**, *6*, 373−380.
(43) Blake, P.; Hill, E. W.; Castro Neto, A. H.; Novoselov, K. S.; Jiang, D.; Yang, R.; Booth, T. J.; Geim, A. K. Making graphene visible. *Appl. Phys. Lett.* **2007**, *91*, 063124.
(44) Cohen-Karni, T.; Qing, Q.; Li, Q.; Fang, Y.; Lieber, C. M. Graphene and nanowire transistors for cellular interfaces and electrical recording. *Nano Lett.* **2010**, *10*, 1098−1102.
(45) Di, C. A.; Wei, D. C.; Yu, G.; Liu, Y. Q.; Guo, Y. L.; Zhu, D. B. Patterned graphene as source/drain electrodes for bottom-contact organic field-effect transistors. *Adv. Mater.* **2008**, *20*, 3289−3293.
(46) Fei, Z.; Andreev, G. O.; Bao, W. Z.; Zhang, L. F. M.; McLeod, A. S.; Wang, C.; Stewart, M. K.; Zhao, Z.; Dominguez, G.; Thiemens, M.; Fogler, M. M.; Tauber, M. J.; Castro-Neto, A. H.; Lau, C. N.; Keilmann, F.; Basov, D. N. Infrared nanoscopy of dirac plasmons at the graphene-SiO_2 interface. *Nano Lett.* **2011**, *11*, 4701−4705.
(47) Kato, T.; Hatakeyama, R. Site- and alignment-controlled growth of graphene nanoribbons from nickel nanobars. *Nat. Nanotechnol.* **2012**, *7*, 651−656.
(48) Chen, J.-H.; Jang, C.; Xiao, S.; Ishigami, M.; Fuhrer, M. S. Intrinsic and extrinsic performance limits of graphene devices on SiO_2. *Nat. Nanotechnol.* **2008**, *3*, 206−209.
(49) Bunch, J. S.; van der Zande, A. M.; Verbridge, S. S.; Frank, I. W.; Tanenbaum, D. M.; Parpia, J. M.; Craighead, H. G.; McEuen, P. L. Electromechanical resonators from graphene sheets. *Science* **2007**, *315*, 490−493.
(50) Liu, M.; Yin, X. B.; Ulin-Avila, E.; Geng, B. S.; Zentgraf, T.; Ju, L.; Wang, F.; Zhang, X. A graphene-based broadband optical modulator. *Nature* **2011**, *474*, 64−67.
(51) Garcia-Sanchez, D.; van der Zande, A. M.; Paulo, A. S.; Lassagne, B.; McEuen, P. L.; Bachtold, A. Imaging mechanical vibrations in suspended graphene sheets. *Nano Lett.* **2008**, *8*, 1399−1403.
(52) Lafkioti, M.; Krauss, B.; Lohmann, T.; Zschieschang, U.; Klauk, H.; von Klitzing, K.; Smet, J. H. Graphene on a hydrophobic substrate: Doping reduction and hysteresis suppression under ambient conditions. *Nano Lett.* **2010**, *10*, 1149−1153.
(53) Frank, I. W.; Tanenbaum, D. M.; Van der Zande, A. M.; McEuen, P. L. Mechanical properties of suspended graphene sheets. *J. Vac. Sci. Technol. B* **2007**, *25*, 2558−2561.
(54) Ishigami, M.; Chen, J. H.; Cullen, W. G.; Fuhrer, M. S.; Williams, E. D. Atomic structure of graphene on SiO_2. *Nano Lett.* **2007**, *7*, 1643−1648.
(55) Du, X.; Skachko, I.; Barker, A.; Andrei, E. Y. Approaching ballistic transport in suspended graphene. *Nat. Nanotechnol.* **2008**, *3*, 491−495.
(56) Seol, J. H.; Jo, I.; Moore, A. L.; Lindsay, L.; Aitken, Z. H.; Pettes, M. T.; Li, X. S.; Yao, Z.; Huang, R.; Broido, D.; Mingo, N.; Ruoff, R. S.; Shi, L. Two-dimensional phonon transport in supported graphene. *Science* **2010**, *328*, 213−216.
(57) First, P. N.; de Heer, W. A.; Seyller, T.; Berger, C.; Stroscio, J. A.; Moon, J. S. Epitaxial graphenes on silicon carbide. *MRS Bull.* **2010**, *35*, 296−305.
(58) Van Bommel, A. J.; Crombeen, J. E.; Van Tooren, A. LEED and Auger electron observations of the SiC(0001) surface. *Surf. Sci.* **1975**, *48*, 463−472.
(59) Berger, C.; Song, Z.; Li, X.; Wu, X.; Brown, N.; Naud, C.; Mayou, D.; Li, T.; Hass, J.; Marchenkov, A. N.; Conrad, E. H.; First, P. N.; de Heer, W. A. Electronic confinement and coherence in patterned epitaxial graphene. *Science* **2006**, *312*, 1191−1196.
(60) Mallet, P.; Varchon, F.; Naud, C.; Magaud, L.; Berger, C.; Veuillen, J. Y. Electron states of mono- and bilayer graphene on SiC probed by scanning-tunneling microscopy. *Phys. Rev. B: Condens. Matter Mater. Phys.* **2007**, *76*, 041403.
(61) de Heer, W. A.; Berger, C.; Wu, X.; First, P. N.; Conrad, E. H.; Li, X.; Li, T.; Sprinkle, M.; Hass, J.; Sadowski, M. L.; Potemski, M.; Martinez, G. Epitaxial graphene. *Solid State Commun.* **2007**, *143*, 92−100.
(62) Lauffer, P.; Emtsev, K. V.; Graupner, R.; Seyller, T.; Ley, L.; Reshanov, S. A.; Weber, H. B. Atomic and electronic structure of few-layer graphene on SiC(0001) studied with scanning tunneling microscopy and spectroscopy. *Phys. Rev. B: Condens. Matter Mater. Phys.* **2008**, *77*, 155426.
(63) Davis, L. E.; MacDonald, N. C.; Palmberg, P. W.; Riach, G. E.; Weber, R. E. *Handbook of Auger Electron Spectroscopy: A Reference Book of Standard Data for Identification and Interpretation of Auger Electron Spectroscopy Data*, 2nd ed.; Physical Electronics Industries, Inc.: Chanhassen, MN, 1976.
(64) Kravets, V. G.; Grigorenko, A. N.; Nair, R. R.; Blake, P.; Anissimova, S.; Novoselov, K. S.; Geim, A. K. Spectroscopic ellipsometry of graphene and an exciton-shifted van Hove peak in absorption. *Phys. Rev. B: Condens. Matter Mater. Phys.* **2010**, *81*, 155413.
(65) Sun, D.; Divin, C.; Berger, C.; de Heer, W. A.; First, P. N.; Norris, T. B. Spectroscopic measurement of interlayer screening in multilayer epitaxial graphene. *Phys. Rev. Lett.* **2010**, *104*, 136802.
(66) Hiebel, F.; Mallet, P.; Varchon, F.; Magaud, L.; Veuillen, J. Y. Graphene-substrate interaction on 6H-SiC(000(1)over bar): A scanning tunneling microscopy study. *Phys. Rev. B: Condens. Matter Mater. Phys.* **2008**, *78*, 153412.
(67) Bostwick, A.; Ohta, T.; McChesney, J. L.; Emtsev, K. V.; Seyller, T.; Horn, K.; Rotenberg, E. Symmetry breaking in few layer graphene films. *New J. Phys.* **2007**, *9*, 385.
(68) Forbeaux, I.; Themlin, J. M.; Debever, J. M. Heteroepitaxial graphite on 6H-SiC(0001): Interface formation through conduction-band electronic structure. *Phys. Rev. B: Condens. Matter Mater. Phys.* **1998**, *58*, 16396−16406.
(69) Lin, Y. M.; Dimitrakopoulos, C.; Jenkins, K. A.; Farmer, D. B.; Chiu, H. Y.; Grill, A.; Avouris, P. 100-GHz transistors from wafer-scale epitaxial graphene. *Science* **2010**, *327*, 662−662.
(70) Lin, Y. M.; Valdes-Garcia, A.; Han, S. J.; Farmer, D. B.; Meric, I.; Sun, Y. N.; Wu, Y. Q.; Dimitrakopoulos, C.; Grill, A.; Avouris, P.; Jenkins, K. A. Wafer-scale graphene integrated circuit. *Science* **2011**, *332*, 1294−1297.
(71) Low, T.; Perebeinos, V.; Tersoff, J.; Avouris, P. Deformation and scattering in graphene over substrate steps. *Phys. Rev. Lett.* **2012**, *108*, 096601.
(72) Strupinski, W.; Grodecki, K.; Wysmolek, A.; Stepniewski, R.; Szkopek, T.; Gaskell, P. E.; Gruneis, A.; Haberer, D.; Bozek, R.; Krupka, J.; Baranowski, J. M. Graphene epitaxy by chemical vapor deposition on SiC. *Nano Lett.* **2011**, *11*, 1786−1791.
(73) Emtsev, K. V.; Bostwick, A.; Horn, K.; Jobst, J.; Kellogg, G. L.; Ley, L.; McChesney, J. L.; Ohta, T.; Reshanov, S. A.; Rohrl, J.; Rotenberg, E.; Schmid, A. K.; Waldmann, D.; Weber, H. B.; Seyller, T.

DOI: 10.1021/cr400607y
Chem. Rev. 2015, 115, 8294−8343

Towards wafer-size graphene layers by atmospheric pressure graphitization of silicon carbide. *Nat. Mater.* **2009**, *8*, 203−207.
(74) Brus, L. E. Electron-electron and electron-hole interactions in small semiconductor crystallites: The size dependence of the lowest excited electronic state. *J. Chem. Phys.* **1984**, *80*, 4403−4409.
(75) Brus, L. Electronic wave functions in semiconduc tor clusters: Experiment and theory. *J. Phys. Chem.* **1986**, *90*, 2555−2560.
(76) Henglein, A. Small-particle research: Physicochemical properties of extremely small colloidal metal and semiconductor particles. *Chem. Rev.* **1989**, *89*, 1861−1873.
(77) Zhang, Q.; Dandeneau, C. S.; Zhou, X.; Cao, G. ZnO Nanostructures for dye-sensitized solar cells. *Adv. Mater.* **2009**, *21*, 4087−4108.
(78) Hwang, J. O.; Lee, D. H.; Kim, J. Y.; Han, T. H.; Kim, B. H.; Park, M.; No, K.; Kim, S. O. Vertical ZnO nanowires/graphene hybrids for transparent and flexible field emission. *J. Mater. Chem.* **2011**, *21*, 3432−3437.
(79) Wang, Z. L.; Song, J. H. Piezoelectric nanogenerators based on zinc oxide nanowire arrays. *Science* **2006**, *312*, 242−246.
(80) Law, M.; Greene, L. E.; Johnson, J. C.; Saykally, R.; Yang, P. D. Nanowire dye-sensitized solar cells. *Nat. Mater.* **2005**, *4*, 455−459.
(81) Kim, Y.-J.; Lee, J.-H.; Yi, G.-C. Vertically aligned ZnO nanostructures grown on graphene layers. *Appl. Phys. Lett.* **2009**, *95*, 213101.
(82) Gfroerer, T. H. Photoluminescence in analysis of surfaces and interfaces. *Encyclopedia of Analytical Chemistry*; John Wiley & Sons, Ltd.: Hoboken, NJ, 2006.
(83) Park, W. I.; Jun, Y. H.; Jung, S. W.; Yi, G. C. Excitonic emissions observed in ZnO single crystal nanorods. *Appl. Phys. Lett.* **2003**, *82*, 964−966.
(84) Tan, S. T.; Sun, X. W.; Yu, Z. G.; Wu, P.; Lo, G. Q.; Kwong, D. L. p-type conduction in unintentional carbon-doped ZnO thin films. *Appl. Phys. Lett.* **2007**, *91*, 072101.
(85) Teke, A.; Özgür, Ü.; Doğan, S.; Gu, X.; Morkoç, H.; Nemeth, B.; Nause, J.; Everitt, H. O. Excitonic fine structure and recombination dynamics in single-crystalline ZnO. *Phys. Rev. B: Condens. Matter Mater. Phys.* **2004**, *70*, 195207.
(86) Lee, J. M.; Pyun, Y. B.; Yi, J.; Choung, J. W.; Park, W. I. ZnO nanorod-graphene hybrid architectures for multifunctional conductors. *J. Phys. Chem. C* **2009**, *113*, 19134−19138.
(87) Li, D.; Mueller, M. B.; Gilje, S.; Kaner, R. B.; Wallace, G. G. Processable aqueous dispersions of graphene nanosheets. *Nat. Nanotechnol.* **2008**, *3*, 101−105.
(88) Eda, G.; Fanchini, G.; Chhowalla, M. Large-area ultrathin films of reduced graphene oxide as a transparent and flexible electronic material. *Nat. Nanotechnol.* **2008**, *3*, 270−274.
(89) Xu, C.; Kim, B.-S.; Lee, J.-H.; Kim, M.; Hwang, S. W.; Choi, B. L.; Lee, E. K.; Kim, J. M.; Whang, D. Seed-free electrochemical growth of ZnO nanotube arrays on single-layer graphene. *Mater. Lett.* **2012**, *72*, 25−28.
(90) Choi, D.; Choi, M.-Y.; Choi, W. M.; Shin, H.-J.; Park, H.-K.; Seo, J.-S.; Park, J.; Yoon, S.-M.; Chae, S. J.; Lee, Y. H.; Kim, S.-W.; Choi, J.-Y.; Lee, S. Y.; Kim, J. M. Fully rollable transparent nanogenerators based on graphene electrodes. *Adv. Mater.* **2010**, *22*, 2187−2192.
(91) Hill, E. W.; Geim, A. K.; Novoselov, K.; Schedin, F.; Blake, P. Graphene spin valve devices. *IEEE Trans. Magn.* **2006**, *42*, 2694−2696.
(92) Novoselov, K. S.; Geim, A. K.; Morozov, S. V.; Jiang, D.; Katsnelson, M. I.; Grigorieva, I. V.; Dubonos, S. V.; Firsov, A. A. Two-dimensional gas of massless Dirac fermions in graphene. *Nature* **2005**, *438*, 197−200.
(93) Wang, X.; Zhi, L.; Muellen, K. Transparent, conductive graphene electrodes for dye-sensitized solar cells. *Nano Lett.* **2008**, *8*, 323−327.
(94) Hummers, W. S.; Offeman, R. E. Preparation of graphitic oxide. *J. Am. Chem. Soc.* **1958**, *80*, 1339−1339.
(95) Kovtyukhova, N. I.; Ollivier, P. J.; Martin, B. R.; Mallouk, T. E.; Chizhik, S. A.; Buzaneva, E. V.; Gorchinskiy, A. D. Layer-by-layer assembly of ultrathin composite films from micron-sized graphite oxide sheets and polycations. *Chem. Mater.* **1999**, *11*, 771−778.
(96) Lee, C.-H.; Kim, Y.-J.; Hong, Y. J.; Jeon, S.-R.; Bae, S.; Hong, B. H.; Yi, G.-C. Flexible inorganic nanostructure light-emitting diodes fabricated on graphene films. *Adv. Mater.* **2011**, *23*, 4614−4619.
(97) Kim, Y.-J.; Hadiyawarman; Yoon, A.; Kim, M.; Yi, G.-C.; Liu, C. Hydrothermally grown ZnO nanostructures on few-layer graphene sheets. *Nanotechnology* **2011**, *22*, 245603.
(98) Lin, J.; Penchev, M.; Wang, G.; Paul, R. K.; Zhong, J.; Jing, X.; Ozkan, M.; Ozkan, C. S. Heterogeneous graphene nanostructures: ZnO nanostructures grown on large-area graphene layers. *Small* **2010**, *6*, 2448−2452.
(99) Kumar, B.; Lee, K. Y.; Park, H.-K.; Chae, S. J.; Lee, Y. H.; Kim, S.-W. Controlled growth of semiconducting nanowire, nanowall, and hybrid nanostructures on graphene for piezoelectric nanogenerators. *ACS Nano* **2011**, *5*, 4197−4204.
(100) Kim, Y.-J.; Yoo, H.; Lee, C.-H.; Park, J. B.; Baek, H.; Kim, M.; Yi, G.-C. Position- and morphology-controlled ZnO nanostructures grown on graphene layers. *Adv. Mater.* **2012**, *24*, 5565−9.
(101) Zheng, W. T.; Ho, Y. M.; Tian, H. W.; Wen, M.; Qi, J. L.; Li, Y. A. Field emission from a composite of graphene sheets and ZnO nanowires. *J. Phys. Chem. C* **2009**, *113*, 9164−9168.
(102) Wu, Z.-S.; Pei, S.; Ren, W.; Tang, D.; Gao, L.; Liu, B.; Li, F.; Liu, C.; Cheng, H.-M. Field emission of single-layer graphene films prepared by electrophoretic deposition. *Adv. Mater.* **2009**, *21*, 1756−1760.
(103) Bajic, S.; Latham, R. V. Enhanced cold-cathode emission using composite resin-carbon coatings. *J. Phys. D: Appl. Phys.* **1988**, *21*, 200−204.
(104) Tseng, Y. K.; Huang, C. J.; Cheng, H. M.; Lin, I. N.; Liu, K. S.; Chen, I. C. Characterization and field-emission properties of needle-like zinc oxide nanowires grown vertically on conductive zinc oxide films. *Adv. Funct. Mater.* **2003**, *13*, 811−814.
(105) Lee, C. J.; Lee, T. J.; Lyu, S. C.; Zhang, Y.; Ruh, H.; Lee, H. J. Field emission from well-aligned zinc oxide nanowires grown at low temperature. *Appl. Phys. Lett.* **2002**, *81*, 3648−3650.
(106) Wu, C.; Li, F.; Zhang, Y.; Guo, T. Improving the field emission of graphene by depositing zinc oxide nanorods on its surface. *Carbon* **2012**, *50*, 3622−3626.
(107) Fu, X. W.; Liao, Z. M.; Zhou, Y. B.; Wu, H. C.; Bie, Y. Q.; Xu, J.; Yu, D. P. Graphene/ZnO nanowire/graphene vertical structure based fast-response ultraviolet photodetector. *Appl. Phys. Lett.* **2012**, *100*, 223114.
(108) Bai, J.; Zhong, X.; Jiang, S.; Huang, Y.; Duan, X. Graphene nanomesh. *Nat. Nanotechnol.* **2010**, *5*, 190−194.
(109) Kuo, T.-J.; Lin, C.-N.; Kuo, C.-L.; Huang, M. H. Growth of ultralong ZnO nanowires on silicon substrates by vapor transport and their use as recyclable photocatalysts. *Chem. Mater.* **2007**, *19*, 5143−5147.
(110) Akhavan, O. Graphene Nanomesh by ZnO nanorod photocatalysts. *ACS Nano* **2010**, *4*, 4174−4180.
(111) Hui, Y. Y.; Tai, G. A.; Sun, Z. H.; Xu, Z. H.; Wang, N.; Yan, F.; Lau, S. P. n- and p-Type modulation of ZnO nanomesh coated graphene field effect transistors. *Nanoscale* **2012**, *4*, 3118−3122.
(112) Dutta, M.; Sarkar, S.; Ghosh, T.; Basak, D. ZnO/graphene quantum dot solid-state solar cell. *J. Phys. Chem. C* **2012**, *116*, 20127−20131.
(113) Kim, S.; Janes, D. B.; Choi, S.-Y.; Ju, S. Nanoscale contacts between semiconducting nanowires and metallic graphenes. *Appl. Phys. Lett.* **2012**, *101*, 063122.
(114) Liao, Z.-M.; Lu, Y.; Wu, H.-C.; Bie, Y.-Q.; Zhou, Y.-B.; Yu, D.-P. Improved performance of ZnO nanowire field-effect transistors via focused ion beam treatment. *Nanotechnology* **2011**, *22*, 375201.
(115) Williams, G.; Kamat, P. V. Graphene-semiconductor nanocomposites: Excited-state interactions between ZnO nanoparticles and graphene oxide. *Langmuir* **2009**, *25*, 13869−13873.
(116) Luo, Q. P.; Yu, X. Y.; Lei, B. X.; Chen, H. Y.; Kuang, D. B.; Su, C. Y. Reduced graphene oxide-hierarchical ZnO hollow sphere

DOI: 10.1021/cr400607y
Chem. Rev. 2015, 115, 8294−8343

composites with enhanced photocurrent and photocatalytic activity. *J. Phys. Chem. C* **2012**, *116*, 8111−8117.
(117) Kumar, P.; Panchakarla, L. S.; Venkataprasad Bhat, S.; Maitra, U.; Subrahmanyam, K. S.; Rao, C. N. R. Photoluminescence, white light emitting properties and related aspects of ZnO nanoparticles admixed with graphene and GaN. *Nanotechnology* **2010**, *21*, 385701.
(118) Akhavan, O. Photocatalytic reduction of graphene oxides hybridized by ZnO nanoparticles in ethanol. *Carbon* **2011**, *49*, 11−18.
(119) Baby, T. T.; Ramaprabhu, S. Experimental study on the field emission properties of metal oxide nanoparticle-decorated graphene. *J. Appl. Phys.* **2012**, *111*, 034311.
(120) Vietmeyer, F.; Seger, B.; Kamat, P. V. Anchoring ZnO particles on functionalized single wall carbon nanotubes. Excited state interactions and charge collection. *Adv. Mater.* **2007**, *19*, 2935−2940.
(121) Zou, W.; Zhu, J.; Sun, Y.; Wang, X. Depositing ZnO nanoparticles onto graphene in a polyol system. *Mater. Chem. Phys.* **2011**, *125*, 617−620.
(122) Yu, D.; Nagelli, E.; Naik, R.; Dai, L. Asymmetrically functionalized graphene for photodependent diode rectifying behavior. *Angew. Chem., Int. Ed.* **2011**, *50*, 6575−6578.
(123) Xu, T.; Zhang, L.; Cheng, H.; Zhu, Y. Significantly enhanced photocatalytic performance of ZnO via graphene hybridization and the mechanism study. *Appl. Catal., B* **2011**, *101*, 382−387.
(124) Yang, Y.; Ren, L.; Zhang, C.; Huang, S.; Liu, T. Facile fabrication of functionalized graphene sheets (FGS)/ZnO nanocomposites with photocatalytic property. *ACS Appl. Mater. Interfaces* **2011**, *3*, 2779−2785.
(125) Wang, J.; Tsuzuki, T.; Tang, B.; Hou, X.; Sun, L.; Wang, X. Reduced graphene oxide/ZnO composite: Reusable adsorbent for pollutant management. *ACS Appl. Mater. Interfaces* **2012**, *4*, 3084−3090.
(126) Wang, Z.; Zhan, X.; Wang, Y.; Muhammad, S.; Huang, Y.; He, J. A flexible UV nanosensor based on reduced graphene oxide decorated ZnO nanostructures. *Nanoscale* **2012**, *4*, 2678−2684.
(127) Chang, H.; Sun, Z.; Ho, K. Y.-F.; Tao, X.; Yan, F.; Kwok, W.-M.; Zheng, Z. A highly sensitive ultraviolet sensor based on a facile in situ solution-grown ZnO nanorod/graphene heterostructure. *Nanoscale* **2011**, *3*, 258−264.
(128) Huang, Q.; Zeng, D.; Li, H.; Xie, C. Room temperature formaldehyde sensors with enhanced performance, fast response and recovery based on zinc oxide quantum dots/graphene nanocomposites. *Nanoscale* **2012**, *4*, 5651−5658.
(129) Singh, G.; Choudhary, A.; Haranath, D.; Joshi, A. G.; Singh, N.; Singh, S.; Pasricha, R. ZnO decorated luminescent graphene as a potential gas sensor at room temperature. *Carbon* **2012**, *50*, 385−394.
(130) Yoo, D.-H.; Cuong, T. V.; Luan, V. H.; Khoa, N. T.; Kim, E. J.; Hur, S. H.; Hahn, S. H. Photocatalytic performance of a Ag/ZnO/CCG multidimensional heterostructure prepared by a solution-based method. *J. Phys. Chem. C* **2012**, *116*, 7180−7184.
(131) Allen, E. T.; Crenshaw, J. L. Effect of temperature and acidity in the formation of marcasite (FeS_2) and wurtzite (ZnS): A contribution to the genesis of unstable forms. *Am. J. Sci.* **1914**, *38*, 393−431.
(132) Fang, X. S.; Zhai, T. Y.; Gautam, U. K.; Li, L.; Wu, L. M.; Bando, Y.; Golberg, D. ZnS nanostructures: From synthesis to applications. *Prog. Mater. Sci.* **2011**, *56*, 175−287.
(133) Fang, X. S.; Wu, L. M.; Hu, L. F. ZnS nanostructure arrays: A developing material star. *Adv. Mater.* **2011**, *23*, 585−598.
(134) Hu, J. S.; Ren, L. L.; Guo, Y. G.; Liang, H. P.; Cao, A. M.; Wan, L. J.; Bai, C. L. Mass production and high photocatalytic activity of ZnS nanoporous nanoparticles. *Angew. Chem., Int. Ed.* **2005**, *44*, 1269−1273.
(135) Yanagida, S.; Azuma, T.; Midori, Y.; Pac, C.; Sakurai, H. Semiconductor photocatalysis. Part 4. Hydrogen evolution and photoredox reactions of cyclic ethers catalysed by zinc sulphide. *J. Chem. Soc., Perkin Trans. 2* **1985**, 1487−1493.
(136) Hu, H.; Wang, X.; Liu, F.; Wang, J.; Xu, C. Rapid microwave-assisted synthesis of graphene nanosheets-zinc sulfide nanocomposites: Optical and photocatalytic properties. *Synth. Met.* **2011**, *161*, 404−410.
(137) Subramanian, V.; Wolf, E. E.; Kamat, P. V. Green emission to probe photoinduced charging events in ZnO-Au nanoparticles. Charge distribution and fermi-level equilibration. *J. Phys. Chem. B* **2003**, *107*, 7479−7485.
(138) Rabek, J. F. *Polymer Photodegradation: Mechanisms and Experimental Methods*; Springer: Dordrecht, The Netherlands, 1995.
(139) Wang, P.; Jiang, T.; Zhu, C.; Zhai, Y.; Wang, D.; Dong, S. One-step, solvothermal synthesis of graphene-CdS and graphene-ZnS quantum dot nanocomposites and their interesting photovoltaic properties. *Nano Res.* **2010**, *3*, 794−799.
(140) Nethravathi, C.; Nisha, T.; Ravishankar, N.; Shivakumara, C.; Rajamathi, M. Graphene-nanocrystalline metal sulphide composites produced by a one-pot reaction starting from graphite oxide. *Carbon* **2009**, *47*, 2054−2059.
(141) Fernandez-Garcia, M.; Martinez-Arias, A.; Hanson, J. C.; Rodriguez, J. A. Nanostructured oxides in chemistry: Characterization and properties. *Chem. Rev.* **2004**, *104*, 4063−4104.
(142) Moriarty, P. Nanostructured materials. *Rep. Prog. Phys.* **2001**, *64*, 297−381.
(143) Yang, Y.; Liu, T. Fabrication and characterization of graphene oxide/zinc oxide nanorods hybrid. *Appl. Surf. Sci.* **2011**, *257*, 8950−8954.
(144) Li, Y.; Liu, Y.; Shen, W.; Yang, Y.; Wen, Y.; Wang, M. Graphene-ZnS quantum dot nanocomposites produced by solvothermal route. *Mater. Lett.* **2011**, *65*, 2518−2521.
(145) Li, C.; Jiang, D.; Zhang, L.; Xia, J.; Li, Q. Controlled Synthesis of ZnS Quantum Dots and ZnS Quantum Flakes with Graphene as a Template. *Langmuir* **2012**, *28*, 9729−9734.
(146) Fang, X. S.; Bando, Y.; Shen, G. Z.; Ye, C. H.; Gautam, U. K.; Costa, P. M. F. J.; Zhi, C. Y.; Tang, C. C.; Golberg, D. Ultrafine ZnS nanobelts as field emitters. *Adv. Mater.* **2007**, *19*, 2593−2596.
(147) Kim, S.; Choi, H.; Jung, M.; Choi, S.-Y.; Ju, S. Hybrid nanowire-multilayer graphene film light-emitting sources. *Nanotechnology* **2010**, *21*, 425203.
(148) Matsumura, M.; Furukawa, S.; Saho, Y.; Tsubomura, H. Cadmium sulfide photocatalyzed hydrogen production from aqueous solutions of sulfite: Effect of crystal structure and preparation method of the catalyst. *J. Phys. Chem.* **1985**, *89*, 1327−1329.
(149) Radecka, M.; Rekas, M.; Trenczek-Zajac, A.; Zakrzewska, K. Importance of the band gap energy and flat band potential for application of modified TiO_2 photoanodes in water photolysis. *J. Power Sources* **2008**, *181*, 46−55.
(150) Gelderman, K.; Lee, L.; Donne, S. W. Flat-band potential of a semiconductor: Using the Mott-Schottky equation. *J. Chem. Educ.* **2007**, *84*, 685−688.
(151) Bott, A. W. Electrochemistry of semiconductors. *Curr. Sep.* **1998**, *17*, 87−92.
(152) Reber, J. F.; Rusek, M. Photochemical hydrogen production with platinized suspensions of cadmium sulfide and cadmium zinc sulfide modified by silver sulfide. *J. Phys. Chem.* **1986**, *90*, 824−834.
(153) Meissner, D.; Memming, R.; Kastening, B.; Bahnemann, D. Fundamental problems of water splitting at cadmium sulfide. *Chem. Phys. Lett.* **1986**, *127*, 419−423.
(154) Honma, I.; Sano, T.; Komiyama, H. Surface-enhanced Raman scattering (SERS) for semiconductor microcrystallites observed in Ag-CdS hybrid particles. *J. Phys. Chem.* **1993**, *97*, 6692−6695.
(155) Ye, J.; Hou, Y.; Zhang, G.; Wu, C. Temperature-induced aggregation of poly(N-isopropylacrylamide)-stabilizecd CdS quantum dots in water. *Langmuir* **2008**, *24*, 2727−2731.
(156) Weller, H. Colloidal semiconductor Q-particles: Chemistry in the transition region between solid state and molecules. *Angew. Chem., Int. Ed. Engl.* **1993**, *32*, 41−53.
(157) Han, S. C.; Hu, L. F.; Gao, N.; Al-Ghamdi, A. A.; Fang, X. S. Efficient Self-assembly synthesis of uniform CdS spherical nanoparticles-Au nanoparticles hybrids with enhanced photoactivity. *Adv. Funct. Mater.* **2014**, *24*, 3725−3733.

DOI: 10.1021/cr400607y
Chem. Rev. 2015, 115, 8294−8343

(158) Hirai, T.; Okubo, H.; Komasawa, I. Size-selective incorporation of CdS nanoparticles into mesoporous silica. *J. Phys. Chem. B* **1999**, *103*, 4228−4230.
(159) Bao, N. Z.; Shen, L. M.; Takata, T.; Domen, K. Self-templated synthesis of nanoporous CdS nanostructures for highly efficient photocatalytic hydrogen production under visible. *Chem. Mater.* **2008**, *20*, 110−117.
(160) Jing, D. W.; Guo, L. J. A novel method for the preparation of a highly stable and active CdS photocatalyst with a special surface nanostructure. *J. Phys. Chem. B* **2006**, *110*, 11139−11145.
(161) Cao, A. N.; Liu, Z.; Chu, S. S.; Wu, M. H.; Ye, Z. M.; Cai, Z. W.; Chang, Y. L.; Wang, S. F.; Gong, Q. H.; Liu, Y. F. A facile one-step method to produce graphene-CdS quantum dot nanocomposites as promising optoelectronic materials. *Adv. Mater.* **2010**, *22*, 103−106.
(162) Li, Q.; Guo, B. D.; Yu, J. G.; Ran, J. R.; Zhang, B. H.; Yan, H. J.; Gong, J. R. Highly efficient visible-light-driven photocatalytic hydrogen production of CdS-cluster-decorated graphene nanosheets. *J. Am. Chem. Soc.* **2011**, *133*, 10878−10884.
(163) Alonsovante, N.; Colell, H.; Stimming, U.; Tributsch, H. Anomalous low-temperature kinetic effects for oxygen evolution on RuO_2 and Pt electrodes. *J. Phys. Chem.* **1993**, *97*, 7381−7384.
(164) Bamwenda, G. R.; Tsubota, S.; Nakamura, T.; Haruta, M. Photoassisted hydrogen production from a water-ethanol solution: A comparison of activities of Au-TiO_2 and Pt-TiO_2. *J. Photochem. Photobiol., A* **1995**, *89*, 177−189.
(165) Jia, L.; Wang, D. H.; Huang, Y. X.; Xu, A. W.; Yu, H. Q. Highly durable N-doped graphene/CdS nanocomposites with enhanced photocatalytic hydrogen evolution from water under visible light irradiation. *J. Phys. Chem. C* **2011**, *115*, 11466−11473.
(166) Zhang, N.; Zhang, Y. H.; Pan, X. Y.; Fu, X. Z.; Liu, S. Q.; Xu, Y. J. Assembly of CdS nanoparticles on the two-dimensional graphene scaffold as visible-light-driven photocatalyst for selective organic transformation under ambient conditions. *J. Phys. Chem. C* **2011**, *115*, 23501−23511.
(167) Liu, X. J.; Pan, L. K.; Lv, T.; Zhu, G.; Sun, Z.; Sun, C. Q. Microwave-assisted synthesis of CdS-reduced graphene oxide composites for photocatalytic reduction of Cr(VI). *Chem. Commun.* **2011**, *47*, 11984−11986.
(168) Santra, P. K.; Kamat, P. V. Mn-doped quantum dot sensitized solar cells: A strategy to boost efficiency over 5%. *J. Am. Chem. Soc.* **2012**, *134*, 2508−2511.
(169) Lv, T.; Pan, L. K.; Liu, X. J.; Lu, T.; Zhu, G.; Sun, Z.; Sun, C. Q. One-step synthesis of CdS-TiO_2-chemically reduced graphene oxide composites via microwave-assisted reaction for visible-light photocatalytic degradation of methyl orange. *Catal. Sci. Technol.* **2012**, *2*, 754−758.
(170) Zhao, W.; Bai, Z.; Ren, A.; Guo, B.; Wu, C. Sunlight photocatalytic activity of CdS modified TiO_2 loaded on activated carbon fibers. *Appl. Surf. Sci.* **2010**, *256*, 3493−3498.
(171) Dufaux, T.; Boettcher, J.; Burghard, M.; Kern, K. Photocurrent distribution in graphene-CdS nanowire devices. *Small* **2010**, *6*, 1868−1872.
(172) Lee, H.; Heo, K.; Park, J.; Park, Y.; Noh, S.; Kim, K. S.; Lee, C.; Hong, B. H.; Jian, J.; Hong, S. Graphene-nanowire hybrid structures for high-performance photoconductive devices. *J. Mater. Chem.* **2012**, *22*, 8372−8376.
(173) Foll, H.; Langa, S.; Carstensen, J.; Christophersen, M.; Tiginyanu, I. M. Pores in III-V semiconductors. *Adv. Mater.* **2003**, *15*, 183−198.
(174) Dick, K. A.; Deppert, K.; Karlsson, L. S.; Wallenberg, L. R.; Samuelson, L.; Seifert, W. A new understanding of au-assisted growth of III-V semiconductor nanowires. *Adv. Funct. Mater.* **2005**, *15*, 1603−1610.
(175) Matsukura, F.; Ohno, H.; Dietl, T. *III-V Ferromagnetic Semiconductors*; Elsevier Science BV: Amsterdam, 2002; Vol. *14*, pp 1−87.
(176) Vurgaftman, I.; Meyer, J. R.; Ram-Mohan, L. R. Band parameters for III-V compound semiconductors and their alloys. *J. Appl. Phys.* **2001**, *89*, 5815−5875.
(177) del Alamo, J. A. Nanometre-scale electronics with III-V compound semiconductors. *Nature* **2011**, *479*, 317−323.
(178) Watanabe, K.; Taniguchi, T.; Kanda, H. Direct-bandgap properties and evidence for ultraviolet lasing of hexagonal boron nitride single crystal. *Nat. Mater.* **2004**, *3*, 404−409.
(179) Golberg, D.; Bando, Y.; Huang, Y.; Terao, T.; Mitome, M.; Tang, C. C.; Zhi, C. Y. Boron nitride nanotubes and nanosheets. *ACS Nano* **2010**, *4*, 2979−2993.
(180) Song, L.; Ci, L. J.; Lu, H.; Sorokin, P. B.; Jin, C. H.; Ni, J.; Kvashnin, A. G.; Kvashnin, D. G.; Lou, J.; Yakobson, B. I.; Ajayan, P. M. Large scale growth and characterization of atomic hexagonal boron nitride Layers. *Nano Lett.* **2010**, *10*, 3209−3215.
(181) Lee, C.; Li, Q.; Kalb, W.; Liu, X.-Z.; Berger, H.; Carpick, R. W.; Hone, J. Frictional characteristics of atomically thin sheets. *Science* **2010**, *328*, 76−80.
(182) Pacile, D.; Meyer, J. C.; Girit, C. O.; Zettl, A. The two-dimensional phase of boron nitride: Few-atomic-layer sheets and suspended membranes. *Appl. Phys. Lett.* **2008**, *92*, 133107.
(183) Pakdel, A.; Wang, X. B.; Bando, Y.; Golberg, D. Nonwetting "white graphene" films. *Acta Mater.* **2013**, *61*, 1266−1273.
(184) Yu, J.; Qin, L.; Hao, Y.; Kuang, S.; Bai, X.; Chong, Y.-M.; Zhang, W.; Wang, E. Vertically aligned boron nitride nanosheets: Chemical vapor synthesis, ultraviolet light emission, and superhydrophobicity. *ACS Nano* **2010**, *4*, 414−422.
(185) Ci, L.; Song, L.; Jin, C. H.; Jariwala, D.; Wu, D. X.; Li, Y. J.; Srivastava, A.; Wang, Z. F.; Storr, K.; Balicas, L.; Liu, F.; Ajayan, P. M. Atomic layers of hybridized boron nitride and graphene domains. *Nat. Mater.* **2010**, *9*, 430−435.
(186) Castro Neto, A. H.; Guinea, F.; Peres, N. M. R.; Novoselov, K. S.; Geim, A. K. The electronic properties of graphene. *Rev. Mod. Phys.* **2009**, *81*, 109−162.
(187) Dean, C. R.; Young, A. F.; Meric, I.; Lee, C.; Wang, L.; Sorgenfrei, S.; Watanabe, K.; Taniguchi, T.; Kim, P.; Shepard, K. L.; Hone, J. Boron nitride substrates for high-quality graphene electronics. *Nat. Nanotechnol.* **2010**, *5*, 722−726.
(188) Xue, J. M.; Sanchez-Yamagishi, J.; Bulmash, D.; Jacquod, P.; Deshpande, A.; Watanabe, K.; Taniguchi, T.; Jarillo-Herrero, P.; Leroy, B. J. Scanning tunnelling microscopy and spectroscopy of ultra-flat graphene on hexagonal boron nitride. *Nat. Mater.* **2011**, *10*, 282−285.
(189) Gannett, W.; Regan, W.; Watanabe, K.; Taniguchi, T.; Crommie, M. F.; Zettl, A. Boron nitride substrates for high mobility chemical vapor deposited graphene. *Appl. Phys. Lett.* **2011**, *98*, 242105.
(190) Wang, H.; Taychatanapat, T.; Hsu, A.; Watanabe, K.; Taniguchi, T.; Jarillo-Herrero, P.; Palacios, T. BN/graphene/BN transistors for RF applications. *IEEE Electron Device Lett.* **2011**, *32*, 1209−1211.
(191) Haigh, S. J.; Gholinia, A.; Jalil, R.; Romani, S.; Britnell, L.; Elias, D. C.; Novoselov, K. S.; Ponomarenko, L. A.; Geim, A. K.; Gorbachev, R. Cross-sectional imaging of individual layers and buried interfaces of graphene-based heterostructures and superlattices. *Nat. Mater.* **2012**, *11*, 764−767.
(192) Lee, K. H.; Shin, H. J.; Lee, J.; Lee, I. Y.; Kim, G. H.; Choi, J. Y.; Kim, S. W. Large-scale synthesis of high-quality hexagonal boron nitride nanosheets for large-area graphene electronics. *Nano Lett.* **2012**, *12*, 714−718.
(193) Luo, Z. T.; Lu, Y.; Singer, D. W.; Berck, M. E.; Somers, L. A.; Goldsmith, B. R.; Johnson, A. T. C. Effect of substrate roughness and feedstock concentration on growth of wafer-scale graphene at atmospheric pressure. *Chem. Mater.* **2011**, *23*, 1441−1447.
(194) Han, G. H.; Guenes, F.; Bae, J. J.; Kim, E. S.; Chae, S. J.; Shin, H.-J.; Choi, J.-Y.; Pribat, D.; Lee, Y. H. Influence of copper morphology in forming nucleation seeds for graphene growth. *Nano Lett.* **2011**, *11*, 4144−4148.
(195) Liu, Z.; Song, L.; Zhao, S. Z.; Huang, J. Q.; Ma, L. L.; Zhang, J. N.; Lou, J.; Ajayan, P. M. Direct growth of graphene/hexagonal boron nitride stacked layers. *Nano Lett.* **2011**, *11*, 2032−2037.
(196) Ding, X. L.; Ding, G. Q.; Xie, X. M.; Huang, F. Q.; Jiang, M. H. Direct growth of few layer graphene on hexagonal boron nitride by chemical vapor deposition. *Carbon* **2011**, *49*, 2522−2525.

DOI: 10.1021/cr400607y
Chem. Rev. 2015, 115, 8294−8343

(197) Adachi, S. *Gaas and Related Materials: Bulk Semiconducting and Superlattice Properties*; World Scientific Publishing Co., Inc.: Singapore, 1994.
(198) Blakemore, J. S. Semiconducting and other major properties of gallium arsenide. *J. Appl. Phys.* **1982**, *53*, R123−R181.
(199) Duan, X. F.; Wang, J. F.; Lieber, C. M. Synthesis and optical properties of gallium arsenide nanowires. *Appl. Phys. Lett.* **2000**, *76*, 1116−1118.
(200) Alferov, Z. I. Nobel Lecture: The double heterostructure concept and its applications in physics, electronics, and technology. *Rev. Mod. Phys.* **2001**, *73*, 767−782.
(201) Ferrari, A. C.; Meyer, J. C.; Scardaci, V.; Casiraghi, C.; Lazzeri, M.; Mauri, F.; Piscanec, S.; Jiang, D.; Novoselov, K. S.; Roth, S.; Geim, A. K. Raman spectrum of graphene and graphene layers. *Phys. Rev. Lett.* **2006**, *97*, 187401.
(202) Gupta, A.; Chen, G.; Joshi, P.; Tadigadapa, S.; Eklund, P. C. Raman scattering from high-frequency phonons in supported n-graphene layer films. *Nano Lett.* **2006**, *6*, 2667−2673.
(203) Calizo, I.; Bao, W. Z.; Miao, F.; Lau, C. N.; Balandin, A. A. The effect of substrates on the Raman spectrum of graphene: Graphene-on-sapphire and graphene-on-glass. *Appl. Phys. Lett.* **2007**, *91*, 201904.
(204) Calizo, I.; Ghosh, S.; Bao, W. Z.; Miao, F.; Lau, C. N.; Balandin, A. A. Raman nanometrology of graphene: Temperature and substrate effects. *Solid State Commun.* **2009**, *149*, 1132−1135.
(205) Friedemann, M.; Pierz, K.; Stosch, R.; Ahlers, F. J. Graphene on gallium arsenide: Engineering the visibility. *Appl. Phys. Lett.* **2009**, *95*, 102103.
(206) Woszczyna, M.; Friedemann, M.; Pierz, K.; Weimann, T.; Ahlers, F. J. Magneto-transport properties of exfoliated graphene on GaAs. *J. Appl. Phys.* **2011**, *110*, 043712.
(207) Simon, J.; Simmonds, P. J.; Woodall, J. M.; Lee, M. L. Graphitized carbon on GaAs(100) substrates. *Appl. Phys. Lett.* **2011**, *98*, 073113.
(208) Tang, C. C.; Li, M. Y.; Li, L. J.; Chi, C. C.; Chen, J. C. Graphene-GaAs/AlxGa1-xAs heterostructure dual-function field-effect transistor. *Appl. Phys. Lett.* **2012**, *101*, 202104.
(209) Peters, K.; Tittel, A.; Gayer, N.; Graf, A.; Paulava, V.; Wurstbauer, U.; Hansen, W. Enhancing the visibility of graphene on GaAs. *Appl. Phys. Lett.* **2011**, *99*, 191912.
(210) Teo, G.; Wang, H.; Wu, Y.; Guo, Z.; Zhang, J.; Ni, Z.; Shen, Z. Visibility study of graphene multilayer structures. *J. Appl. Phys.* **2008**, *103*, 124302.
(211) Goncalves, G.; Marques, P.; Barros-Timmons, A.; Bdkin, I.; Singh, M. K.; Emami, N.; Gracio, J. Graphene oxide modified with PMMA via ATRP as a reinforcement filler. *J. Mater. Chem.* **2010**, *20*, 9927−9934.
(212) Stoberl, U.; Wurstbauer, U.; Wegscheider, W.; Weiss, D.; Eroms, J. Morphology and flexibility of graphene and few-layer graphene on various substrates. *Appl. Phys. Lett.* **2008**, *93*, 051906.
(213) Lee, J. M.; Choung, J. W.; Yi, J.; Lee, D. H.; Samal, M.; Yi, D. K.; Lee, C. H.; Yi, G. C.; Paik, U.; Rogers, J. A.; Park, W. I. Vertical pillar-superlattice array and graphene hybrid light emitting diodes. *Nano Lett.* **2010**, *10*, 2783−2788.
(214) Munshi, A. M.; Dheeraj, D. L.; Fauske, V. T.; Kim, D. C.; van Helvoort, A. T. J.; Fimland, B. O.; Weman, H. Vertically aligned GaAs nanowires on graphite and few-layer graphene: Generic model and epitaxial growth. *Nano Lett.* **2012**, *12*, 4570−4576.
(215) Pearton, S. J.; Zolper, J. C.; Shul, R. J.; Ren, F. GaN: Processing, defects, and devices. *J. Appl. Phys.* **1999**, *86*, 1−78.
(216) Morkoc, H.; Strite, S.; Gao, G. B.; Lin, M. E.; Sverdlov, B.; Burns, M. Large - band - gap SiC, III - V nitride, and II - VI ZnSe - based semiconductor device technologies. *J. Appl. Phys.* **1994**, *76*, 1363−1398.
(217) Strite, S.; Morkoc, H. GaN, AIN and InN: A review. *J. Vac. Sci. Technol., B: Microelectron. Process. Phenom.* **1992**, *10*, 1237−1266.
(218) Jain, S. C.; Willander, M.; Narayan, J.; Van Overstraeten, R. III-nitrides: Growth, characterization, and properties. *J. Appl. Phys.* **2000**, *87*, 965−1006.
(219) Chung, K.; Lee, C.-H.; Yi, G.-C. Transferable GaN layers grown on ZnO-coated graphene layers for optoelectronic devices. *Science* **2010**, *330*, 655−657.
(220) Chung, K.; Park, S. I.; Baek, H.; Chung, J. S.; Yi, G. C. High-quality GaN films grown on chemical vapor-deposited graphene films. *NPG Asia Mater.* **2012**, *4*, e24.
(221) Han, N.; Cuong, T. V.; Han, M.; Ryu, B. D.; Chandramohan, S.; Park, J. B.; Kang, J. H.; Park, Y. J.; Ko, K. B.; Kim, H. Y.; Kim, H. K.; Ryu, J. H.; Katharria, Y. S.; Choi, C. J.; Hong, C. H. Improved heat dissipation in gallium nitride light-emitting diodes with embedded graphene oxide pattern. *Nat. Commun.* **2013**, *4*, 1452.
(222) Subrina, S.; Kotchetkov, D.; Balandin, A. A. Heat removal in silicon-on-insulator integrated circuits with graphene lateral heat spreaders. *IEEE Electron Device Lett.* **2009**, *30*, 1281−1283.
(223) Yan, Z.; Liu, G. X.; Khan, J. M.; Balandin, A. A. Graphene quilts for thermal management of high-power GaN transistors. *Nat. Commun.* **2012**, *3*, 827.
(224) Jo, G.; Choe, M.; Cho, C. Y.; Kim, J. H.; Park, W.; Lee, S.; Hong, W. K.; Kim, T. W.; Park, S. J.; Hong, B. H.; Kahng, Y. H.; Lee, T. Large-scale patterned multi-layer graphene films as transparent conducting electrodes for GaN light-emitting diodes. *Nanotechnology* **2010**, *21*, 175201.
(225) Kim, B. J.; Mastro, M. A.; Hite, J.; Eddy, C. R.; Kim, J. Transparent conductive graphene electrode in GaN-based ultra-violet light emitting diodes. *Opt. Express* **2010**, *18*, 23030−23034.
(226) Kim, B. J.; Lee, C.; Jung, Y.; Baik, K. H.; Mastro, M. A.; Hite, J. K.; Eddy, C. R.; Kim, J. Large-area transparent conductive few-layer graphene electrode in GaN-based ultra-violet light-emitting diodes. *Appl. Phys. Lett.* **2011**, *99*, 143101.
(227) Caldwell, J. D.; Anderson, T. J.; Culbertson, J. C.; Jernigan, G. G.; Hobart, K. D.; Kub, F. J.; Tadjer, M. J.; Tedesco, J. L.; Hite, J. K.; Mastro, M. A.; Myers-Ward, R. L.; Eddy, C. R.; Campbell, P. M.; Gaskill, D. K. Technique for the dry transfer of epitaxial graphene onto arbitrary substrates. *ACS Nano* **2010**, *4*, 1108−1114.
(228) Lee, J. M.; Jeong, H. Y.; Choi, K. J.; Il Park, W. Metal/graphene sheets as p-type transparent conducting electrodes in GaN light emitting diodes. *Appl. Phys. Lett.* **2011**, *99*, 041115.
(229) Chandramohan, S.; Kang, J. H.; Katharria, Y. S.; Han, N.; Beak, Y. S.; Ko, K. B.; Park, J. B.; Kim, H. K.; Suh, E. K.; Hong, C. H. Work-function-tuned multilayer graphene as current spreading electrode in blue light-emitting diodes. *Appl. Phys. Lett.* **2012**, *100*, 023502.
(230) Choe, M.; Cho, C. Y.; Shim, J. P.; Park, W.; Lim, S. K.; Hong, W. K.; Lee, B. H.; Lee, D. S.; Park, S. J.; Lee, T. Au nanoparticle-decorated graphene electrodes for GaN-based optoelectronic devices. *Appl. Phys. Lett.* **2012**, *101*, 031115.
(231) Seo, T. H.; Lee, K. J.; Oh, T. S.; Lee, Y. S.; Jeong, H.; Park, A. H.; Kim, H.; Choi, Y. R.; Suh, E. K.; Cuong, T. V.; Pham, V. H.; Chung, J. S.; Kim, E. J. Graphene network on indium tin oxide nanodot nodes for transparent and current spreading electrode in InGaN/GaN light emitting diode. *Appl. Phys. Lett.* **2011**, *98*, 251114.
(232) Seo, T. H.; Lee, K. J.; Park, A. H.; Hong, C. H.; Suh, E. K.; Chae, S. J.; Lee, Y. H.; Cuong, T. V.; Pham, V. H.; Chung, J. S.; Kim, E. J.; Jeon, S. R. Enhanced light output power of near UV light emitting diodes with graphene/indium tin oxide nanodot nodes for transparent and current spreading electrode. *Opt. Express* **2011**, *19*, 23111−23117.
(233) Liao, L.; Bai, J. W.; Cheng, R.; Lin, Y. C.; Jiang, S.; Qu, Y. Q.; Huang, Y.; Duan, X. F. Sub-100 nm channel length graphene transistors. *Nano Lett.* **2010**, *10*, 3952−3956.
(234) Hosono, H. Recent progress in transparent oxide semiconductors: Materials and device application. *Thin Solid Films* **2007**, *515*, 6000−6014.
(235) Hosono, H. Ionic amorphous oxide semiconductors: Material design, carrier transport, and device application. *J. Non-Cryst. Solids* **2006**, *352*, 851−858.
(236) Fukumura, T.; Toyosaki, H.; Yamada, Y. Magnetic oxide semiconductors. *Semicond. Sci. Technol.* **2005**, *20*, S103−S111.

DOI: 10.1021/cr400607y
Chem. Rev. 2015, 115, 8294−8343

(237) Miyauchi, M.; Nakajima, A.; Hashimoto, K.; Watanabe, T. A highly hydrophilic thin film under 1 μW/cm^2 UV illumination. *Adv. Mater.* **2000**, *12*, 1923−1927.
(238) Yan, Y. Y.; Gao, N.; Barthlott, W. Mimicking natural superhydrophobic surfaces and grasping the wetting process: A review on recent progress in preparing superhydrophobic surfaces. *Adv. Colloid Interface Sci.* **2011**, *169*, 80−105.
(239) Fujishima, A.; Zhang, X. T. Titanium dioxide photocatalysis: Present situation and future approaches. *C. R. Chim.* **2006**, *9*, 750−760.
(240) Wang, R.; Hashimoto, K.; Fujishima, A.; Chikuni, M.; Kojima, E.; Kitamura, A.; Shimohigoshi, M.; Watanabe, T. Photogeneration of highly amphiphilic TiO_2 surfaces. *Adv. Mater.* **1998**, *10*, 135−138.
(241) Zhang, H. Z.; Banfield, J. F. Understanding polymorphic phase transformation behavior during growth of nanocrystalline aggregates: Insights from TiO_2. *J. Phys. Chem. B* **2000**, *104*, 3481−3487.
(242) Fujishima, A.; Zhang, X.; Tryk, D. A. TiO_2 photocatalysis and related surface phenomena. *Surf. Sci. Rep.* **2008**, *63*, 515−582.
(243) Burnside, S. D.; Shklover, V.; Barbe, C.; Comte, P.; Arendse, F.; Brooks, K.; Gratzel, M. Self-organization of TiO_2 nanoparticles in thin films. *Chem. Mater.* **1998**, *10*, 2419−2425.
(244) Leary, R.; Westwood, A. Carbonaceous nanomaterials for the enhancement of TiO_2 photocatalysis. *Carbon* **2011**, *49*, 741−772.
(245) Malato, S.; Fernandez-Ibanez, P.; Maldonado, M. I.; Blanco, J.; Gernjak, W. Decontamination and disinfection of water by solar photocatalysis: Recent overview and trends. *Catal. Today* **2009**, *147*, 1−59.
(246) Williams, G.; Seger, B.; Kamat, P. V. TiO_2-graphene nanocomposites. UV-assisted photocatalytic reduction of graphene oxide. *ACS Nano* **2008**, *2*, 1487−1491.
(247) Becerril, H. A.; Mao, J.; Liu, Z.; Stoltenberg, R. M.; Bao, Z.; Chen, Y. Evaluation of solution-processed reduced graphene oxide films as transparent conductors. *ACS Nano* **2008**, *2*, 463−470.
(248) Stankovich, S.; Dikin, D. A.; Dommett, G. H. B.; Kohlhaas, K. M.; Zimney, E. J.; Stach, E. A.; Piner, R. D.; Nguyen, S. T.; Ruoff, R. S. Graphene-based composite materials. *Nature* **2006**, *442*, 282−286.
(249) Kotov, N. A.; Dekany, I.; Fendler, J. H. Ultrathin graphite oxide-polyelectrolyte composites prepared by self-assembly: Transition between conductive and non-conductive states. *Adv. Mater.* **1996**, *8*, 637−641.
(250) Kamat, P. V.; Bedja, I.; Hotchandani, S. Photoinduced charge transfer between carbon and semiconductor clusters-one-electron reduction of C_{60} in colloidal TiO_2 semiconductor suspensions. *J. Phys. Chem.* **1994**, *98*, 9137−9142.
(251) Robel, I.; Bunker, B. A.; Kamat, P. V. Single-walled carbon nanotube-CdS nanocomposites as light-harvesting assemblies: Photoinduced charge-transfer interactions. *Adv. Mater.* **2005**, *17*, 2458−2463.
(252) Kongkanand, A.; Kamat, P. V. Electron storage in single wall carbon nanotubes. Fermi level equilibration in semiconductor-SWCNT suspensions. *ACS Nano* **2007**, *1*, 13−21.
(253) Lightcap, I. V.; Kosel, T. H.; Kamat, P. V. Anchoring semiconductor and metal nanoparticles on a two-dimensional catalyst mat. storing and shuttling electrons with reduced graphene oxide. *Nano Lett.* **2010**, *10*, 577−583.
(254) Ng, Y. H.; Lightcap, I. V.; Goodwin, K.; Matsumura, M.; Kamat, P. V. To what extent do graphene scaffolds improve the photovoltaic and photocatalytic response of TiO_2 nanostructured films? *J. Phys. Chem. Lett.* **2010**, *1*, 2222−2227.
(255) Tan, Y. W.; Zhang, Y.; Bolotin, K.; Zhao, Y.; Adam, S.; Hwang, E. H.; Das Sarma, S.; Stormer, H. L.; Kim, P. Measurement of scattering rate and minimum conductivity in graphene. *Phys. Rev. Lett.* **2007**, *99*, 246803.
(256) Zhang, H.; Lv, X. J.; Li, Y. M.; Wang, Y.; Li, J. H. P25-Graphene composite as a high performance photocatalyst. *ACS Nano* **2010**, *4*, 380−386.
(257) Wang, X.; Zhi, L. J.; Mullen, K. Transparent, conductive graphene electrodes for dye-sensitized solar cells. *Nano Lett.* **2008**, *8*, 323−327.
(258) Wang, D. H.; Choi, D. W.; Li, J.; Yang, Z. G.; Nie, Z. M.; Kou, R.; Hu, D. H.; Wang, C. M.; Saraf, L. V.; Zhang, J. G.; Aksay, I. A.; Liu, J. Self-assembled TiO_2-graphene hybrid nanostructures for enhanced Li-ion insertion. *ACS Nano* **2009**, *3*, 907−914.
(259) Akhavan, O.; Ghaderi, E. Photocatalytic reduction of graphene oxide nanosheets on TiO_2 thin film for photoinactivation of bacteria in solar light irradiation. *J. Phys. Chem. C* **2009**, *113*, 20214−20220.
(260) Sato, T.; Taya, M. Copper-aided photo sterilization of microbial cells on TiO_2 film under irradiation from a white light fluorescent lamp. *Biochem. Eng. J.* **2006**, *30*, 199−204.
(261) Vamathevan, V.; Amal, R.; Beydoun, D.; Low, G.; McEvoy, S. Photocatalytic oxidation of organics in water using pure and silver-modified titanium dioxide particles. *J. Photochem. Photobiol., A* **2002**, *148*, 233−245.
(262) Gaya, U. I.; Abdullah, A. H. Heterogeneous photocatalytic degradation of organic contaminants over titanium dioxide: A review of fundamentals, progress and problems. *J. Photochem. Photobiol., C* **2008**, *9*, 1−12.
(263) Akhavan, O.; Abdolahad, M.; Esfandiar, A.; Mohatashamifar, M. Photodegradation of graphene oxide sheets by TiO_2 nanoparticles after a photocatalytic reduction. *J. Phys. Chem. C* **2010**, *114*, 12955−12959.
(264) Zhang, X. Y.; Li, H. P.; Cui, X. L.; Lin, Y. H. Graphene/TiO_2 nanocomposites: Synthesis, characterization and application in hydrogen evolution from water photocatalytic splitting. *J. Mater. Chem.* **2010**, *20*, 2801−2806.
(265) Chou, P. W.; Wang, Y. S.; Lin, C. C.; Chen, Y. J.; Cheng, C. L.; Wong, M. S. Effect of carbon and oxygen on phase transformation of titania films during annealing. *Surf. Coat. Technol.* **2009**, *204*, 834−839.
(266) Lee, J. S.; You, K. H.; Park, C. B. Highly photoactive, low bandgap TiO_2 nanoparticles wrapped by graphene. *Adv. Mater.* **2012**, *24*, 1084−1088.
(267) Lei, Z.; Xiao, Y.; Dang, L.; You, W.; Hu, G.; Zhang, J. Nickel-catalyzed fabrication of SiO_2, TiO_2/graphitized carbon, and the resultant graphitized carbon with periodically macroporous structure. *Chem. Mater.* **2007**, *19*, 477−484.
(268) Shanmugam, S.; Gabashvili, A.; Jacob, D. S.; Yu, J. C.; Gedanken, A. Synthesis and characterization of TiO_2@C core-shell composite nanoparticles and evaluation of their photocatalytic activities. *Chem. Mater.* **2006**, *18*, 2275−2282.
(269) Zhang, L. W.; Fu, H. B.; Zhu, Y. F. Efficient TiO_2 photocatalysts from surface hybridization of TiO_2 particles with graphite-like carbon. *Adv. Funct. Mater.* **2008**, *18*, 2180−2189.
(270) Murphy, A. B. Band-gap determination from diffuse reflectance measurements of semiconductor films, and application to photoelectrochemical water-splitting. *Sol. Energy Mater. Sol. Cells* **2007**, *91*, 1326−1337.
(271) Kim, H. I.; Moon, G. H.; Monllor-Satoca, D.; Park, Y.; Choi, W. Solar photoconversion using graphene/TiO_2 composites: Nanographene shell on TiO_2 core versus TiO_2 nanoparticles on graphene sheet. *J. Phys. Chem. C* **2012**, *116*, 1535−1543.
(272) Chen, C.; Cai, W. M.; Long, M. C.; Zhou, B. X.; Wu, Y. H.; Wu, D. Y.; Feng, Y. J. Synthesis of visible-light responsive graphene oxide/TiO_2 composites with p/n heterojunction. *ACS Nano* **2010**, *4*, 6425−6432.
(273) Schniepp, H. C.; Saville, D. A.; Aksay, I. A. Self-healing of surfactant surface micelles on millisecond time scales. *J. Am. Chem. Soc.* **2006**, *128*, 12378−12379.
(274) Andrea, D. *Battery Management Systems for Large Lithium Ion Battery Packs*; Artech House: Boston, MA, 2010.
(275) Winter, M.; Brodd, R. J. What are batteries, fuel cells, and supercapacitors? *Chem. Rev.* **2004**, *104*, 4245−4269.
(276) Young, K.; Wang, C.; Wang, L.; Strunz, K. Electric vehicle battery technologies. In *Electric Vehicle Integration into Modern Power Networks*; Garcia-Valle, R., Peças Lopes, J. A., Eds.; Springer: New York, 2013; pp 15−56.
(277) McAllister, M. J.; Li, J.-L.; Adamson, D. H.; Schniepp, H. C.; Abdala, A. A.; Liu, J.; Herrera-Alonso, M.; Milius, D. L.; Car, R.; Prud'homme, R. K.; Aksay, I. A. Single sheet functionalized graphene

DOI: 10.1021/cr400607y
Chem. Rev. 2015, 115, 8294−8343

by oxidation and thermal expansion of graphite. *Chem. Mater.* **2007**, *19*, 4396−4404.
(278) Schniepp, H. C.; Li, J. L.; McAllister, M. J.; Sai, H.; Herrera-Alonso, M.; Adamson, D. H.; Prud'homme, R. K.; Car, R.; Saville, D. A.; Aksay, I. A. Functionalized single graphene sheets derived from splitting graphite oxide. *J. Phys. Chem. B* **2006**, *110*, 8535−8539.
(279) Lambert, T. N.; Chavez, C. A.; Hernandez-Sanchez, B.; Lu, P.; Bell, N. S.; Ambrosini, A.; Friedman, T.; Boyle, T. J.; Wheeler, D. R.; Huber, D. L. Synthesis and characterization of titania-graphene nanocomposites. *J. Phys. Chem. C* **2009**, *113*, 19812−19823.
(280) Subrahmanyam, K. S.; Vivekchand, S. R. C.; Govindaraj, A.; Rao, C. N. R. A study of graphenes prepared by different methods: Characterization, properties and solubilization. *J. Mater. Chem.* **2008**, *18*, 1517−1523.
(281) Liu, J. C.; Bai, H. W.; Wang, Y. J.; Liu, Z. Y.; Zhang, X. W.; Sun, D. D. Self-sssembling TiO_2 nanorods on large graphene oxide sheets at a two-phase interface and their anti-recombination in photocatalytic applications. *Adv. Funct. Mater.* **2010**, *20*, 4175−4181.
(282) Liang, Y. Y.; Wang, H. L.; Casalongue, H. S.; Chen, Z.; Dai, H. J. TiO_2 nanocrystals grown on graphene as advanced photocatalytic hybrid materials. *Nano Res.* **2010**, *3*, 701−705.
(283) Wang, W. D.; Serp, P.; Kalck, P.; Faria, J. L. Photocatalytic degradation of phenol on MWNT and titania composite catalysts prepared by a modified sol-gel method. *Appl. Catal., B* **2005**, *56*, 305−312.
(284) Han, S. C.; Hu, L. F.; Liang, Z. Q.; Wageh, S.; Al-Ghamdi, A. A.; Chen, Y. S.; Fang, X. S. One-step hydrothermal synthesis of 2D hexagonal nanoplates of α-Fe_2O_3/graphene composites with enhanced photocatalytic activity. *Adv. Funct. Mater.* **2014**, *24*, 5719−5727.
(285) Chen, L.; Yang, X.; Chen, J.; Liu, J.; Wu, H.; Zhan, H.; Liang, C.; Wu, M. Continuous shape- and spectroscopy-tuning of hematite nanocrystals. *Inorg. Chem.* **2010**, *49*, 8411−8420.
(286) Lee, Y.-C.; Chueh, Y.-L.; Hsieh, C.-H.; Chang, M.-T.; Chou, L.-J.; Wang, Z. L.; Lan, Y.-W.; Chen, C.-D.; Kurata, H.; Isoda, S. p-Type α-Fe_2O_3 nanowires and their n-Type transition in a reductive ambient. *Small* **2007**, *3*, 1356−1361.
(287) Chirita, M.; Grozescu, I. Fe_2O_3—Nanoparticles, physical properties and their photochemical and photoelectrochemical applications. *Bul. Stiint. Univ. "Politeh." Timisoara, Ser. Chim. Ing. Mediului* **2009**, *54*, 1−8.
(288) Al-Kuhaili, M.; Saleem, M.; Durrani, S. Optical properties of iron oxide (α- Fe_2O_3) thin films deposited by the reactive evaporation of iron. *J. Alloys Compd.* **2012**, *521*, 178−182.
(289) Luan, P.; Xie, M.; Liu, D.; Fu, X.; Jing, L. Effective charge separation in the rutile TiO_2 nanorod-coupled α-Fe_2O_3 with exceptionally high visible activities. *Sci. Rep.* **2014**, *4*, 6180.
(290) Wheeler, D. A.; Wang, G.; Ling, Y.; Li, Y.; Zhang, J. Z. Nanostructured hematite: Synthesis, characterization, charge carrier dynamics, and photoelectrochemical properties. *Energy Environ. Sci.* **2012**, *5*, 6682−6702.
(291) Sivula, K.; Le Formal, F.; Grätzel, M. Solar water splitting: Progress using hematite (α-Fe_2O_3) photoelectrodes. *ChemSusChem* **2011**, *4*, 432−449.
(292) Cesar, I.; Sivula, K.; Kay, A.; Zboril, R.; Grätzel, M. Influence of feature size, film thickness, and silicon doping on the performance of nanostructured hematite photoanodes for solar water splitting. *J. Phys. Chem. C* **2009**, *113*, 772−782.
(293) Bae, S.; Kim, H.; Lee, Y.; Xu, X. F.; Park, J. S.; Zheng, Y.; Balakrishnan, J.; Lei, T.; Kim, H. R.; Song, Y. I.; Kim, Y. J.; Kim, K. S.; Ozyilmaz, B.; Ahn, J. H.; Hong, B. H.; Iijima, S. Roll-to-roll production of 30-in. graphene films for transparent electrodes. *Nat. Nanotechnol.* **2010**, *5*, 574−578.
(294) Gomez De Arco, L.; Zhang, Y.; Schlenker, C. W.; Ryu, K.; Thompson, M. E.; Zhou, C. W. Continuous, highly flexible, and transparent graphene films by chemical vapor deposition for organic photovoltaics. *ACS Nano* **2010**, *4*, 2865−2873.
(295) Kim, H.; Gilmore, C. M.; Pique, A.; Horwitz, J. S.; Mattoussi, H.; Murata, H.; Kafafi, Z. H.; Chrisey, D. B. Electrical, optical, and structural properties of indium-tin-oxide thin films for organic light-emitting devices. *J. Appl. Phys.* **1999**, *86*, 6451−6461.
(296) Nisha, M.; Anusha, S.; Antony, A.; Manoj, R.; Jayaraj, M. K. Effect of substrate temperature on the growth of ITO thin films. *Appl. Surf. Sci.* **2005**, *252*, 1430−1435.
(297) Terzini, E.; Thilakan, P.; Minarini, C. Properties of ITO thin films deposited by RF magnetron sputtering at elevated substrate temperature. *Mater. Sci. Eng., B* **2000**, *77*, 110−114.
(298) Hong, W. J.; Xu, Y. X.; Lu, G. W.; Li, C.; Shi, G. Q. Transparent graphene/PEDOT-PSS composite films as counter electrodes of dye-sensitized solar cells. *Electrochem. Commun.* **2008**, *10*, 1555−1558.
(299) Groenendaal, B. L.; Jonas, F.; Freitag, D.; Pielartzik, H.; Reynolds, J. R. Poly(3,4-ethylenedioxythiophene) and its derivatives: Past, present, and future. *Adv. Mater.* **2000**, *12*, 481−494.
(300) Kirchmeyer, S.; Reuter, K. Scientific importance, properties and growing applications of poly(3,4-ethylenedioxythiophene). *J. Mater. Chem.* **2005**, *15*, 2077−2088.
(301) O'Regan, B.; Gratzel, M. A low-cost, high-efficiency solar cell based on dye-sensitized colloidal TiO_2 films. *Nature* **1991**, *353*, 737−740.
(302) Papageorgiou, N. Counter-electrode function in nanocrystalline photoelectrochemical cell configurations. *Coord. Chem. Rev.* **2004**, *248*, 1421−1446.
(303) Chen, Y.; Zhang, X.; Yu, P.; Ma, Y. W. Stable dispersions of graphene and highly conducting graphene films: A new approach to creating colloids of graphene monolayers. *Chem. Commun.* **2009**, 4527−4529.
(304) Li, S. S.; Tu, K. H.; Lin, C. C.; Chen, C. W.; Chhowalla, M. Solution-processable graphene oxide as an efficient hole transport layer in polymer solar cells. *ACS Nano* **2010**, *4*, 3169−3174.
(305) Liu, S.; Wang, J. Q.; Zeng, J.; Ou, J. F.; Li, Z. P.; Liu, X. H.; Yang, S. R. "Green" electrochemical synthesis of Pt/graphene sheet nanocomposite film and its electrocatalytic property. *J. Power Sources* **2010**, *195*, 4628−4633.
(306) Feng, X. M.; Li, R. M.; Ma, Y. W.; Chen, R. F.; Shi, N. E.; Fan, Q. L.; Huang, W. One-step electrochemical synthesis of graphene/polyaniline composite film and its applications. *Adv. Funct. Mater.* **2011**, *21*, 2989−2996.
(307) Zhuang, X.-D.; Chen, Y.; Liu, G.; Li, P.-P.; Zhu, C.-X.; Kang, E.-T.; Noeh, K.-G.; Zhang, B.; Zhu, J.-H.; Li, Y.-X. Conjugated-polymer-functionalized graphene oxide: Synthesis and nonvolatile rewritable memory effect. *Adv. Mater.* **2010**, *22*, 1731−1735.
(308) Das, A.; Chakraborty, B.; Sood, A. K. Raman spectroscopy of graphene on different substrates and influence of defects. *Bull. Mater. Sci.* **2008**, *31*, 579−584.
(309) Kou, R.; Shao, Y. Y.; Mei, D. H.; Nie, Z. M.; Wang, D. H.; Wang, C. M.; Viswanathan, V. V.; Park, S.; Aksay, I. A.; Lin, Y. H.; Wang, Y.; Liu, J. Stabilization of electrocatalytic metal nanoparticles at metal-metal oxide-graphene triple junction points. *J. Am. Chem. Soc.* **2011**, *133*, 2541−2547.
(310) Matsui, T.; Fujiwara, K.; Okanishi, T.; Kikuchi, R.; Takeguchi, T.; Eguchi, K. Electrochemical oxidation of CO over tin oxide supported platinum catalysts. *J. Power Sources* **2006**, *155*, 152−156.
(311) Zheng, N.; Stucky, G. D. A general synthetic strategy for oxide-supported metal nanoparticle catalysts. *J. Am. Chem. Soc.* **2006**, *128*, 14278−14280.
(312) Singh, V.; Joung, D.; Zhai, L.; Das, S.; Khondaker, S. I.; Seal, S. Graphene based materials: Past, present and future. *Prog. Mater. Sci.* **2011**, *56*, 1178−1271.
(313) Soldano, C.; Mahmood, A.; Dujardin, E. Production, properties and potential of graphene. *Carbon* **2010**, *48*, 2127−2150.
(314) Forbeaux, I.; Themlin, J. M.; Charrier, A.; Thibaudau, F.; Debever, J. M. Solid-state graphitization mechanisms of silicon carbide 6H-SiC polar faces. *Appl. Surf. Sci.* **2000**, *162*−*163*, 406−412.
(315) Hass, J.; de Heer, W. A.; Conrad, E. H. The growth and morphology of epitaxial multilayer graphene. *J. Phys.: Condens. Matter* **2008**, *20*, 323202.

DOI: 10.1021/cr400607y
Chem. Rev. 2015, 115, 8294−8343

(316) Kedzierski, J.; Hsu, P. L.; Healey, P.; Wyatt, P. W.; Keast, C. L.; Sprinkle, M.; Berger, C.; de Heer, W. A. Epitaxial graphene transistors on SiC substrates. *IEEE Trans. Electron Devices* **2008**, *55*, 2078−2085.
(317) May, J. W. Platinum surface LEED rings. *Surf. Sci.* **1969**, *17*, 267−270.
(318) Somani, P. R.; Somani, S. P.; Umeno, M. Planer nano-graphenes from camphor by CVD. *Chem. Phys. Lett.* **2006**, *430*, 56−59.
(319) Choi, W.; Lahiri, I.; Seelaboyina, R.; Kang, Y. S. Synthesis of graphene and its applications: A review. *Crit. Rev. Solid State Mater. Sci.* **2010**, *35*, 52−71.
(320) Batzill, M. The surface science of graphene: Metal interfaces, CVD synthesis, nanoribbons, chemical modifications, and defects. *Surf. Sci. Rep.* **2012**, *67*, 83−115.
(321) Cui, Y.; Fu, Q.; Zhang, H.; Tan, D.; Bao, X. Dynamic characterization of graphene growth and etching by oxygen on Ru(0001) by photoemission electron microscopy. *J. Phys. Chem. C* **2009**, *113*, 20365−20370.
(322) Reina, A.; Jia, X.; Ho, J.; Nezich, D.; Son, H.; Bulovic, V.; Dresselhaus, M. S.; Kong, J. Large area, few-layer graphene films on arbitrary substrates by chemical vapor deposition. *Nano Lett.* **2009**, *9*, 30−35.
(323) Wei, D.; Liu, Y.; Wang, Y.; Zhang, H.; Huang, L.; Yu, G. Synthesis of N-doped graphene by chemical vapor deposition and its electrical properties. *Nano Lett.* **2009**, *9*, 1752−1758.
(324) Lv, R.; Li, Q.; Botello-Mendez, A. R.; Hayashi, T.; Wang, B.; Berkdemir, A.; Hao, Q.; Elias, A. L.; Cruz-Silva, R.; Gutierrez, H. R.; Kim, Y. A.; Muramatsu, H.; Zhu, J.; Endo, M.; Terrones, H.; Charlier, J.-C.; Pan, M.; Terrones, M. Nitrogen-doped graphene: Beyond single substitution and enhanced molecular sensing. *Sci. Rep.* **2012**, *2*, 586.
(325) Malesevic, A.; Vitchev, R.; Schouteden, K.; Volodin, A.; Zhang, L.; Van Tendeloo, G.; Vanhulsel, A.; Van Haesendonck, C. Synthesis of few-layer graphene via microwave plasma-enhanced chemical vapour deposition. *Nanotechnology* **2008**, *19*, 305604.
(326) Zhu, M.; Wang, J.; Holloway, B. C.; Outlaw, R. A.; Zhao, X.; Hou, K.; Shutthanandan, V.; Manos, D. M. A mechanism for carbon nanosheet formation. *Carbon* **2007**, *45*, 2229−2234.
(327) Shin, H.-J.; Kim, K. K.; Benayad, A.; Yoon, S.-M.; Park, H. K.; Jung, I.-S.; Jin, M. H.; Jeong, H.-K.; Kim, J. M.; Choi, J.-Y.; Lee, Y. H. Efficient reduction of graphite oxide by sodium borohydride and its effect on electrical conductance. *Adv. Funct. Mater.* **2009**, *19*, 1987−1992.
(328) Gomez-Navarro, C.; Weitz, R. T.; Bittner, A. M.; Scolari, M.; Mews, A.; Burghard, M.; Kern, K. Electronic transport properties of individual chemically reduced graphene oxide sheets. *Nano Lett.* **2007**, *7*, 3499−3503.
(329) Bourlinos, A. B.; Gournis, D.; Petridis, D.; Szabo, T.; Szeri, A.; Dekany, I. Graphite oxide: Chemical reduction to graphite and surface modification with primary aliphatic amines and amino acids. *Langmuir* **2003**, *19*, 6050−6055.
(330) Hernandez, Y.; Nicolosi, V.; Lotya, M.; Blighe, F. M.; Sun, Z.; De, S.; McGovern, I. T.; Holland, B.; Byrne, M.; Gun'Ko, Y. K.; Boland, J. J.; Niraj, P.; Duesberg, G.; Krishnamurthy, S.; Goodhue, R.; Hutchison, J.; Scardaci, V.; Ferrari, A. C.; Coleman, J. N. High-yield production of graphene by liquid-phase exfoliation of graphite. *Nat. Nanotechnol.* **2008**, *3*, 563−568.
(331) Furtado, C. A.; Kim, U. J.; Gutierrez, H. R.; Pan, L.; Dickey, E. C.; Eklund, P. C. Debundling and dissolution of single-walled carbon nanotubes in amide solvents. *J. Am. Chem. Soc.* **2004**, *126*, 6095−6105.
(332) Blake, P.; Brimicombe, P. D.; Nair, R. R.; Booth, T. J.; Jiang, D.; Schedin, F.; Ponomarenko, L. A.; Morozov, S. V.; Gleeson, H. F.; Hill, E. W.; Geim, A. K.; Novoselov, K. S. Graphene-based liquid crystal device. *Nano Lett.* **2008**, *8*, 1704−1708.
(333) Lotya, M.; Hernandez, Y.; King, P. J.; Smith, R. J.; Nicolosi, V.; Karlsson, L. S.; Blighe, F. M.; De, S.; Wang, Z.; McGovern, I. T.; Duesberg, G. S.; Coleman, J. N. Liquid phase production of graphene by exfoliation of graphite in surfactant/water solutions. *J. Am. Chem. Soc.* **2009**, *131*, 3611−3620.
(334) Jiao, L.; Zhang, L.; Wang, X.; Diankov, G.; Dai, H. Narrow graphene nanoribbons from carbon nanotubes. *Nature* **2009**, *458*, 877−880.
(335) Kosynkin, D. V.; Higginbotham, A. L.; Sinitskii, A.; Lomeda, J. R.; Dimiev, A.; Price, B. K.; Tour, J. M. Longitudinal unzipping of carbon nanotubes to form graphene nanoribbons. *Nature* **2009**, *458*, 872−876.
(336) Yang, X.; Dou, X.; Rouhanipour, A.; Zhi, L.; Rader, H. J.; Mullen, K. Two-dimensional graphene nanoribbons. *J. Am. Chem. Soc.* **2008**, *130*, 4216−4217.
(337) Kim, K. S.; Zhao, Y.; Jang, H.; Lee, S. Y.; Kim, J. M.; Kim, K. S.; Ahn, J.-H.; Kim, P.; Choi, J.-Y.; Hong, B. H. Large-scale pattern growth of graphene films for stretchable transparent electrodes. *Nature* **2009**, *457*, 706−710.
(338) O'Donnell, K. P.; Chen, X. Temperature dependence of semiconductor band gaps. *Appl. Phys. Lett.* **1991**, *58*, 2924−2926.
(339) Bermel, P.; Luo, C.; Zeng, L.; Kimerling, L. C.; Joannopoulos, J. D. Improving thin-film crystalline silicon solar cell efficiencies with photonic crystals. *Opt. Express* **2007**, *15*, 16986−17000.
(340) Green, M. A. The path to 25% silicon solar cell efficiency: History of silicon cell evolution. *Prog. Photovoltaics* **2009**, *17*, 183−189.
(341) Miller, J. K.; Qi, J.; Xu, Y.; Cho, Y. J.; Liu, X.; Furdyna, J. K.; Perakis, I.; Shahbazyan, T. V.; Tolk, N. Near-bandgap wavelength dependence of long-lived traveling coherent longitudinal acoustic phonons in GaSb-GaAs heterostructures. *Phys. Rev. B: Condens. Matter Mater. Phys.* **2006**, *74*, 113313.
(342) Mattheis, J.; Rau, U.; Werner, J. H. Light absorption and emission in semiconductors with band gap fluctuations - A study on Cu(In,Ga)Se_2 thin films. *J. Appl. Phys.* **2007**, *101*, 113519.
(343) Blase, X.; Rubio, A.; Louie, S. G.; Cohen, M. L. Stability and band gap constancy of boron nitride nanotubes. *Europhys. Lett.* **1994**, *28*, 335.
(344) Rubio, A.; Corkill, J. L.; Cohen, M. L. Theory of graphitic boron nitride nanotubes. *Phys. Rev. B: Condens. Matter Mater. Phys.* **1994**, *49*, 5081.
(345) Elim, H. I.; Ji, W.; Zhu, F. Carrier concentration dependence of optical Kerr nonlinearity in indium tin oxide films. *Appl. Phys. B: Lasers Opt.* **2006**, *82*, 439−442.
(346) Laux, S.; Kaiser, N.; Zoller, A.; Gotzelmann, R.; Lauth, H.; Bernitzki, H. Room-temperature deposition of indium tin oxide thin films with plasma ion-assisted evaporation. *Thin Solid Films* **1998**, *335*, 1−5.
(347) Weiher, R. L.; Ley, R. P. Optical properties of indium oxide. *J. Appl. Phys.* **1966**, *37*, 299−302.
(348) Avouris, P. Graphene: Electronic and photonic properties and devices. *Nano Lett.* **2010**, *10*, 4285−4294.
(349) Shirasaki, Y.; Supran, G. J.; Bawendi, M. G.; Bulovic, V. Emergence of colloidal quantum-dot light-emitting technologies. *Nat. Photonics* **2013**, *7*, 13−23.
(350) Abbas, A. N.; Liu, G.; Narita, A.; Orosco, M.; Feng, X.; Mullen, K.; Zhou, C. Deposition, characterization, and thin-film-based chemical sensing of ultra-long chemically synthesized graphene nanoribbons. *J. Am. Chem. Soc.* **2014**, *136*, 7555−7558.
(351) Wu, J. S.; Pisula, W.; Mullen, K. Graphenes as potential material for electronics. *Chem. Rev.* **2007**, *107*, 718−747.
(352) Zheng, Y.; Qian, L.; Yang, Y.; Titov, A.; Hyvonen, J.; Cao, W.; Xue, J.; Holloway, P. H. 19.5L: Late-news paper: high efficiency and long lifetime quantum-dot light-emitting diodes for flat panel display applications. *Dig. Tech. Pap. - Soc. Inf. Disp. Int. Symp.* **2013**, *44*, 221−223.
(353) Oh, J. H.; Lee, K. H.; Yoon, H. C.; Yang, H.; Do, Y. R. Color-by-blue display using blue quantum dot light-emitting diodes and green/red color converting phosphors. *Opt. Express* **2014**, *22*, A511−A520.
(354) Bourzac, K. Quantum dots go on display. *Nature* **2013**, *493*, 283.
(355) Lightcap, I. V.; Kamat, P. V. Fortification of CdSe quantum dots with graphene oxide. excited state interactions and light energy conversion. *J. Am. Chem. Soc.* **2012**, *134*, 7109−7116.

DOI: 10.1021/cr400607y
Chem. Rev. 2015, 115, 8294−8343

(356) Guo, S. R.; Bao, D. D.; Upadhyayula, S.; Wang, W.; Guvenc, A. B.; Kyle, J. R.; Hosseinibay, H.; Bozhilov, K. N.; Vullev, V. I.; Ozkan, C. S.; Ozkan, M. Photoinduced electron transfer between pyridine coated cadmium selenide quantum dots and single sheet graphene. *Adv. Funct. Mater.* **2013**, *23*, 5199−5211.
(357) Wong, W. S.; Sands, T.; Cheung, N. W.; Kneissl, M.; Bour, D. P.; Mei, P.; Romano, L. T.; Johnson, N. M. Fabrication of thin-film InGaN light-emitting diode membranes by laser lift-off. *Appl. Phys. Lett.* **1999**, *75*, 1360−1362.
(358) David, A.; Fujii, T.; Moran, B.; Nakamura, S.; DenBaars, S. P.; Weisbuch, C.; Benisty, H. Photonic crystal laser lift-off GaN light-emitting diodes. *Appl. Phys. Lett.* **2006**, *88*, 133514.
(359) Bajpai, R.; Roy, S.; Kulshrestha, N.; Rafiee, J.; Koratkar, N.; Misra, D. S. Graphene supported nickel nanoparticle as a viable replacement for platinum in dye sensitized solar cells. *Nanoscale* **2012**, *4*, 926−930.
(360) Roy-Mayhew, J. D.; Boschloo, G.; Hagfeldt, A.; Aksay, I. A. Functionalized graphene sheets as a versatile replacement for platinum in dye-sensitized solar cells. *ACS Appl. Mater. Interfaces* **2012**, *4*, 2794−2800.
(361) Du, J. H.; Pei, S. F.; Ma, L. P.; Cheng, H. M. 25th anniversary article: Carbon nanotube- and graphene- based transparent conductive films for optoelectronic devices. *Adv. Mater.* **2014**, *26*, 1958−1991.
(362) Kaempgen, M.; Duesberg, G. S.; Roth, S. Transparent carbon nanotube coatings. *Appl. Surf. Sci.* **2005**, *252*, 425−429.
(363) Li, Z. R.; Kandel, H. R.; Dervishi, E.; Saini, V.; Biris, A. S.; Biris, A. R.; Lupu, D. Does the wall number of carbon nanotubes matter as conductive transparent material? *Appl. Phys. Lett.* **2007**, *91*, 053115.
(364) Yang, N.; Zhai, J.; Wang, D.; Chen, Y.; Jiang, L. Two-dimensional graphene bridges enhanced photoinduced charge transport in dye-sensitized solar cells. *ACS Nano* **2010**, *4*, 887−894.
(365) Nair, R.; Blake, P.; Grigorenko, A.; Novoselov, K.; Booth, T.; Stauber, T.; Peres, N.; Geim, A. Fine structure constant defines visual transparency of graphene. *Science* **2008**, *320*, 1308−1308.
(366) Dawlaty, J. M.; Shivaraman, S.; Strait, J.; George, P.; Chandrashekhar, M.; Rana, F.; Spencer, M. G.; Veksler, D.; Chen, Y. Measurement of the optical absorption spectra of epitaxial graphene from terahertz to visible. *Appl. Phys. Lett.* **2008**, *93*, 131905.
(367) Xia, F.; Mueller, T.; Golizadeh-Mojarad, R.; Freitag, M.; Lin, Y.-m.; Tsang, J.; Perebeinos, V.; Avouris, P. Photocurrent imaging and efficient photon detection in a graphene transistor. *Nano Lett.* **2009**, *9*, 1039−1044.
(368) Lee, E. J.; Balasubramanian, K.; Weitz, R. T.; Burghard, M.; Kern, K. Contact and edge effects in graphene devices. *Nat. Nanotechnol.* **2008**, *3*, 486−490.
(369) Hwang, E.; Adam, S.; Sarma, S. D. Carrier transport in two-dimensional graphene layers. *Phys. Rev. Lett.* **2007**, *98*, 186806.
(370) Martin, J.; Akerman, N.; Ulbricht, G.; Lohmann, T.; Smet, J.; Von Klitzing, K.; Yacoby, A. Observation of electron−hole puddles in graphene using a scanning single-electron transistor. *Nat. Phys.* **2008**, *4*, 144−148.
(371) Cheianov, V. V.; Fal'ko, V. I.; Altshuler, B. L.; Aleiner, I. L. Random resistor network model of minimal conductivity in graphene. *Phys. Rev. Lett.* **2007**, *99*, 176801.
(372) Xia, F.; Mueller, T.; Lin, Y.-m.; Valdes-Garcia, A.; Avouris, P. Ultrafast graphene photodetector. *Nat. Nanotechnol.* **2009**, *4*, 839−843.
(373) Hass, J.; Varchon, F.; Millan-Otoya, J. E.; Sprinkle, M.; Sharma, N.; De Heer, W. A.; Berger, C.; First, P. N.; Magaud, L.; Conrad, E. H. Why multilayer graphene on 4H-SiC(000(1)over-bar) behaves like a single sheet of graphene. *Phys. Rev. Lett.* **2008**, *100*, 125504.
(374) Geim, A.; Grigorieva, I. Van der Waals heterostructures. *Nature* **2013**, *499*, 419−425.
(375) Gobre, V. V.; Tkatchenko, A. Scaling laws for van der Waals interactions in nanostructured materials. *Nat. Commun.* **2013**, *4*, 2341.
(376) Shi, Y.; Zhou, W.; Lu, A.-Y.; Fang, W.; Lee, Y.-H.; Hsu, A. L.; Kim, S. M.; Kim, K. K.; Yang, H. Y.; Li, L.-J.; Idrobo, J.-C.; Kong, J. Van der Waals epitaxy of MoS_2 layers using graphene as growth templates. *Nano Lett.* **2012**, *12*, 2784−2791.
(377) Brown, L.; Hovden, R.; Huang, P.; Wojcik, M.; Muller, D. A.; Park, J. Twinning and twisting of tri-and bilayer graphene. *Nano Lett.* **2012**, *12*, 1609−1615.
(378) Ohta, T.; Bostwick, A.; McChesney, J.; Seyller, T.; Horn, K.; Rotenberg, E. Interlayer interaction and electronic screening in multilayer graphene investigated with angle-resolved photoemission spectroscopy. *Phys. Rev. Lett.* **2007**, *98*, 206802.

DOI: 10.1021/cr400607y
Chem. Rev. 2015, 115, 8294−8343